

11-2016

## Safety Assurance of Non-Deterministic Flight Controllers in Aircraft Applications

Alfonso Noriega

Follow this and additional works at: <https://commons.erau.edu/edt>



Part of the [Aerospace Engineering Commons](#), and the [Aviation Commons](#)

---

### Scholarly Commons Citation

Noriega, Alfonso, "Safety Assurance of Non-Deterministic Flight Controllers in Aircraft Applications" (2016). *Dissertations and Theses*. 288.  
<https://commons.erau.edu/edt/288>

This Dissertation - Open Access is brought to you for free and open access by Scholarly Commons. It has been accepted for inclusion in Dissertations and Theses by an authorized administrator of Scholarly Commons. For more information, please contact [commons@erau.edu](mailto:commons@erau.edu).

SAFETY ASSURANCE OF NON-DETERMINISTIC FLIGHT CONTROLLERS  
IN AIRCRAFT APPLICATIONS

A Dissertation

Submitted to the Faculty

of

Embry-Riddle Aeronautical University

by

Alfonso Noriega

In Partial Fulfillment of the

Requirements for the Degree

of

Doctor of Philosophy in Aerospace Engineering

November 2016

Embry-Riddle Aeronautical University

Daytona Beach, Florida

SAFETY ASSURANCE OF NON-DETERMINISTIC FLIGHT CONTROLLERS  
IN AIRCRAFT APPLICATIONS

by

Alfonso Noriega

A Dissertation prepared under the direction of the candidate's Committee Co-Chairmen, Dr. Richard 'Pat' Anderson and Dr. Mark J. Balas, Department of Aerospace Engineering, and has been approved by the members of the Dissertation Committee. It was submitted to the School of Graduate Studies and Research and was accepted in partial fulfillment of the requirements for the degree of Doctor of Philosophy in Aerospace Engineering.

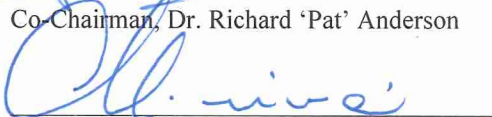
DISSERTATION COMMITTEE



Co-Chairman, Dr. Richard 'Pat' Anderson



Co-Chairman, Dr. Mark J. Balas



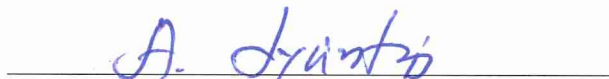
Member, Dr. Maj D. Mirmirani



Member, Dr. Richard J. Prazenica




Member, Dr. Borja Martos



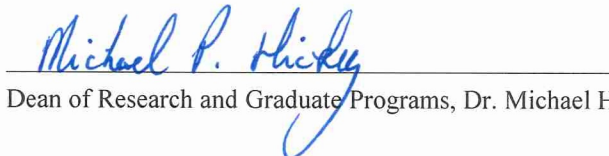
Department Chair, Dr. Anastasios Lyrantzis

10/31/16  
Date



Dean of College of Engineering, Dr. Maj Mirmirani

10/31/16  
Date



Dean of Research and Graduate Programs, Dr. Michael Hickey

10/31/2016  
Date

## ACKNOWLEDGMENTS

I would like to thank everyone who has, directly or indirectly, helped me to complete this work. First, I would like to thank my parents for their unconditional support. When I left home 9 years ago I had no idea I would make it this far, but I think that somehow, they did.

I would like to thank Dr. Pat Anderson for mentoring me since the beginning of my Master's degree. His knowledge of aircraft dynamics and control systems inspired me to pursue a PhD in this field. I thank him for the countless discussions that have helped me become a better engineer, and for believing in me since the beginning.

None of this would have been possible without the help of Dr. Mark Balas. His work is impressive and his knowledge on all things adaptive is simply unmatched. It is inspiring to see a person of his stature remain so humble and eager to help. I thank him for working so closely, for being patient when I didn't understand things, and for helping me get a better understanding of adaptive control theory.

I would also like to thank Dr. Borja Martos for helping me throughout this investigation. His support has ranged from very specific discussions of General Aviation aircraft, actuators, and sensors, to general moral support that helped me stay sane. I thank him for showing me that sometimes we need to take a step back and look at the big picture instead of drowning in a glass of water.

I thank Dr. Maj Mirmirani for his help in this investigation. He is the most eloquent and warm person that I have met. I thank him for finding time in his very busy schedule to review my work. I also thank him for the financial support provided for my graduate studies. I would also like to thank Dr. Richard Prazenica for all of his help. He introduced

me to the world of modern controls. His open door policy and eagerness to help are greatly appreciated.

Last, but not least, I would like to thank everyone at EFRC. I thank Shirley Koelker for making every day an enjoyable one, and for her help in the preparation of this document. I would like to thank Vinod Gehlot, Zachery Kern, Javier Cisneros, and everyone else for creating a friendly and enjoyable atmosphere, and for all the discussions and help they provided. I thank Alex Spradlin for all of her support and for her help in the preparation of this document.

## TABLE OF CONTENTS

LIST OF TABLES .....	vii
LIST OF FIGURES .....	viii
SYMBOLS.....	x
ABBREVIATIONS .....	xii
ABSTRACT.....	xiii
1. Introduction.....	1
1.1. Motivation.....	1
1.2. Problem Statement .....	6
1.2.1. Significance of the Proposed Work.....	9
2. Objectives .....	11
2.1. General Objective.....	11
2.2. Specific Objectives.....	12
2.2.1. Technical Objective 1.....	12
2.2.2. Technical Objective 2.....	12
2.2.3. Technical Objective 3.....	13
2.2.4. Technical Objective 4.....	14
2.2.5. Technical Objective 5.....	15
2.2.6. Technical Objective 6.....	15
2.2.7. Assumptions .....	16
3. Literature Review .....	18
3.1. Loss of Control .....	18
3.2. Adaptive Controls.....	20
3.2.1. Adaptive Controls in Aircraft .....	22
3.2.2. Certification of Adaptive Flight Controllers.....	26
3.3. Adaptive Robust Tracking with Disturbance Rejection .....	27
3.3.1. Plant and Robust Direct Adaptive Controller Structure.....	28
3.3.2. Ideal Trajectories .....	29
3.3.3. Existence and Uniqueness of the Ideal Trajectories.....	30
3.3.4. Stability of the Error System .....	33
3.3.5. Summary of Assumptions.....	35
3.4. Sensor Blending.....	36
3.4.1. Sensor Blending for a Single-Input-Single-Output System .....	36
3.4.2. Sensor Blending for a Multi-Input-Multi-Output System .....	38
4. Methodology.....	40
4.1. Aircraft Notation and Sign Conventions.....	40
4.2. General Aviation Aircraft Considerations .....	43
4.2.1. Selection of the Blending Variables.....	43
4.2.2. Longitudinal Linear Model of an Aircraft .....	46

4.2.3.	Lateral-Directional Linear Model of an Aircraft .....	48
4.3.	Simulation Environment .....	50
4.3.1.	Sensor Models .....	51
4.3.2.	Actuator Models .....	52
4.3.3.	Atmospheric Disturbances .....	52
4.4.	Autopilot Architecture.....	53
4.4.1.	Longitudinal Controller.....	54
4.4.2.	Lateral Controller .....	55
4.4.3.	Navigation Controller.....	56
4.5.	Test Cases .....	57
4.5.1.	Mathematical Requirements .....	57
4.5.2.	Test Scenario.....	58
4.6.	Autopilot Transfer .....	60
5.	Results.....	62
5.1.	Adaptive Controllers .....	62
5.1.1.	Longitudinal MRAC .....	62
5.1.2.	Lateral MRAC .....	67
5.2.	Conventional Controllers .....	72
5.2.1.	Altitude Controller.....	72
5.2.2.	Heading Angle Controller.....	73
5.2.3.	Airspeed Controller .....	73
5.3.	Test Scenario Results .....	74
5.3.1.	Test Case 1: No disturbances.....	74
5.3.2.	Test Case 2: Internal Disturbances .....	79
5.3.3.	Test Case 3: Internal and External Disturbances.....	83
5.4.	Autopilot Transfer Results .....	88
6.	Conclusion .....	94
7.	Recommendations.....	98
	REFERENCES .....	100
A.	Robust Stabilization Theorem Proof .....	105

## LIST OF TABLES

Table 4.1. Aircraft body axes variable notation.....	41
Table 4.2. Natural frequency and random noise of each sensor. ....	52
Table 4.3. Summary of disturbances present on each test case. ....	60
Table 5.1. Comparison between longitudinal original and blended outputs.....	66
Table 5.2. Comparison between lateral original and blended outputs.....	71
Table 5.3. Longitudinal conventional controller gains. ....	73
Table 5.4. Zeros and high frequency gain of blended outputs in the Navion aircraft. ....	89

## LIST OF FIGURES

Figure 1.1. Representative aircraft of the GA fleet.....	1
Figure 1.2. Gross weight versus cruise speed of several GA aircraft. ....	2
Figure 1.3. Cost of entry-level, four-seat airplanes over time (Anderson, 2013). ....	5
Figure 3.1. Fatal accidents in GA in CY2001-CY2011 (General Aviation Joint Steering Committee, 2014). ....	19
Figure 3.2. Indirect adaptive control.....	21
Figure 3.3. Direct adaptive control. ....	22
Figure 4.1. Aircraft body axes notation (Klein & Morelli, 2006).....	41
Figure 4.2. Control surface deflection sign convention (Klein & Morelli, 2006). ....	42
Figure 4.3. Sign convention of the Euler angles (CH Robotics, n.d.). ....	43
Figure 4.4. Cirrus SR22 in flight. ....	50
Figure 4.5. Stability derivatives of the SR22 model used.....	51
Figure 4.6. Longitudinal controller architecture. ....	54
Figure 4.7. Lateral controller architecture. ....	55
Figure 4.8. Aircraft's heading, waypoint heading, and heading error.....	56
Figure 4.9. Localizer and glideslope errors. ....	57
Figure 4.10. Horizontal navigation profile of the test scenario. ....	59
Figure 4.11. Vertical navigation profile of the test scenario.....	59
Figure 4.12. Navion aircraft in flight. ....	60
Figure 5.1. Time history comparison of original and blended outputs. ....	66
Figure 5.2. Plant input for output comparison. ....	66
Figure 5.3. Time history of original and blended outputs response.....	71
Figure 5.4. Noise-free vertical navigation results for the SR22 aircraft. ....	74
Figure 5.5. Noise-free pitch angle tracking results for the SR22 aircraft. ....	75
Figure 5.6. Time history of longitudinal adaptive gains for the SR22 aircraft. ....	76
Figure 5.7. Noise-free horizontal navigation results for the SR22 aircraft.....	77
Figure 5.8. Noise-free bank angle tracking results for the SR22 aircraft. ....	77
Figure 5.9. Noise-free localizer time history results for the SR22 aircraft.....	78
Figure 5.10. Time histories for the lateral adaptive gains for the SR22 aircraft.....	78
Figure 5.11. Vertical navigation results for the SR22 aircraft with sensor noise. ....	79
Figure 5.12. Pitch angle tracking results for the SR22 aircraft with sensor noise. ....	80

Figure 5.13. Longitudinal adaptive gains time history for the SR22 aircraft with sensor noise. ....	80
Figure 5.14. Horizontal navigation results for the SR22 aircraft with sensor noise. ....	81
Figure 5.15. Bank angle tracking results for the SR22 aircraft with sensor noise. ....	82
Figure 5.16. Localizer error time history for the SR22 aircraft with sensor noise. ....	82
Figure 5.17. Lateral adaptive gains time history for the SR22 aircraft with sensor noise. ....	83
Figure 5.18. Vertical navigation results for the SR22 aircraft. ....	84
Figure 5.19. Pitch angle tracking results for the SR22 aircraft. ....	85
Figure 5.20. Longitudinal adaptive gains time history for the SR22 aircraft. ....	85
Figure 5.21. Horizontal navigation results for the SR22 aircraft. ....	86
Figure 5.22. Localizer error time history for the SR22 aircraft. ....	86
Figure 5.23. Bank angle tracking results for the SR22 aircraft. ....	87
Figure 5.24. Lateral adaptive gains time history for the SR22 aircraft. ....	88
Figure 5.25. Vertical navigation results for the Navion aircraft. ....	90
Figure 5.26. Pitch angle tracking results for the Navion aircraft. ....	90
Figure 5.27. Longitudinal adaptive gains time history for the Navion aircraft. ....	91
Figure 5.28. Horizontal navigation results for the Navion aircraft. ....	91
Figure 5.29. Localizer error time history for the Navion aircraft. ....	92
Figure 5.30. Bank angle tracking results for the Navion aircraft. ....	92
Figure 5.31. Lateral adaptive gains time history for the Navion aircraft. ....	93

## SYMBOLS

$x$	State vector
$A$	A matrix
$B$	Control matrix
$C$	Output matrix
$\Gamma$	Disturbance matrix
$u$	Control vector
$u_D$	Disturbance vector
$\phi_D$	Disturbance basis vector
$y$	Output vector
$e_y$	Output error
$t$	Time
$G_m$	Adaptive gain
$G_u$	Adaptive gain
$G_e$	Adaptive gain
$G_D$	Adaptive gain
$a$	Damping term
$\gamma$	Weighing factor
$x_*$	Ideal state trajectory
$u_*$	Ideal control trajectory
$P_1$	Bounded projection
$P_2$	Bounded projection
$I$	Identity matrix
$R( \ )$	Range
$N( \ )$	Nullspace
$v$	Disturbance vector
$\  \ \ $	Norm
$tr( \ )$	Trace
$C_b$	Blended output
$K$	DC gain
$u$	Forward velocity
$w$	Down velocity
$q$	Pitch rate
$\theta$	Pitch angle
$X_u$	Change in forward force due to forward velocity
$X_w$	Change in forward force due to down velocity
$Z_u$	Change in vertical force due to forward velocity
$Z_w$	Change in vertical force due to down velocity
$g$	Acceleration due to gravity
$u_0$	Trim forward velocity
$M_u$	Change in pitching moment due to forward velocity
$M_w$	Change in pitching moment due to down velocity
$M_{\{w\}}$	Change in pitching moment due to rate of down velocity

$M_q$	Change in pitching moment due to pitch rate
$X_{\delta_e}$	Change in forward force due to elevator deflection
$Z_{\delta_e}$	Change in vertical force due to elevator deflection
$M_{\delta_e}$	Change in pitching moment due to elevator deflection
$\delta_e$	Elevator deflection
$\zeta$	Damping ratio
$\omega$	Natural frequency
$k_\theta$	Pitch transfer function gain
$T_{\theta_1}$	First pitch time constant
$T_{\theta_2}$	Second pitch time constant
$\beta$	Sideslip angle
$p$	Roll rate
$r$	Yaw rate
$\phi$	Bank angle
$Y_\beta$	Change in side force due to sideslip angle
$Y_p$	Change in side force due to roll rate
$Y_r$	Change in side force due to yaw rate
$L_\beta$	Change in rolling moment due to sideslip
$L_p$	Change in rolling moment due to roll rate
$L_r$	Change in rolling moment due to yaw rate
$N_\beta$	Change in yawing moment due to sideslip
$N_p$	Change in yawing moment due to roll rate
$N_r$	Change in yawing moment due to yaw rate
$\delta_a$	Aileron deflection
$\delta_r$	Rudder deflection
$L_{\delta_a}$	Change in rolling moment due to aileron deflection
$N_{\delta_a}$	Change in yawing moment due to aileron deflection
$a_x$	Longitudinal acceleration
$a_y$	Lateral acceleration
$a_z$	Vertical acceleration

## ABBREVIATIONS

GA	General Aviation
CFR	Code of Federal Regulations
LOC	Loss of Control
CAST	Commercial Aviation Safety Team
JSAT	Joint Safety Analysis Team
CFIT	Controlled Flight Into Terrain
GPS	Global Positioning System
IFR	Instrument Flight Rules
AOPA	Aircraft Owners and Pilots Association
IMC	Instrument Meteorological Conditions
GAJSC	General Aviation Joint Steering Committee
OOP	Owner/Operator/Pilot
LOCWG	Loss of Control Working Groups
SE	Safety Enhancements
SISO	Single-Input-Single-Output
SD	Strictly Dissipative
ASD	Almost Strictly Dissipative
FAA	Federal Aviation Administration
MIMO	Multi-Input-Multi-Output
ILS	Instrument Landing System
CPS	Certification Process Study
GTM	Generic Transport Model
MRAC	Model Reference Adaptive Control

## ABSTRACT

Noriega, Alfonso. PhD, Embry-Riddle Aeronautical University, November 2016. Safety Assurance of Non-Deterministic Flight Controllers in Aircraft Applications.

Loss of control is a serious problem in aviation that primarily affects General Aviation. Technological advancements can help mitigate the problem, but the FAA certification process makes certain solutions economically unfeasible. This investigation presents the design of a generic adaptive autopilot that could potentially lead to a single certification for use in several makes and models of aircraft. The autopilot consists of a conventional controller connected in series with a robust direct adaptive model reference controller. In this architecture, the conventional controller is tuned once to provide outer-loop guidance and navigation to a reference model. The adaptive controller makes unknown aircraft behave like the reference model, allowing the conventional controller to successfully provide navigation without the need for retuning.

A strong theoretical foundation is presented as an argument for the safety and stability of the controller. The stability proof of direct adaptive controllers require that the plant being controlled has no unstable transmission zeros and has a nonzero high frequency gain. Because most conventional aircraft do not readily meet these requirements, a process known as sensor blending was used. Sensor blending consists of using a linear combination of the plant's outputs that has no unstable transmission zeros and has a nonzero high frequency gain to drive the adaptive controller. Although this method does not present a problem for regulators, it can lead to a steady state error in tracking applications. The sensor blending theory was expanded to take advantage of the system's dynamics to allow for zero steady state error tracking. This method does not need knowledge of the specific

system's dynamics, but instead uses the structure of the A and B matrices to perform the blending for the general case.

The generic adaptive autopilot was tested in two high-fidelity nonlinear simulators of two typical General Aviation aircraft. The results show that the autopilot was able to adapt appropriately to the different aircraft and was able to perform three-dimensional navigation and an ILS approach, without any modification to the controller. The autopilot was tested in moderate atmospheric turbulence, using consumer-grade sensors and actuators currently available in General Aviation aircraft. The generic adaptive autopilot was shown to be robust to atmospheric turbulence and sensor and actuator random noise. In both aircraft simulators, the autopilot adapted successfully to changes in airspeed, altitude, and configuration.

This investigation proves the feasibility of a generic autopilot using direct adaptive controller. The autopilot does not need *a priori* information of the specific aircraft's dynamics to maintain its safety and stability arguments. Real-time parameter estimation of the aircraft dynamics are not needed. Recommendations for future work are provided.

## 1. Introduction

### 1.1. Motivation

General Aviation (GA) is defined as all civil aircraft that are certified under Part 23 of the Title 14 Code of Federal Regulations (CFR). Figure 1.1 shows the wide range of aircraft that comprise GA.



(a) Cessna 172



(b) Beechcraft King Air 250



(c) Cessna Citation Jet 2

Figure 1.1. Representative aircraft of the GA fleet.

GA aircraft have a gross takeoff weight of 12,500 lb or less for the normal and utility categories (nine seats or less, excluding pilots) and 19,000 lb or less for multiengine airplanes in the commuter category (19 seats or less, excluding pilots) (Federal Aviation Administration, 2015). These weight ranges lead to a wide variety of aircraft, from small piston engine airplanes to corporate business jets, as seen in Figure 1.1. Figure 1.2 shows a plot of cruise speed versus gross weight of several GA aircraft. The plot illustrates the wide performance range of aircraft classified as GA.

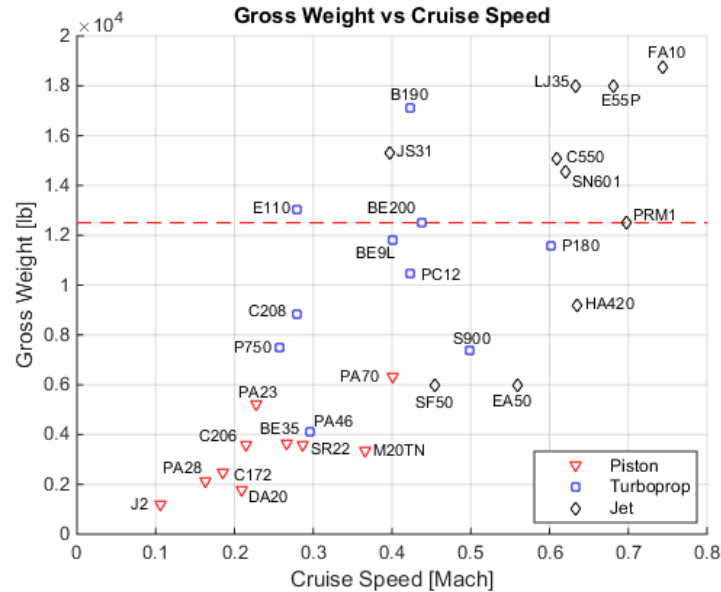


Figure 1.2. Gross weight versus cruise speed of several GA aircraft.

In the period between 1998 and 2004, GA accounted for more than half of the total number of hours flown by civilian aircraft with an accident rate of more than double that of commercial flights (Jacobson, 2010). There are several causal factors of GA accidents, the top three have been identified as loss of control inflight, controlled flight into terrain, and powerplant failure (Federal Aviation Administration, 2015). Although accidents due to controlled flight into terrain and powerplant failure have seen a decrease in occurrence over the past few years, loss of control remains the main cause of fatal accidents in GA (General Aviation Joint Steering Committee, 2014).

Loss of Control (LOC) was defined by the 2000 Commercial Aviation Safety Team (CAST) Joint Safety Analysis Team (JSAT) Report on Loss of Control as “a significant, unintended departure of an aircraft from controlled flight, the operational flight envelope, or usual flight attitudes, including ground events (Jacobson, 2010).” Some of the causes for LOC include, among others, pilot inexperience, physiological factors, failure to recognize stalls and/or spins, and failure to maintain airspeed (Federal Aviation

Administration, 2015). In order to reduce the number of LOC accidents, the FAA and industry leaders provide several resources to educate and train airmen to prevent LOC. Some of these resources include training sessions and seminars. Additionally, the implementation of newer technology could help reduce LOC accidents.

New technology has already proven effective in reducing accident rates. In the period between 2001 and 2010, there was a 60% drop in fatal accidents that were due to Controlled Flight into Terrain (CFIT), the second leading cause of fatal accidents in GA. Most of this technology was implemented in the form of handheld devices that provided Global Positioning Systems (GPS) position on a moving map and weather, terrain, and traffic information (General Aviation Joint Steering Committee, 2014). LOC accidents could be reduced by the installation of autopilots. Autopilots can help prevent LOC accidents through reduced pilot workload, especially during Instrument Flight Rules (IFR) operations. The Aircraft Owners and Pilots Association (AOPA) estimates that night, instrument meteorological conditions (IMC), LOC accidents could be reduced by 50% if autopilots were to be installed in all IFR capable GA aircraft (General Aviation Joint Steering Committee, 2014). By taking control of the aircraft and automating tasks such as maintaining altitude, the pilot has more time to focus on more important tasks such as navigating or monitoring the aircraft systems. If the pilot gets distracted, the autopilot will continue to maintain positive control of the aircraft. It is important to note that the pilot receives help from the autopilot rather than being replaced by it. However, unlike the technology used to prevent CFIT accidents, autopilots must have direct means and authority to deflect the control surfaces of the aircraft directly, and therefore must be installed on the aircraft. This means that if there is a system malfunction, the autopilot can

potentially place the aircraft in a dangerous flight condition. To prevent this, the FAA has established a rigorous certification process for autopilots that is intended to make the probability that the autopilot will malfunction during normal operations highly unlikely. The certification process aims to ensure that the probability of a safety-critical system failure is extremely improbable and does not result from a single failure (Federal Aviation Administration, 2015).

In order to certify an autopilot, manufacturers must demonstrate that the autopilot will perform its intended functions adequately. Each logic path must be tested to demonstrate that the outcome is the intended one and that there are absolutely no unintended functions programmed into the software (Bhattacharyya, Cofer, Musliner, Mueller, & Engstrom, 2015). Deterministic software, software in which the output of the system depends uniquely on the input, can then be certified albeit through a lengthy process. For non-deterministic software, however, this presents a certification challenge that has not yet been solved (Jacklin S. A., 2008). This lengthy certification process leads manufacturers to focus their development of autopilot designs to larger aircraft. Smaller GA aircraft are less commonly equipped with autopilots. Since autopilots help reduce the leading cause of accidents, the question arises as to why autopilots are not found on every aircraft. The answer lies in the overwhelming cost of purchasing an autopilot when compared to the total cost of the aircraft.

Due to FAA regulations, each autopilot needs to be certified for each particular make and model of aircraft. This means that a significant amount of resources is required to perform gain tuning and flight testing. This additional cost is ultimately transferred to the consumer who ends up paying significantly more money for the certification process

than for the product itself. Evidence of this fact can be found in autopilots for aircraft certified in the experimental category. These autopilots do not need to be certified and, therefore, cost a fraction of the price of their certified counterparts while they are comprised of essentially the same hardware and software and provide nearly the same functionality. For example, an experimental aircraft can be equipped with an autopilot for as little as \$2,500 while an autopilot for a certified aircraft can cost up to \$15,000 for an aircraft valued between \$20,000 to \$100,000 (General Aviation Joint Steering Committee, 2014). Certification costs not only affect autopilots, but the entire aircraft design process. This fact is more evident when looking at the cost of new aircraft. In the period between 1948 and 2010, the price of new GA airplanes has increased exponentially, at a much faster rate than standard inflation, as can be seen in Figure 1.3 (Anderson, 2013).

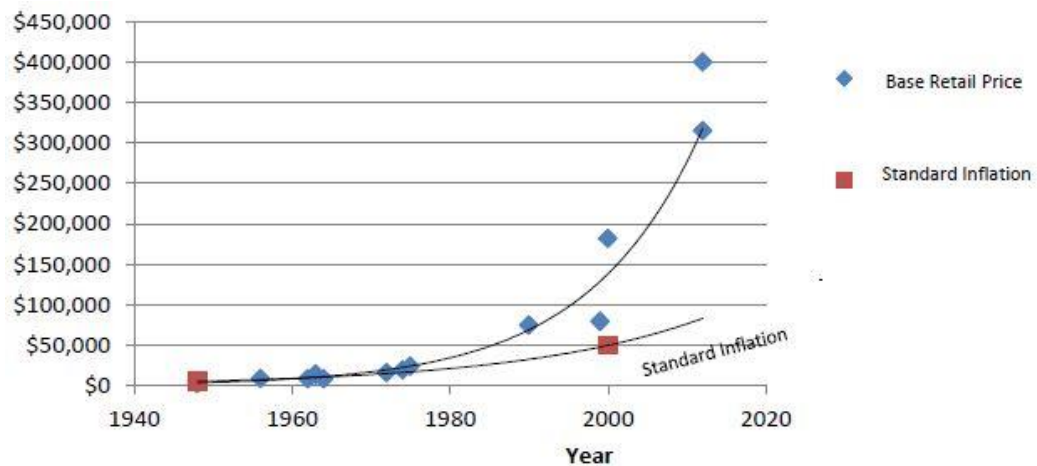


Figure 1.3. Cost of entry-level, four-seat airplanes over time (Anderson, 2013).

Expensive autopilots often lead to the owner/operator/pilot (OOP) not purchasing them. Making autopilots more affordable would lead to more OOPs installing them, increasing the overall safety of GA through reduced pilot workload, and envelope protection. Adaptive control theory offers an attractive solution to this problem. Designing an autopilot with little to no knowledge of the aircraft and allowing the gains to adapt would

lead to a generic autopilot that could potentially work for all makes and models of aircraft. If it could be demonstrated that a generic autopilot is safe and reliable to a level of confidence acceptable by the FAA, the time and cost savings would be significant for manufacturers, operators, and regulating agencies alike.

This investigation determined the feasibility of developing formal methods for the safety assurance of a non-deterministic autopilot. This was a necessary step towards increasing automation in GA aircraft. Without the use of adaptive controllers, increasing the automation level in small aircraft is not economically feasible. Working towards a certifiable, non-deterministic autopilot is a sensible approach due to the optional nature of the autopilot. This would allow manufacturers and regulators to become familiar with a new certification process, while still maintaining the possibility to disconnect the adaptive controllers completely and effectively. As the work in this investigation is expanded further, automation can begin to be used for more flight critical duties like envelope protection. Eventually, the results obtained here could lead to a fully fly-by-wire small aircraft that is affordable and safe.

## **1.2. Problem Statement**

Control system design has evolved well beyond its current state of implementation on civilian aircraft. The reason for this is that current regulations prevent the certification of nonlinear controllers. For safety reasons, the FAA has established a rigorous set of rules and processes for the certification of flight control software. These rules, however, were designed for the certification of linear controllers and some of the criteria does not apply to nonlinear systems. The technological advances have outpaced the certification process updates. This has led to newer, safer technology that is uncertifiable due to outdated

regulations (14 CFR Part 23 Reorganization Aviation Rulemaking Committee, 2013). Two of the main problems with the certification of adaptive controllers arise from this fact and are described below, while further description of these and the other major certification gaps can be found in Jacklin (Jacklin S. A., 2008).

- i) Proof of stability and convergence: although stability of a nonlinear controller can be proven, there currently does not exist an equivalent performance metric as to how stable the system is. Uncertainties in the plant could then potentially invalidate those proofs if there does not exist enough ‘margin’. Linear systems do not have this problem because gain and phase margins are well defined for linear cases.
- ii) Verification and validation: during the validation stage of software certification, it must be demonstrated that the software not only performs its intended functions but that it will also never perform any other function. The nonlinear nature of adaptive controls makes this nearly impossible. Although controller gains and trajectories can be shown to be bounded, *how* these trajectories dissipate may vary and is unpredictable.

Developing a certification process for adaptive controllers is a multi-disciplinary process (Jacklin S. A., 2008) and it will presumably take several years before the FAA is willing to accept it. This investigation will explore methods for the safety assurance of adaptive controllers with application considerations specific to GA aircraft. The methods used for this purpose will be a combination of mathematical analysis and simulation in an effort to complement theory with practice. Stability proofs and mathematical analysis are needed to demonstrate feasible deployment of an autopilot that includes an adaptive control

algorithm in a GA aircraft.

In addition to the FAA certification requirements, adaptive controls place certain conditions on the plant which they control that need to be met in order to guarantee the stability of the system. It is important to note that even if these conditions are not met, the controller might still perform its intended function, but there is no theoretical foundation on the stability of the system. Consequently, even if the plant does not meet the conditions, the controller may still work properly, but there is no guarantee on the stability of the system. In the case of direct adaptive control, these conditions are that the system must be minimum phase and have a nonzero high frequency gain (Balas & Fuentes, 2004). The following paragraphs briefly describe these conditions and why they can be problematic for aircraft.

In a Single-Input Single-Output (SISO) system, minimum phase means that the system has no unstable zeros. This is problematic in aircraft applications because most conventional aircraft are non-minimum phase (Snell, 2002). This can be observed in practice by an initial tendency of the system to respond in the opposite direction of where it is being excited. High frequency gain is the amplification of the input at very high frequencies. A non-zero high frequency gain requires the system to have a relative degree of one (or less). Once again, this is not always the case for aircraft. Many aircraft transfer functions have relative degree higher than one. In addition, due to cost constraints, civilian aircraft are equipped with lower-grade sensors and actuators than their military counterparts. This also has a negative impact on high frequency gain, as will be discussed later. Since these two conditions are often violated in aircraft applications, this investigation also aims to implement an aircraft specific solution to meet these conditions.

After these problems have been solved, it is important to test the controller on a different aircraft. For this, the system will be tested in at least one high fidelity model of an aircraft different from that used in development. In summary, the four necessary statements that must be satisfied are listed below:

- i) To identify an adaptive control algorithm suitable for deployment as a single certification autopilot for the general aviation fleet.
- ii) To identify the mathematical challenges associated with the implementation of current state-of-the-art adaptive controllers on GA aircraft.
- iii) To develop the theory required to show feasible deployment that includes demonstration of stability of the adaptive algorithm.
- iv) To test the controller on at least one unknown high fidelity nonlinear simulator.

### **1.2.1. Significance of the Proposed Work**

For decades, adaptive control systems have been applied to aircraft for several different applications ranging from envelope protection to fault tolerant controls (Wang, Santone, & Chengyu, 2012; Boskovic, 2012). A majority of these efforts, however, have been performed in simulation or in advanced, highly maneuverable, turbojet fighter aircraft. A gap exists in bringing this technology to a large number of varying types of aircraft. In addition, the stability proofs of these controllers are mostly limited to address specific aspects of implementation, as opposed to all of them simultaneously. This investigation aims to expand these proofs to include practical considerations. In this effort, it is necessary to ensure that the conditions imposed on the plant by adaptive control theory are met. This presents a challenge because most aircraft do not readily meet these conditions. A method for testing and ensuring minimum phase and non-zero high

frequency gain needs to be established in order to provide a theoretical foundation on the stability of the proposed autopilots.

As mentioned previously, control design has clearly evolved well beyond the capabilities of a conventional autopilot. However, none of the benefits of adaptive controllers will be available for civilian use until the certification issues has been addressed. The safety assurance of adaptive controls with practical considerations is an initial step toward bringing the benefits of advanced flight controls into GA.

Segments of the work presented here have been published or accepted into various conferences. The use of a zero filter to mitigate the minimum phase problem in aircraft was initially used but later abandoned in favor of sensor blending (Noriega, Balas, & Anderson, 2016). The sensor blending methodology in which the blending is performed in a way that it does not alter the ideal trajectories has been submitted and accepted to the 2017 AIAA SciTech conference (Noriega, Balas, & Anderson, 2017). The future work presented in the last chapter has been submitted and accepted to the 2017 AIAA Aviation invited session dealing with Fly-by-Wire control of general aviation aircraft (Noriega, Balas, & Martos, 2017).

## 2. Objectives

### 2.1. General Objective

**The primary objective of this investigation was to identify a suitable adaptive control algorithm that can be deployed as a feasible single certification generic autopilot for the GA fleet. Then, to develop the necessary theory and implementation methodology that guarantees system stability even when controlling an unknown plant in the presence of bounded and persistent internal and external disturbances.**

An adaptive control algorithm is necessary in order to control the wide range of aircraft in GA without manual retuning of the controller gains for each make and model. A generic autopilot means that the controller architecture and stability arguments remain un-affected by the specific aircraft make and model being controlled. An implementation methodology is necessary to ensure that the assumptions used in the theory development are valid for every aircraft that must be controlled by the generic autopilot. System stability means that the controller gains and aircraft states will remain bounded and will not diverge. Internal disturbances refer to those that arise from within the system in the form of sensor or actuator noise and unmodeled dynamics. External disturbances refer to environmental factors such as wind gusts and atmospheric turbulence. To meet the general objective, specific objectives were established. The following section describes each of these objectives and the necessary tasks required to complete them.

## **2.2. Specific Objectives**

### **2.2.1. Technical Objective 1**

**Identification of an adaptive control algorithm with the potential to be developed into a suitable single certification autopilot for GA.**

This objective consisted of identifying an adaptive control algorithm as the starting point of this investigation. This algorithm must be as simple as possible while maintaining sufficient robustness. To meet this objective, the following tasks were performed:

Task 1.1. Literature survey: an extensive literature survey was performed to identify suitable adaptive control algorithms for aircraft applications.

Task 1.2. Preliminary testing: the algorithms with the most desirable properties were subjected to preliminary testing on a linear model. The test consisted of controlling a linear model of an aircraft in an effort to expose the strengths and weaknesses of each algorithm.

Task 1.3. Algorithm selection: after the preliminary testing of the available algorithms was complete, the most promising algorithm was selected for the development of a generic autopilot.

### **2.2.2. Technical Objective 2**

**Identification of the mathematical challenges associated with the implementation of the selected adaptive control algorithm on GA aircraft.**

The next step was to identify the specific challenges in the implementation of the selected algorithm with guaranteed stability. The following tasks were performed:

Task 2.1. Identification of stability challenges: this task involved identifying which

of the assumptions made in the development of the stability theory of the algorithm are not met by the intended plants (GA aircraft).

Task 2.2. Identification of implementation challenges: to ensure the feasibility of a generic autopilot, the hardware used in the implementation must be representative of hardware currently available in GA aircraft. This means that the effects of lower-grade actuators and sensors typically present in GA needed to be analyzed. The operating environment also needs to be included in the analysis, which means that the presence of bounded and periodic atmospheric disturbances needed to be studied. This includes atmospheric turbulence, wind shear, and crosswinds.

### **2.2.3. Technical Objective 3**

**Development of the theory and methodology that address the implementation challenges of the selected algorithm.**

After the implementation challenges were identified, the next step was to develop the necessary theory and implementation methodology to handle them. The following tasks were performed:

Task 3.1. Non-minimum phase: because most conventional aircraft are non-minimum phase in altitude (an important state in autopilot design), a process to deal with this had to be established.

Task 3.2. Non-zero high frequency gain: the addition of second order actuators causes the system to have a zero high frequency gain. This can be mitigated if the velocity of the actuator is fed forward to the output. The measurement of an actuator rate using consumer-grade sensors often leads to noisy signals. This needed to be addressed.

Task 3.3. Consumer-grade hardware: due to FAA regulations, autopilot actuators

are slow and possess low control power. In addition, the sensors implemented are not as precise as those found in military aircraft, leading to a lower signal-to-noise ratio. This needed to be taken into account while demonstrating the safety of the controller.

#### **2.2.4. Technical Objective 4**

**Implementation of the adaptive control algorithm in simulation using a high fidelity GA aircraft model.**

The algorithm was implemented in simulation using the methodology developed in the previous objective. A high fidelity simulator of a GA aircraft was used. This step was still considered to be part of the development and was intended to expose errors and/or weaknesses in the methodology developed. Accurate knowledge of the plant was still made available for further refinement of the methodology. The following tasks were performed for a gradual implementation of the algorithm.

Task 4.1. Linear model implementation: the first step was to implement the algorithm in a linear model of an aircraft in the absence of disturbances.

Task 4.2. Nonlinear model implementation: after the controller was operating as required, it was implemented in a nonlinear, six-degrees-of-freedom simulator in the absence of disturbances.

Task 4.3. Robustness modifications: different robustness modifications to the algorithm were studied, and the most appropriate modifications were implemented.

Task 4.4. Disturbances: internal and external disturbances were added to the model.

### **2.2.5. Technical Objective 5**

**Expansion of the algorithm's stability proofs to include practical and implementation considerations specific to GA aircraft.**

After the practical and implementation challenges of the algorithm had been addressed, the stability theory of the algorithm was expanded to include the methodology developed. The theory developed guaranteed stability of the entire system in the intended operating environment as a whole. The following tasks were performed:

Task 5.1. Theory development: the first task to meet this objective was to develop the mathematical theory that guarantees stability of the system.

Task 5.2. Test cases: after the theory was developed, it was supported with simulation test cases. Extreme conditions at the edge of the operating envelope were tested to validate the theory predictions.

### **2.2.6. Technical Objective 6**

**Implementation of the generic autopilot on a high fidelity simulator of a different GA aircraft while maintaining the algorithm's safety arguments.**

After the stability theory for a generic adaptive autopilot has been developed and validated with simulation test cases, the generic autopilot was implemented on a different aircraft model following the proposed methodology. This objective was designed to test the transferability of the safety and stability arguments to an unknown plant. Accurate knowledge of the plant was not needed in this step. The following tasks were performed:

Task 6.1. Aircraft analysis: a new aircraft was tested for the assumptions made for the theory. It was analyzed for minimum phase and non-zero high frequency gain. Knowledge of the plant was not made available in this step, and the controller architecture

and implementation methodology were not modified.

Task 6.2. Generic autopilot implementation: once the requirements were met, the generic autopilot was implemented on a high fidelity simulator of a GA aircraft.

Task 6.3. Stability analysis: the stability of the system was tested. Knowledge of the plant was used for this analysis. Additionally, simulation test cases were performed to ensure that the system was stable and that the adaptive gains remained bounded.

### **2.2.7. Assumptions**

The following assumptions were made throughout this investigation:

#### **Autopilot Design**

- i) The autopilot was implemented in a simulation model of a Cirrus SR22 in cruise condition (160 kts at 6000 ft). This flight condition was chosen because it represents a typical cruise altitude and airspeed for the aircraft.
- ii) The autopilot consisted of decoupled longitudinal and lateral controllers. The longitudinal mode controls vertical speed, and the lateral mode controls bank angle.
- iii) The autopilot was always engaged from a trim condition.
- iv) No pilot inputs were applied after the autopilot is engaged.
- v) Disturbances were moderate and bounded. This is a conservative assumption because most GA autopilots disengage in the presence of moderate turbulence.
- vi) The actuators were represented as second order systems with a natural frequency of 22.6 rad/s and a damping ratio of 0.7 (Berger T. , Tischler, Hagerott, Gangsaas, & Saeed, 2013). The actuators can fully deflect the control

surfaces of the aircraft to the limits specified within the type certificate data sheet.

- vii) The sensors are represented as second order systems with natural frequency of 25 rad/s and a damping ratio of 1 (Berger T. , Tischler, Hagerott, Gangsaas, & Saeed, 2012).
- viii) All aircraft states were measurable.
- ix) The aircraft was equipped with roll and pitch axes servos.
- x) The autopilot performance must be equivalent to current GA autopilots.

### **Autopilot Implementation**

- i) The autopilot was transferred to a Navion aircraft in cruise condition (150 kts at 6000 ft).
- ii) Control requirements were established prior to testing the autopilot.
- iii) The controller structure was to remain unchanged unless otherwise determined by the previous step.

### **3. Literature Review**

#### **3.1. Loss of Control**

Loss of control (LOC) was defined by the 2000 Commercial Aviation Safety Team (CAST) Joint Safety Analysis Team (JSAT) Report on Loss of Control as “a significant, unintended departure of the aircraft from controlled flight, the operational flight envelope, or usual flight attitudes, including ground events (Jacobson, 2010).” LOC is the leading cause for fatal accidents in aviation worldwide (Belcastro & Foster, 2010). From 1998 to 2004, the LOC accidents per million flight hours for General Aviation (GA) aircraft was 11.24, with over half of these accidents leading to fatalities (Jacobson, 2010). This is a significantly higher number than that for commercial aircraft (0.1 for Part 121 and 4.03 for Part 135). These alarming rates have led to several studies. The NASA Aviation Safety Program conducted a study on the subject and the results grouped the causal factors into three major categories: pilot induced, environmentally induced, and system induced (Jacobson, 2010). Of the three, pilot induced appears to be the most common (Belcastro & Foster, 2010).

To address these issues, the General Aviation Joint Steering Committee (GAJSC) was re-established in 2011 after being inactive for several years following its creation in the mid-1990s (General Aviation Joint Steering Committee, 2014). The findings specific to GA were similar to those for aviation in general; LOC contributes to the highest number of accidents by a significant margin. Figure 3.1 shows a breakdown of the causes of GA accidents between 2001 and 2011. To investigate this issue and to propose solutions, the GAJSC created two Loss of Control Working Groups (LOCWG). The first LOCWG (LOCWG 1.0) dealt with LOC accidents that occurred on approach and landing, while

LOCWG 2.0 dealt with en route and departure accidents. The two LOCWGs developed a series of 34 Safety Enhancements (SE), which they prioritized based on their effectiveness at preventing accidents and their implementation feasibility.

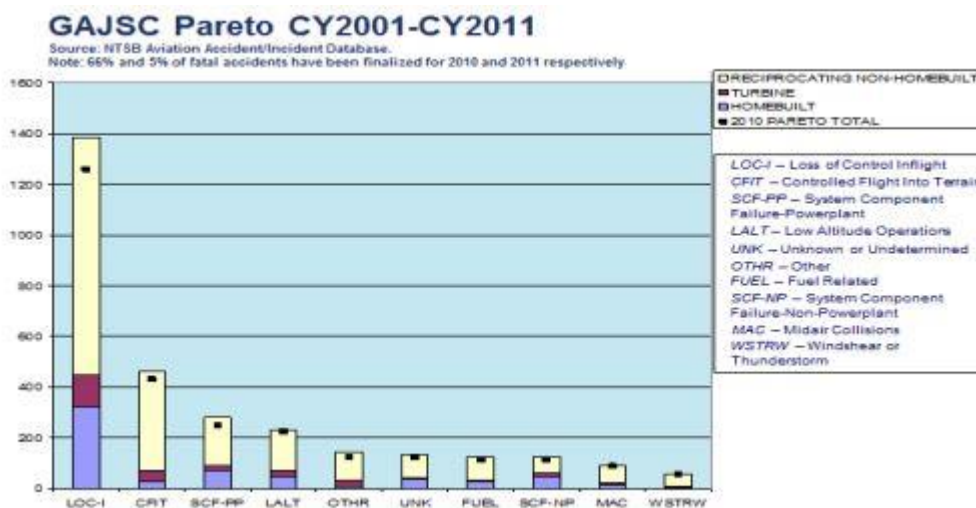


Figure 3.1. Fatal accidents in GA in CY2001-CY2011 (General Aviation Joint Steering Committee, 2014).

The first two SEs deal with angle of attack systems. A major contributing factor to LOC is aerodynamic stall. Installing low cost angle of attack indicators in the GA fleet would prevent a significant number of accidents. In addition, having a stall protection system onboard the aircraft could lead to the stall region of the airframe never being reached. Autopilot related SEs are found in SE 25 through 27. These SEs deal with the reduction of regulatory roadblocks for the installation of state-of-the-art technology in GA aircraft. An example of the safety benefits of newer technology can be found in the second leading cause for accidents in GA, namely Controlled Flight into Terrain (CFIT). Between 2001 and 2010, CFIT-related accidents have decreased by 60% (General Aviation Joint Steering Committee, 2014). Owner/Operator/Pilots (OOPs) have opted for handheld devices to prevent CFIT because the technology is available and relatively inexpensive. However, this is not the case for LOC.

The Aircraft Owners and Pilots Association (AOPA) estimates that night, Instrument Meteorological Conditions (IMC), LOC accidents could be reduced by 50% if autopilots were to be installed in all IFR capable GA aircraft (General Aviation Joint Steering Committee, 2014). However, while autopilots for experimental aircraft can be purchased for as little as \$2,500, a certified autopilot with similar capabilities can cost up to \$25,000. This expense is not reasonable, since in most cases it accounts for more than 10% of the total vehicle cost (General Aviation Joint Steering Committee, 2014). To change this, a new certification methodology must be adopted so that the cost of this safety enhancing technology can be reduced significantly. In 2009, the Part 23 Certification Process Study (CPS) resulted in recommendations to make safety modifications more affordable and feasible (Anderson, 2013; Federal Aviation Administration, 2009). Because the GA fleet consists of over 200,000 aircraft, most recommendations were focused on keeping the existing fleet safe (Federal Aviation Administration, n.d.). Using state-of-the-art technology can provide an answer to reducing the cost of certified autopilots. The use of adaptive controllers can provide a generic autopilot that adapts to the individual aircraft. The following section analyzes the advancement of adaptive controllers from military aircraft to GA.

### **3.2. Adaptive Controls**

An adaptive control process is defined as one in which “the controller has to learn to improve its performance through the observation of the outputs of the process (Bellman & Kalaba, 1959).” Although several definitions exist, the one presented by Bellman and Kalaba has the widest degree of acceptance among control theorists (Narendra &

Annaswamy, 1989). When a plant is fully known and a controller has complete knowledge of the plant dynamics, Bellman and Kabala referred to it as a deterministic process. When unknown factors are present, but are known to be random with known probability functions, they referred to it as a stochastic process. Because adaptive controllers have less information of the plant than deterministic and stochastic processes, they are often referred to by the FAA as non-deterministic (Federal Aviation Administration, 2016).

There exist two approaches to the adaptive control of a plant with unknown parameters: direct and indirect (Narendra & Annaswamy, 1989). In indirect adaptive control, the plant parameters are estimated on-line and used to adjust the controller parameters. This method is also referred as *explicit identification* (Astrom, 1980). In direct adaptive control, no attempt is made at identifying the plant parameters. The control parameters are directly adjusted to improve a performance index. This is also known as *implicit identification*. Figure 3.2 shows a block diagram of indirect adaptive control and Figure 3.3 shows a block diagram of direct adaptive control (Narendra & Annaswamy, 1989).

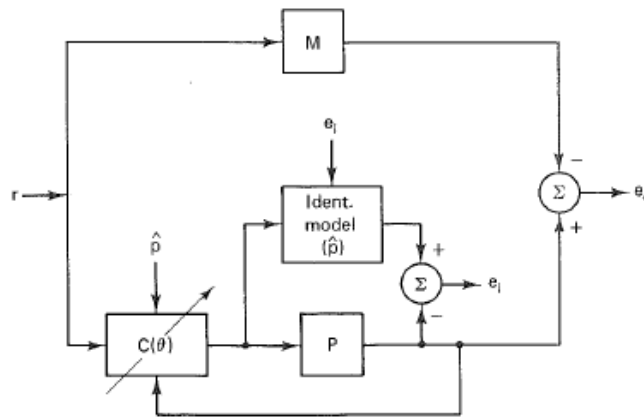


Figure 3.2. Indirect adaptive control.

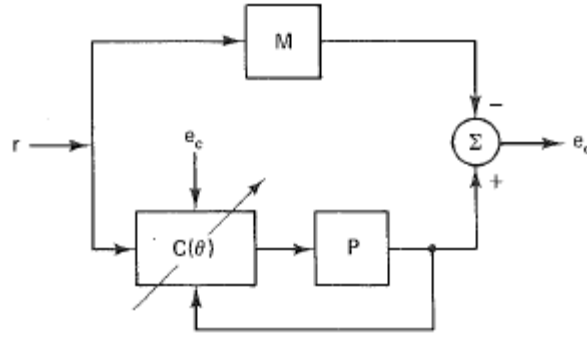


Figure 3.3. Direct adaptive control.

### 3.2.1. Adaptive Controls in Aircraft

The use of adaptive controllers in aircraft has been successfully demonstrated for several purposes. From simplifying the flying task by decoupling the aircraft modes (Bruner, 2007) to fault tolerance of asymmetric damage (Liu, Tao, & Joshi, 2010), adaptive control theory has demonstrated great potential to increase aviation safety.

Both direct and indirect adaptive control methods have been successfully tested on aircraft. An indirect adaptive self designing controller was flight tested on the VISTA/F-16 (Ward, 1998). NASA has successfully tested both direct and indirect adaptive controllers on a modified F-15 (Urnes, 1999). In unmanned aircraft, Wise et al presented a reconfigurable flight controller for a tailless advanced fighter (Wise, et al., 1999). Adaptive controls has also been used for guidance and control of advanced weapon systems. McFarland and Calise presented a neural networks adaptive controller for an agile anti-air missile (McFarland & Calise, 1997). Sharma et al presented an adaptive augmentation controller for precision guided munitions (Sharma, Lavretsky, & Wise, 2006). Regardless of the adaptive control method used, a trend becomes apparent. After a new controller architecture has been identified, it almost invariantly is implemented first in highly maneuverable aircraft. Only a fraction of the controllers tested on these aircraft are

eventually implemented in GA aircraft. The following paragraphs describe the main adaptive controller architectures that were eventually implemented in GA aircraft from controller conception to their implementation in GA.

Kim and Calise developed an adaptive flight controller using neural networks (Kim & Calise, 1997). The neural networks were first trained off-line using a nominal mathematical model of an aircraft. Learning neural networks were used on-line to compensate for any inversion errors between the nominal model and actual aircraft. They presented successful results using a simulation of an F/A-18 turbojet fighter aircraft. This work was expanded by Rysdyk et al, by the addition of a nonlinear damper for improved robustness (Rysdyk, Nardi, & Calise, 1999). This work was tested on a simulation of an XV-15 tilt-rotor aircraft.

Steck et al recognized the benefits of the neural networks based adaptive controllers on military aircraft and proposed their use on GA (Steck, Rokhsaz, Pesonen, & Duerksen, 2004). The authors designed an adaptive controller to decouple the flight controls and to improve the handling qualities, even in the presence of hardware failures and configuration changes. Simulation results were presented for a typical single-engine GA aircraft. The authors presented a brief discussion of the effects of adaptive controllers in aircraft, pilot, and software certification.

In 2007, Bruner expanded the work of Kim and Calise by removing the need of dynamic feedback of the state variables (Bruner, 2007). Rajagopal et al expanded this work further by proposing a general observer structure that separates the design of the nominal closed loop dynamics from the estimation error dynamics, allowing for fast adaptation without inducing high frequency oscillations (Rajagopal, Mannava, Balakrishnan, Nguyen,

& Krishnakumar, 2009). Rajagopal et al developed a neural networks based adaptive controller using that general observer structure. The controller was used to design a robust adaptive controller for a GA aircraft (Rajagopal, Balakrishnan, Steck, & Kimball, 2010). The controller consisted of a dynamic inversion controller augmented with a neural network to compensate for model uncertainties. The results showed that the adaptive controller was able to compensate for model uncertainties and drastic system failures such as 50% loss of elevator and thrust effectiveness.

Dynamic inversion augmented with neural networks to correct for model uncertainties was implemented on a GA aircraft simulator by Chandramohan et al (Chandramohan, Steck, Rokhsaz, & Ferrari, 2007). Kimberly et al adapted the control architecture and implemented it on a Bonanza Fly-by-Wire research testbed (Lemon, Steck, Hinson, Nguyen, & Dimball, 2010). Hardware-in-the-loop simulation results were successful, but engagement of the flight controller in flight resulted in un-commanded unstable oscillations. Meikel et al adjusted the simulator model used and re-tuned the controllers (Meikel, Steele, Lemon, Steck, & Rokhsaz, 2013). Flight test results, however, were still unsuccessful.

Cao and Hovakimyan presented the L1 adaptive control architecture that has a low-pass filter in the feedback channel to prevent high adaptation rates from inducing high frequency oscillations in the plant (Cao & Hovakimyan, 2007). This controller architecture has been widely implemented in aircraft applications. Patel et al, implemented a neural networks-based L1 controller on a simulation of an unstable X-45A UCAV (Patel, Cao, Hovakimyan, Wise, & Lavretsky, 2007). This controller provided improved performance over the neural networks Model Reference Adaptive Controller (MRAC) that was

previously implemented on the same simulation by Lavretsky and Wise (Lavretsky & Wise, 2005).

Gregory et al designed an L1 adaptive controller for NASA's Generic Transport Model (GTM) (Gregory, Cao, Xargay, Hovakimyan, & Zou, 2009). The authors provided nonlinear simulation results along with primary pilot evaluations. Campbell and Kaneshige presented different implementation of a baseline controller with an L1 adaptive augmentation on a simulation of NASA's GTM (Campbell & Kaneshige, 2010). Results showed that the L1 adaptive augmentation improved the baseline controller performance in the presence of disturbances and actuator saturation. Gregory et al presented flight test results of an L1 controller onboard the GTM (Gregory, Xargay, Cao, & Hovakimyan, 2010).

Stroosma et al implemented an L1 adaptive controller on a simulation of a GA business jet (Stroosma, et al., 2011). The controller was used to improve the aircraft's handling qualities and to prevent unfavorable aircraft-pilot interactions in the presence of hardware failures. The results show that the adaptive controller provided consistent handling qualities in the presence of configuration changes and hardware failures.

Steinberg identify the potential of fuzzy logic controllers for aircraft applications and proposed several applications (Steinberg, 1992). A fuzzy logic generic autopilot was then designed and presented by Duerksen (Duerksen, 1996). Duerksen used two decoupled longitudinal fuzzy logic controllers. Fuzzy logic controllers have been found to be less sensitive to plant variations (Mamdani, 1993). This fact makes them a suitable candidate to design a generic autopilot. Duerksen demonstrated successful simulation results for a business jet and single engine piston aircraft with the same controller. Shuguang presented

a fuzzy logic controller to improve the bank angle tracking of aircraft at high angle of attack and low dynamic pressure (Shuguang, 1994). Simulation results are presented that indicate that the fuzzy logic controller performs significantly better than the un-augmented aircraft. However, the controller had to be carefully designed around zero error to avoid unexpected behavior. Baker presented some of the limitations of fuzzy logic controllers as applied to flight controls (Baker, 1993).

Kaneshige et al used neural networks and dynamic inversion to design a generic autopilot (Kaneshige, Bull, & Totah, 2000). A base aerodynamic model of an aircraft is used to design a dynamic inversion flight controller. The neural networks compensates for inversion errors and reduces the tuning time needed to transfer the autopilot to different makes and models of aircraft. The authors successfully transferred the autopilot from a mid-sized twin engine commercial jet transport aircraft to a modified F-15 with movable canards. Jacklin et al presented the certification problems associated with the use of such learning neural networks, specifically in the area of software verification and validation (Jacklin, et al., 2005).

### **3.2.2. Certification of Adaptive Flight Controllers**

Despite all the efforts made to increase the safety of aviation through adaptive controllers, certification of non-deterministic controllers is still not possible. Jacklin presented the new certification guidelines of DO-178C (Jacklin S. A., 2012), while Romanski described the challenges of software certification as difficult even for deterministic software (Romanski, 2001). One of the main problems with the certification of autonomous systems is determining the level of autonomy. Clough presented a scale which could be used to determine the level of autonomy and criticality of flight controllers

(Clough, 2002).

Another problem in the certification of non-deterministic software is the lack of performance metrics. It is impossible to assess the margin of stability of a non-deterministic controllers in the same manner it is done for deterministic software. To address this issue, Stepanyan et al developed stability and performance metrics for adaptive flight controllers (Stepanyan, Krishnakumar, Nguyen, & Van Eykeren, 2009).

Instead of developing new performance metrics to certify non-deterministic flight controllers in the same manner as deterministic controllers, Galloway et al proposed the use of technology substitution for actual testing with the intent of lowering certification costs (Galloway, et al., 2005). For example, they proposed the use of theoretical proofs in lieu of flight test demonstrations. Rushby proposed a similar goal-oriented certification process, in which unconditional goals are proposed and the system is then certified based on its ability to achieve those goals (Rushby, 2007). While several teams, comprised of flight controller manufacturers and regulators, are trying to determine new methods for the certification of non-deterministic flight controllers, Gat presented an optimistic view on the future of non-deterministic software certification, claiming that all present certification issues can be solved using techniques that already exist (Gat, 2004).

### **3.3. Adaptive Robust Tracking with Disturbance Rejection**

The stability and convergence properties of the adaptive controller used in this investigation are divided, for simplicity, into four parts. First, the plant's and the adaptive controller's structures are defined. Second, *ideal trajectories* are defined that will lead to tracking of the reference model. Third, the existence and uniqueness of these ideal trajectories is demonstrated. Finally, an error system is defined between the plant and ideal

trajectories and stability and convergence for this system are proven. Regulation of the error system translates into the plant converging to the ideal trajectories and, thus, tracking the reference model. No knowledge of the plant is used, but general assumptions are noted when they are needed. The last subsection contains a summary of these assumptions.

### 3.3.1. Plant and Robust Direct Adaptive Controller Structure

Consider the linear plant given by:

$$\begin{aligned}\dot{x} &= Ax + Bu + \Gamma u_D; x(0) = x_0 \in \mathfrak{R}^N \\ y &= Cx\end{aligned}\tag{1}$$

where  $x(t) \in \mathfrak{R}^N$  is the plant state,  $u(t), y(t) \in \mathfrak{R}^M$  are the control input and plant output  $m$ -dimensional vectors respectively, and  $u_D(t)$  is a disturbance with known basis functions  $\phi_D(t)$ .

The control objective is for the plant output,  $y(t)$ , to robustly asymptotically track the output  $y_m(t)$  of a linear finite-dimensional Reference Model given by:

$$\begin{aligned}\dot{x}_m &= A_m x_m + B_m u_m; x_m(0) = x_0^m \\ y_m &= C_m x_m\end{aligned}\tag{2}$$

where the reference model state  $x_m(t)$  is an  $N_m$ -dimensional vector with reference model output  $y_m(t)$  of the same dimension as the plant output  $y(t)$ . While the plant and reference model outputs must be of the same dimension, the reference model does not need to be of the same dimension as the plant. The reference model parameters will be completely known. Robust asymptotic tracking means that the output error vector,  $e_y$ , tends to a predetermined neighborhood of the vector zero,  $N(0)$ , as time tends to infinity. That is:

$$e_y \equiv y - y_m \xrightarrow[t \rightarrow \infty]{} N(0)\tag{3}$$

The control objective will be accomplished by a direct adaptive control law of the form (Fuentes & Balas, 2000):

$$u = G_m x_m + G_u u_m + G_e e_y + G_D \phi_D \quad (4)$$

with adaptive gains given by:

$$\begin{aligned} \dot{G}_u &= -aG_u - e_y u_m^* \gamma_u; \gamma_u > 0 \\ \dot{G}_m &= -aG_m - e_y x_m^* \gamma_m; \gamma_m > 0 \\ \dot{G}_e &= -aG_e - e_y e_y^* \gamma_e; \gamma_e > 0 \\ \dot{G}_D &= -aG_D - e_y \phi_D^* \gamma_D; \gamma_D > 0 \end{aligned} \quad (5)$$

### 3.3.2. Ideal Trajectories

The *Ideal Trajectories* for the system in (1) are defined in the following way (Wen & Balas, 1989):

$$\begin{cases} x_* = S_{11}^* x_m + S_{12}^* u_m + S_{13}^* z_D = S_1 z \\ u_* = S_{21}^* x_m + S_{22}^* u_m + S_{23}^* z_D = S_2 z \end{cases} \quad \text{with } z \equiv \begin{bmatrix} x_m \\ u_m \\ z_D \end{bmatrix} \in \mathfrak{R}^L \quad (6)$$

Where the *ideal trajectory*  $x_*(t)$  is generated by the *ideal control*  $u_*(t)$  from:

$$\begin{aligned} \dot{x}_* &= Ax_* + Bu_* + \Gamma u_D \\ y_* &= Cx_* = y_m \end{aligned} \quad (7)$$

If the ideal trajectories can be shown to exist, they will produce exact output tracking in a disturbance-free plant (7).

Substituting (6) into (7) and grouping like terms yields the following linear *Model Matching Conditions*:

$$AS_{11}^* + BS_{21}^* = S_{11}^* A_m \quad (8)$$

$$AS_{12}^* + BS_{22}^* = S_{12}^* F_m + S_{11}^* B_m \quad (9)$$

$$CS_{11}^* = C_m \quad (10)$$

$$CS_{12}^* = 0 \quad (11)$$

$$AS_{13}^* + BS_{23}^* + \Gamma\theta = S_{13}^*F \quad (12)$$

$$CS_{13}^* = 0 \quad (13)$$

which can be rewritten as:

$$\begin{cases} AS_1 + BS_2 = S_1L_m + H_1 \\ CS_1 = H_2 \end{cases} \quad (14)$$

where  $S_1 \equiv [S_{11}^* \ S_{12}^* \ S_{13}^*]$ ,  $S_2 \equiv [S_{21}^* \ S_{22}^* \ S_{23}^*]$ ,  $H_1 \equiv [0 \ 0 \ -\Gamma\theta]$ ,

$$H_2 \equiv [C_m \ 0 \ 0], \text{ and } L_m \equiv \begin{bmatrix} A_m & B_m & 0 \\ 0 & F_m & 0 \\ 0 & 0 & F \end{bmatrix}.$$

The *Model Matching Conditions* are *necessary and sufficient* conditions for the existence of the ideal trajectories in the form of (6).

### 3.3.3. Existence and Uniqueness of the Ideal Trajectories

To prove the existence and uniqueness of the ideal trajectories, the first assumption on the plant is made:  $CB$  is nonsingular. For a Single-Input Single-Output (SISO) this translates to having non-zero high frequency gain. If  $CB$  is in fact nonsingular, then  $P_1 \equiv B(CB)^{-1}C$  is a non-orthogonal, bounded projection onto the range of  $B$ ,  $R(B)$ , along the nullspace of  $C$ ,  $N(C)$  with a complementary bounded projection  $P_2 \equiv I - P_1$ , and  $X = R(B) \oplus N(C)$  (Balas & Fuentes, 2004). Under these definitions, the following identities apply:

$$P_1x + P_2x = P_1x + (I - P_1)x = x \quad (15)$$

$$P_1^2 = B(CB)^{-1}CB(CB)^{-1}C = B(CB)^{-1}C = P_1 \quad (16)$$

$$P_2^2 = (1 - P_1)(1 - P_1) = 1 - 2P_1 + P_1^2 = 1 - P_1 = P_2 \quad (17)$$

$$\begin{aligned} (P_1AP_1)P_1x + (P_1AP_2)P_2x &= (P_1AP_1^2 + P_1AP_2^2)x = (P_1AP_1 + P_1AP_2)x \\ &= (P_1AP_1 + P_1A(1 - P_1))x \\ &= (P_1AP_1 + P_1A - P_1AP_1)x \\ &= P_1Ax \end{aligned} \quad (18)$$

$$\begin{aligned} (P_2AP_1)P_1x + (P_2AP_2)P_2x &= (P_2AP_1^2 + P_2AP_2^2)x = (P_2AP_1 + P_2AP_2)x \\ &= (P_2AP_1 + P_2A(1 - P_1))x \\ &= (P_2AP_1 + P_2A - P_2AP_1)x \\ &= P_2Ax \end{aligned} \quad (19)$$

$$P_1B = B(CB)^{-1}CB = B \quad (20)$$

$$CP_1x = CB(CB)^{-1}Cx = Cx = y \quad (21)$$

$$CP_2 = C(1 - P_1) = C - C(B(CB)^{-1}C) = 0 \quad (22)$$

$$P_2B = (1 - P_1)B = B - B(CB)^{-1}CB = 0 \quad (23)$$

Now, for the above pair  $(P_1, P_2)$ :

$$\begin{cases} \frac{dP_1x}{dt} = P_1\dot{x} = P_1Ax + P_1Bu \\ \frac{dP_2x}{dt} = P_2\dot{x} = P_2Ax + P_2Bu \\ y = Cx \end{cases} \quad (24)$$

Using the identities in (16) through (23), (24) can be rewritten as:

$$\begin{cases} \frac{dP_1x}{dt} = (P_1AP_1)P_1Ax + (P_1AP_2)P_2Ax + (P_1B)u \\ \frac{dP_2x}{dt} = (P_2AP_1)P_1Ax + (P_2AP_2)P_2Ax + (P_2B)u \\ y = Cx \end{cases} \quad (25)$$

If  $CB$  is nonsingular, then there exists an invertible, bounded linear operator  $W \equiv \begin{bmatrix} C \\ W_2^T P_2 \end{bmatrix}$ , where  $W_2$  forms an orthonormal basis for  $N(C)$ , such that  $\bar{B} \equiv WB = \begin{bmatrix} CB \\ 0 \end{bmatrix}$  and  $\bar{C} \equiv CW^{-1} = [I_m \quad 0]$  and  $\bar{A} \equiv WAW^{-1}$ . This coordinate transformation can be used to transform the system in (1) into *normal form* (Balas & Fuentes, 2004):

$$\begin{cases} \dot{y} = \bar{A}_{11}y + \bar{A}_{12}z_2 + CBu \\ \dot{z}_2 = \bar{A}_{21}y + \bar{A}_{22}z_2 \end{cases} \quad (26)$$

where the subsystem  $(\bar{A}_{22}, \bar{A}_{12}, \bar{A}_{21})$  are called the *zero dynamics* of (1), and the eigenvalues of the matrix  $\bar{A}_{22}$  are equal to the *transmission zeros* of  $(A, B, C)$  (Balas & Frost, 2016). The set of transmission zeros,  $Z$ , of  $(A, B, C)$  can be computed as shown below (Kailath, 1980):

$$Z = Z(A, B, C) \equiv \left\{ \lambda \mid V(\lambda) \equiv \begin{bmatrix} A - \lambda I & B \\ C & 0 \end{bmatrix} \text{ is singular} \right\} \quad (27)$$

The matching conditions in (14) can be pre-multiplied by  $W$ :

$$\begin{cases} WAS_1 + WBS - WH_1 = WS_1 L_m \\ CS_1 = H_2 \end{cases} \quad (28)$$

Since  $W^{-1}W = I$ , this can be rewritten as:

$$\begin{cases} WAW^{-1}WS_1 + WBS - WH_1 = WS_1 L_m = \bar{A}\bar{S}_1 + \bar{B}S_2 - \bar{H}_1 \\ CW^{-1}WS_1 = \bar{C}\bar{S}_1 = [I \quad 0]\bar{S}_1 = \bar{S}_a = H_2 \end{cases} \quad (29)$$

where  $\bar{S}_1 \equiv WS_1 = \begin{bmatrix} \bar{S}_a \\ \bar{S}_b \end{bmatrix}$  and  $\bar{H}_1 \equiv WH_1 = \begin{bmatrix} \bar{H}_a \\ \bar{H}_b \end{bmatrix}$ . The first matching condition can be

expressed as:

$$\begin{bmatrix} H_2 \\ \bar{S}_b \end{bmatrix} L_m = \begin{bmatrix} \bar{A}_{11} & \bar{A}_{12} \\ \bar{A}_{21} & \bar{A}_{22} \end{bmatrix} \begin{bmatrix} H_2 \\ \bar{S}_b \end{bmatrix} + \begin{bmatrix} CB \\ 0 \end{bmatrix} S_2 - \begin{bmatrix} \bar{H}_a \\ \bar{H}_b \end{bmatrix} \quad (30)$$

$$\begin{aligned} S_2 &= (CB)^{-1} \left[ H_2 L_m + \bar{H}_a - (\bar{A}_{11} H_2 + \bar{A}_{12} \bar{S}_b) \right] \\ \bar{S}_b L_m &= \bar{A}_{22} \bar{S}_b + (\bar{A}_{21} H_2 - \bar{H}_b) \end{aligned} \quad (31)$$

Equation (31) can be solved for a unique  $\bar{S}_b$  if and only if  $L_m$  does not share any eigenvalues with  $\bar{A}_{22}$  (Balas M. J., 1995). The solution of the matching conditions exists and is unique if the transmission zeros of  $(A, B, C)$  do not coincide with the eigenvalues of  $L_m$ . The eigenvalues of  $L_m$  are the union of the eigenvalues of  $A_m$ ,  $F_m$  and  $F$ .

### 3.3.4. Stability of the Error System

The error between the plant in (1) and the ideal trajectories in (7) can be defined by  $e \equiv x - x_*$  and  $\Delta u = u - u_*$ . The error system can then be defined as:

$$\begin{cases} \dot{e} = Ae + B\Delta u + v \\ e_y = y - y_m = y - y_* = Ce \end{cases} \quad (32)$$

where  $v$  is a vector of bounded disturbances. The system  $(A_c, B, C)$  is said to be *Strictly Dissipative (SD)* if  $A_c \equiv A + BG_*C$  and there exist symmetric positive bounded operators  $P$  and  $Q$  on  $X$  such that  $0 \leq p_{\min} \|e\|^2 \leq (Pe, e) \leq p_{\max} \|e\|^2$ ;  $0 \leq q_{\min} \|e\|^2 \leq (Qe, e) \leq q_{\max} \|e\|^2$  and

$$\begin{cases} \operatorname{Re}(PA_c e, e) \equiv \frac{1}{2} \left[ (PA_c e, e) + \overline{(PA_c e, e)} \right] = \frac{1}{2} \left[ (PA_c e, e) + (e, PA_c e) \right] \\ \quad = -(Qe, e) \leq -q_{\min} \|e\|^2 \\ PB = C^* \end{cases} \quad (33)$$

The system  $(A, B, C)$  is *almost strictly dissipative (ASD)* if there exists a gain  $G_* \in \mathfrak{R}^{m \times m}$  such that  $(A_c, B, C)$  is SD with  $A_c \equiv A + BG_*C$ . The following assumptions on the plant are needed: the plant  $(A, B, C)$  is ASD, and the disturbance basis  $\phi_D$  is bounded.

Substituting (4) for  $u$  and (6) for  $u_*$  into  $\Delta u = u - u_*$  yields:

$$\begin{aligned}\Delta u = u - u_* &= (G_m x_m + G_u u_m + G_e e_y + G_D \phi_D) - (S_{21}^* x_m + S_{22}^* u_m + S_{23}^* z_D) \\ &= G_e^* e_y + \Delta G_e e_y + [\Delta G_m \quad \Delta G_u \quad \Delta G_D] \begin{bmatrix} x_m \\ u_m \\ \phi_D \end{bmatrix} = G_e^* e_y + \Delta G \eta\end{aligned}\quad (34)$$

where  $\Delta G \equiv G - G_*$ ;  $G \equiv [G_e \quad G_m \quad G_u \quad G_D]$ ;  $G_* \equiv [G_e^* \quad S_{21}^* \quad S_{22}^* \quad S_{23}^* L]$ ; and  $\eta \equiv [e_y \quad x_m \quad u_m \quad \phi_D]^T$ . The error system then becomes:

$$\begin{cases} \dot{e} = (A + BG_e^* C)e + B\Delta G\eta + v = A_c e + B\rho + v; v \equiv \Delta G\eta \\ e_y = Ce \\ \Delta \dot{G} = \dot{G} - \dot{G}_* = -e_y \eta^* \gamma; \gamma \equiv \begin{bmatrix} \gamma_e & 0 & 0 & 0 \\ 0 & \gamma_m & 0 & 0 \\ 0 & 0 & \gamma_u & 0 \\ 0 & 0 & 0 & \gamma_D \end{bmatrix} \end{cases}\quad (35)$$

where  $\begin{bmatrix} e \\ G \end{bmatrix} \in \Re^N \mathcal{X} \Re^{mxm}$  is a Hilbert space with inner product

$$\left( \begin{bmatrix} e_1 \\ G_1 \end{bmatrix}, \begin{bmatrix} e_2 \\ G_2 \end{bmatrix} \right) \equiv (e_1, e_2) + \text{tr}(G_1 \gamma^{-1} G_2), \quad \text{norm} \quad \left\| \begin{bmatrix} e \\ G \end{bmatrix} \right\| \equiv (\|e\|^2 + \text{tr}(G \gamma^{-1} G))^{1/2} \quad \text{and}$$

where  $G(t)$  is the  $mxm$  adaptive gain matrix, and  $\gamma$  is any positive definite constant matrix.

Using  $\|M\|_2 \equiv \sqrt{\text{tr}(M \gamma^{-1} M^T)}$  as the trace of a matrix  $M$  where  $\gamma > 0$  and assuming the following:

- i.  $(A, B, C)$  is ASD with  $A_c \equiv A + BG_* C$
- ii. There exists  $M_G > 0$  such that  $\sqrt{\text{tr}(G^* G^{*T})} \leq M_G$
- iii. There exists  $M_v > 0$  such that  $\sup_{t \geq 0} \|v(t)\| \leq M_v < \infty$

- iv. There exists  $a > 0$  such that  $a \leq \frac{q_{min}}{p_{max}}$
- v. The positive definite matrix  $\gamma$  satisfies  $tr(\gamma^{-1}) \leq \left(\frac{M_v}{aM_G}\right)^2$

then the *Robust Stabilization Theorem* (Balas & Frost, 2014) states that for the system in (35), the gain matrix,  $G(t)$ , is bounded, and the state  $e(t)$  exponentially, with rate  $e^{-at}$ , approaches the ball of radius:

$$R_* \equiv \frac{(1 + \sqrt{p_{max}})}{a\sqrt{p_{min}}} M_v \quad (36)$$

The proof of the Robust Stabilization Theorem can be found in Appendix A.

### 3.3.5. Summary of Assumptions

The following assumptions regarding the plant were made in the stability proof of the Robust Direct Adaptive Controller:

- i. The plant  $(A, B, C)$  is ASD
- ii.  $CB$  is nonsingular
- iii. The model input  $u_m$  is bounded
- iv. The disturbance vector  $v$  is bounded

Assumptions i and ii are required to ensure that the energy of the system will be dissipated. Assumption iii requires that the input to the reference model is bounded. With unbounded reference model input, even if the plant tracks the model perfectly, both the model and the plant would be unbounded. Similarly, with an unbounded disturbance vector, the plant states would automatically be unbounded.

### 3.4. Sensor Blending

If the system of interest is not minimum phase or has a nonzero high frequency gain, sensor blending can be used. Sensor blending consists of creating a linear combination of two or more of the system states in such a way that the resulting blended output is minimum phase and nonzero high frequency gain. This means adjusting the coefficients of the output matrix,  $C$ , in order to obtain the desired properties. The following sections describe the sensor blending process.

#### 3.4.1. Sensor Blending for a Single-Input-Single-Output System

For a SISO system, a coordinate transformation can be used to compute the required output matrix that will make the output minimum phase and nonzero high frequency gain (Hartman, 2011). The state space system in (1) can be transformed to controllable canonical form through a coordinate transformation,  $T$ . First, the controllability matrix,  $H$ , is computed:

$$H = \begin{bmatrix} B & A^1 B & A^2 B & A^3 B & \cdots & A^{n-1} B \end{bmatrix} \quad (37)$$

$$\tilde{A} = \begin{bmatrix} 0 & 0 & -a_0 \\ 1 & \vdots & \vdots \\ 0 & 1 & -a_n \end{bmatrix} \quad (38)$$

$$\bar{A} = \tilde{A}^T \quad (39)$$

$$\bar{B} = \begin{bmatrix} 0 & \cdots & 1 \end{bmatrix}^T \quad (40)$$

Then, the new controllability matrix,  $\bar{H}$ , can be computed:

$$\bar{H} = \begin{bmatrix} \bar{B} & \bar{A}^1 \bar{B} & \bar{A}^2 \bar{B} & \bar{A}^3 \bar{B} & \cdots & \bar{A}^{n-1} \bar{B} \end{bmatrix} \quad (41)$$

The coordinate transformation matrix,  $T$ , that will place the system in the desired

form can then be computed as:

$$T = H\bar{H}^{-1} \quad (42)$$

The new output matrix,  $\bar{C}$ , is computed by:

$$\bar{C} = CT = [\bar{c}_o \quad \bar{c}_1 \quad \cdots \quad \bar{c}_{n-1}] \quad (43)$$

The new output matrix,  $\bar{C}$ , contains the coefficients of the transfer function that describes the system as shown below:

$$P(s) = \frac{n(s)}{d(s)} = \frac{\bar{c}_0 + \bar{c}_1 s + \cdots + \bar{c}_{n-1} s^{n-1}}{a_0 + a_1 s + \cdots + a_{n-1} s^{n-1} + s^n} \quad (44)$$

The numerator coefficients can be factored as follows:

$$(s + z_1)(s + z_2)(s - z_p) \cdots (s + z_{n-1}) \quad (45)$$

Any problematic zeros,  $z_p$ , can be modified to be minimum phase (Aditya, Balas, & Doman, 2016). It is desirable to modify the zero locations enough to make the output minimum phase, while leaving the output as close to the original output as possible and maintaining a nonzero high frequency gain. The polynomial is then expanded to obtain the blended output matrix in canonical controllable form,  $\bar{C}_b$ :

$$\bar{C}_b = [\bar{c}_{b0} \quad \bar{c}_{b1} \quad \cdots \quad \bar{c}_{b(n-1)}] \quad (46)$$

This matrix is then transformed back to the original system coordinates to obtain:

$$C_b = \bar{C}_b T^{-1} \quad (47)$$

If the new blended output matrix,  $C_b$ , is used instead of the original  $C$  matrix, the system will have the modified zeros. This sensor blending method provides an intuitive understanding of the blending process for the SISO case. When applied to Multi-Input-Multi-Output (MIMO), the zeros of interest are the transmission zeros, and this process can

be tedious. Balas and Frost presented a systematic approach to sensor blending that works for both SISO and MIMO plants (Balas & Frost, 2017). The following subsection describes this process.

### 3.4.2. Sensor Blending for a Multi-Input-Multi-Output System

A systematic approach to sensor blending was developed by Balas and Frost (Balas & Frost, 2017). This approach uses the fact that in normal form, the eigenvalues of the  $\bar{A}_{22}$  matrix are the transmission zeros of the plant. The approach then converts the sensor blending process into an eigenvalue placement process. It begins by expressing the output matrix as the sum of the original output matrix and a blending matrix:

$$C_b = C + \Delta C \quad (48)$$

If  $CB$  is nonsingular, the system is transformed into normal form through a coordinate transformation,  $W$ . The output matrix is transformed as shown:

$$C_b W^{-1} = (C + \Delta C) W^{-1} = C W^{-1} + \Delta C W^{-1} \quad (49)$$

$$\bar{C}_b = \bar{C} + \Delta \bar{C} \quad (50)$$

The  $\Delta \bar{C}$  matrix is then split into two matrices:

$$\Delta \bar{C} = \begin{bmatrix} \Delta \bar{C}_1 & \Delta \bar{C}_2 \end{bmatrix} \quad (51)$$

Where  $\Delta \bar{C}_1$  consists of the first column and  $\Delta \bar{C}_2$  consists of  $n - 1$  columns, where  $n$  is the number of states in the plant. Theorem 6 in (Balas & Frost, 2017) shows that if the pair  $(\bar{A}_{22}, \bar{A}_{21})$  is controllable, then there exists a matrix  $\Delta \bar{C}_2$  so that the eigenvalues of  $(\bar{A}_{22} - \bar{A}_{21} \Delta \bar{C}_2)$  are all stable and that those eigenvalues are the transmission zeros of the plant when the new output matrix  $C_b$  is used. This means that the matrix  $\Delta \bar{C}_2$  can be chosen to place the eigenvalues in a desired stable location. The  $\Delta \bar{C}_2$  matrix can then be

transformed back to original coordinates to obtain the blending matrix:

$$\Delta C = \Delta \bar{C} W \quad (52)$$

If the blended output matrix,  $C_b = C + \Delta C$ , is used then the transmission zeros of the plant will be the same as the eigenvalues of the matrix  $(\bar{A}_{22} - \bar{A}_{21}\Delta\bar{C}_2)$ , which were placed at a desired stable location. The process is taken further in the reference by writing  $\bar{A}_{22}$  in Jordan form to separate the stable and unstable eigenvalues. The blending is then performed only on the unstable zeros, minimizing the amount of blending that needs to be included. This concludes the systematic blending process.

## 4. Methodology

This section describes the process used to design a generic autopilot capable of controlling different GA aircraft without modification. The autopilot was designed and implemented using a high fidelity simulator of a representative GA aircraft: a Cirrus SR22. The autopilot was then tested for performance and functionality. The final step was to transfer the autopilot, without modifications, into a second high fidelity simulator of a different GA aircraft, a Ryan Navion. The performance and functionality tests were repeated on the new aircraft. Additionally, all stability assumptions were checked to make sure they were still valid on the new aircraft. The following subsections describe the simulation environment used, the architecture of each of the autopilot components, and the test cases used in this investigation.

### 4.1. Aircraft Notation and Sign Conventions

The following notation and sign conventions have been used throughout this investigation. Figure 4.1 shows the aircraft body coordinate system along with aircraft forces, moments, linear velocities, linear accelerations, and angular rates defined in that coordinate system. The longitudinal axis,  $X$ , is positive through the nose of the aircraft. The lateral axis,  $Y$ , is positive through the right wing. The vertical axis,  $Z$ , is positive through the bottom of the aircraft. Table 4.1 lists the notation used for these parameters as well as the sign conventions.

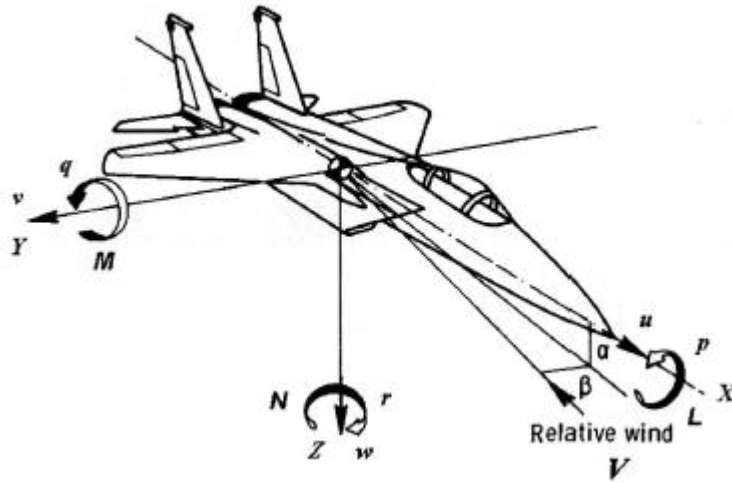


Figure 4.1. Aircraft body axes notation (Klein &amp; Morelli, 2006).

Table 4.1. Aircraft body axes variable notation.

Axis Name	Axis Designation	Physical Quantity	Variable Symbol	Positive
Longitudinal	X	Force	$X$	Forward
		Moment	$L$	Right wing down
		Angular Disp.	$\phi$	Right wing down
		Angular Rate	$p$	Rolling right
		Velocity	$u$	Forward
		Acceleration	$a_x$	Forward
		Force	$Y$	To the right
Lateral	Y	Moment	$M$	Nose up
		Angular Disp.	$\theta$	Nose up
		Angular Rate	$q$	Pitching up
		Velocity	$v$	To the right
		Acceleration	$a_y$	To the right
		Force	$Z$	Down
		Moment	$N$	Nose Right
Vertical	Z	Angular Disp.	$\psi$	Nose Right
		Angular Rate	$r$	Yawing right
		Velocity	$w$	Down
		Acceleration	$a_z$	Down

Control surface deflections have been defined as positive when they generate a negative moment. This means that a down elevator deflection, right aileron down, and left rudder deflection are all positive deflections. Figure 4.2 shows positive control deflections.

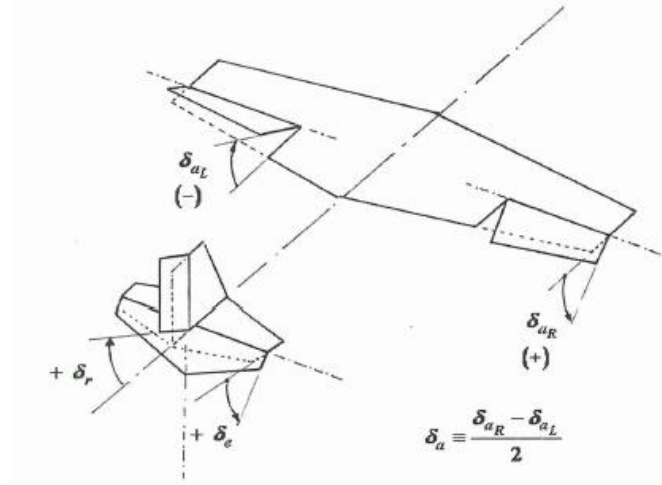


Figure 4.2. Control surface deflection sign convention (Klein & Morelli, 2006).

The velocity and orientation of the relative wind with respect to the aircraft body axes are defined as true airspeed,  $V_{TAS}$ , angle of attack,  $\alpha$ , for the longitudinal angle and sideslip angle,  $\beta$ , for the lateral angle. A positive angle of attack occurs when the relative wind is under the aircraft's longitudinal axis. A positive sideslip angle is defined as the relative wind to the right of the longitudinal axis.

Due to the short duration of the test cases and the low speed of GA aircraft, a flat Earth navigation model was used. The aircraft's displacement to the north of the starting point is represented by  $N$ . The east displacement is represented by  $E$ . The altitude above ground level is represented by  $h$ .

The orientation of the body axes with respect to an Earth fixed frame is defined using Euler angles. The Euler angles are the bank angle,  $\phi$ , for the lateral angle, pitch angle,  $\theta$ , for the longitudinal axis, and the yaw or heading angle,  $\psi$ , for the directional angle. Positive angles are right wing down for bank, nose up for pitch, and nose to the right for yaw. Figure 4.3 shows the orientation of these angles.

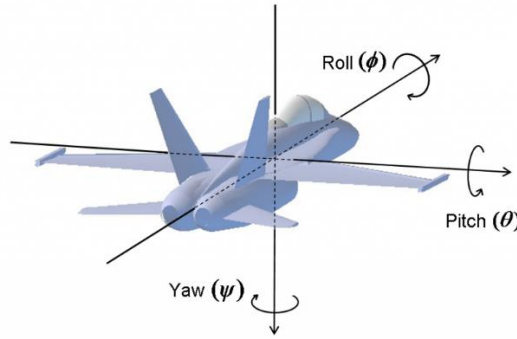


Figure 4.3. Sign convention of the Euler angles (CH Robotics, n.d.).

## 4.2. General Aviation Aircraft Considerations

In order to retain the stability arguments presented in the previous chapter, all assumptions made must be met. GA aircraft of conventional configuration, where the horizontal tail is aft of the center of gravity, do not readily meet all of the assumptions. These type of aircraft are non-minimum phase because the lift of the horizontal tail is in the opposite direction of the intended motion. For example, lowering the altitude of the aircraft would require a positive elevator deflection (down). This deflection would result in an increase of the total lift of the vehicle, leading to a positive acceleration. The aircraft then initially has an upward acceleration before the intended effect takes place. To overcome this, sensor blending was used. The following subsection describes the process used to ensure that the aircraft met all adaptive control assumptions.

### 4.2.1. Selection of the Blending Variables

After the sensor blending process is completed, the blended output will be minimum phase and nonzero high frequency gain. However, the blended output is no longer equal to the original output of interest. This is not a problem if the adaptive controller is being used as a regulator. If the plant states are being driven to zero, any linear

combination of the plant states will also be zero. If the adaptive controller is being used to track a nonzero reference, this could be a problem. The adaptive controller will drive the plant states towards the ideal trajectories. Unlike the regulator case, the ideal trajectories will be modified by the sensor blending. In the tracking case it is highly desirable to choose the blending variables in such a way that the resulting ideal trajectories are equivalent to the original ideal trajectories. If the ideal trajectories remain nearly unchanged by the sensor blending, the original output will still track the reference model even though the blended output is driving the adaptive controller. To select the blending variables that will not have a long term effect on the ideal trajectories, start by defining the blended output,  $C_b$ , as a combination of original output,  $C$ , and a  $\Delta C$  of output candidates that could be used to meet the adaptive control requirements:

$$C_b = C + \Delta C \quad (53)$$

The ideal trajectories in (14) can be simplified, for a disturbance-free case in which the model is a series of steps, into:

$$\begin{cases} AS_1 + BS_2 = 0 \\ C_b S_1 = (C + \Delta C) S_1 = [I \quad 0] \end{cases} \quad (54)$$

If  $A$  is invertible, then the top equation in (54) can be solved for  $S_1$  as shown:

$$S_1 = -A^{-1}BS_2 \quad (55)$$

Substituting (55) into the bottom equation in (54) yields:

$$(C + \Delta C)(-A^{-1}BS_2) = [I \quad 0] \quad (56)$$

Regrouping this expression yields:

$$-CA^{-1}BS_2 - \Delta CA^{-1}BS_2 = [I \quad 0] \quad (57)$$

If the entries of the  $\Delta C$  matrix are chosen so that the  $-\Delta CA^{-1}B$  term is zero, the

ideal trajectories will not be affected by the sensor blending, and the *original* output will track a nonzero reference. If the  $A$  and  $B$  matrices are known,  $\Delta C$  can be chosen so that  $\Delta C A^{-1} B$  is zero using all entries of  $\Delta C$ . If the specific entries of  $A$  and  $B$  are not known but their *structure* is known, the use of  $\Delta C$  entries can be limited to those entries that correspond to a zero entry in the product  $A^{-1} B$ . Note that the term  $-CA^{-1}B$  can be used to compute the DC gain of the transfer function :

$$P(s) = C(sI - A)^{-1} B \quad (58)$$

This means that states whose transfer functions have a zero DC gain will have a zero entry in their corresponding row of  $A^{-1} B$ . If the selection of  $\Delta C$  entries is limited to only the states that have a zero DC gain, the product  $\Delta C A^{-1} B$  will always be zero, regardless of the numerical value chosen for the entry of  $\Delta C$ . If those entries are enough to make the output minimum phase and nonzero high frequency gain, the original output will track the nonzero reference.

After the entries of  $\Delta C$  that have a zero DC gain have been identified, they can be used to place restrictions on  $\Delta \bar{C}$  in normal form. The entries in  $\Delta \bar{C}$  must be chosen so that after they are transformed back to the original coordinates, the only nonzero entries are the ones corresponding to the states that have a zero DC gain:

$$\Delta C = \Delta \bar{C} W \quad (59)$$

The  $W$  matrix depends only on the  $C$  and  $B$  matrices, so detailed knowledge of the dynamics of the system is not needed. If the blending variables are chosen this way, the original output will track the nonzero reference with no steady state error. The following sections demonstrate this process applied specifically to aircraft dynamics.

### 4.2.2. Longitudinal Linear Model of an Aircraft

The longitudinal linear model of an aircraft  $A$  matrix in terms of forward velocity,  $u$ , vertical velocity,  $w$ , pitch rate,  $q$ , and pitch angle,  $\theta$ , in state space form is given by Nelson (Nelson, 1998):

$$x = [u \quad w \quad q \quad \theta]^T \quad (60)$$

$$A = \begin{bmatrix} X_u & X_w & 0 & -g \\ Z_u & Z_w & u_0 & 0 \\ M_u + M_{\dot{w}}Z_u & M_w + M_{\dot{w}}Z_w & M_q + M_{\dot{w}}u_0 & 0 \\ 0 & 0 & 1 & 0 \end{bmatrix} \quad (61)$$

The  $B$  matrix is given by:

$$B = \begin{bmatrix} X_{\delta_e} \\ Z_{\delta_e} \\ M_{\delta_e} + M_{\dot{w}}Z_{\delta_e} \\ 0 \end{bmatrix} \quad (62)$$

The  $C$  matrix for the pitch angle to be the output is given by:

$$C = [0 \quad 0 \quad 0 \quad 1] \quad (63)$$

Adding an elevator actuator with damping ratio,  $\zeta_{\delta_e}$ , and natural frequency,  $\omega_{\delta_e}$ , yields the following matrices:

$$x = [\delta_e \quad \dot{\delta}_e \quad u \quad w \quad q \quad \theta]^T \quad (64)$$

$$A = \begin{bmatrix} 0 & 1 & 0 & 0 & 0 & 0 \\ -\omega_{\delta_e}^2 & -2\zeta_{\delta_e}\omega_{\delta_e} & 0 & 0 & 0 & 0 \\ X_{\delta_e} & 0 & X_u & X_w & 0 & -g \\ Z_{\delta_e} & 0 & Z_u & Z_w & u_0 & 0 \\ M_{\delta_e} + M_{\dot{w}}Z_{\delta_e} & 0 & M_u + M_{\dot{w}}Z_u & M_q + M_{\dot{w}}Z_w & M_q + M_{\dot{w}}u_0 & 0 \\ 0 & 0 & 0 & 0 & 1 & 0 \end{bmatrix} \quad (65)$$

$$B = [0 \quad \omega_{\delta_e}^2 \quad 0 \quad 0 \quad 0 \quad 0]^T \quad (66)$$

$$C = [0 \quad 0 \quad 0 \quad 0 \quad 0 \quad 1] \quad (67)$$

It can be seen that the system has a zero high frequency gain. Some sensor blending is required. The state variable of interest is the pitch angle. Define the blended variable candidates as:

$$\Delta C = [\Delta c_0 \quad \Delta c_1 \quad \Delta c_2 \quad \Delta c_3 \quad \Delta c_4 \quad \Delta c_5] \quad (68)$$

To determine what entries of  $\Delta C$  can be nonzero and still have the product  $\Delta C A^{-1} B$  be zero, compute  $A^{-1} B$ :

$$A^{-1} B = \begin{bmatrix} -1 \\ 0 \\ -\frac{(M_w Z_{\delta} - Z_w M_{\delta})}{(M_u Z_w - M_w Z_u)} \\ \frac{(M_u Z_{\delta} - Z_u M_{\delta})}{(M_u Z_w - M_w Z_u)} \\ 0 \\ \frac{(M_u X_w Z_{\delta} - M_u Z_w X_{\delta} - M_w X_u Z_{\delta} + M_w Z_u X_{\delta} + X_u Z_w M_{\delta} - X_w Z_u M_{\delta})}{g(M_u Z_w - M_w Z_u)} \end{bmatrix} \quad (69)$$

If the entries  $\Delta c_1$  and  $\Delta c_4$  are used to make the output minimum phase and nonzero high frequency gain, the blended output will track the original output at low frequencies.

These states correspond to the actuator rate,  $\dot{\delta}_e$ , and the aircraft's pitch rate,  $q$ , respectively. This means that the blended output will be a linear combination of the pitch angle, the pitch rate, and the elevator rate.

#### 4.2.3. Lateral-Directional Linear Model of an Aircraft

The lateral-directional linear model of an aircraft A matrix is given in terms of sideslip angle,  $\beta$ , roll rate,  $p$ , yaw rate,  $r$ , and bank angle,  $\phi$ , by (Nelson, 1998):

$$x = [\beta \quad \phi \quad p \quad r]^T \quad (70)$$

$$A = \begin{bmatrix} \frac{Y_\beta}{u_0} & \frac{Y_p}{u_0} & \frac{Y_r}{u_0} - 1 & \frac{g \cos(\theta_0)}{u_0} \\ L_\beta & L_p & L_r & 0 \\ N_\beta & N_p & N_r & 0 \\ 0 & 1 & 0 & 0 \end{bmatrix} \quad (71)$$

The  $B$  matrix is given by:

$$B = \begin{bmatrix} 0 \\ L_{\delta_a} \\ N_{\delta_a} \\ 0 \end{bmatrix} \quad (72)$$

The  $C$  matrix for a bank angle output is given by:

$$C = [0 \quad 0 \quad 0 \quad 1] \quad (73)$$

Adding a second order aileron actuator with damping ratio,  $\zeta_{\delta_a}$ , and natural frequency,  $\omega_{\delta_a}$ , yields the following matrices:

$$x = [\delta_a \quad \dot{\delta}_a \quad \beta \quad \phi \quad p \quad r]^T \quad (74)$$

$$A = \begin{bmatrix} 0 & 1 & 0 & 0 & 0 & 0 \\ -\omega_{\delta_a}^2 & -2\zeta_{\delta_a}\omega_{\delta_a} & 0 & 0 & 0 & 0 \\ 0 & 0 & \frac{Y_\beta}{u_0} & \frac{Y_p}{u_0} & \frac{Y_r}{u_0} - 1 & \frac{g \cos(\theta_0)}{u_0} \\ L_{\delta_a} & 0 & L_\beta & L_p & L_r & 0 \\ N_{\delta_a} & 0 & N_\beta & N_p & N_r & 0 \\ 0 & 0 & 0 & 1 & 0 & 0 \end{bmatrix} \quad (75)$$

$$B = \begin{bmatrix} 0 & \omega_{\delta_a}^2 & 0 & 0 & 0 & 0 \end{bmatrix}^T \quad (76)$$

$$C = \begin{bmatrix} 0 & 0 & 0 & 0 & 0 & 1 \end{bmatrix} \quad (77)$$

It can be seen that the system has a zero high frequency gain. Some sensor blending is required. The state variable of interest is the bank angle. Define the blended variable candidates as:

$$\Delta C = \begin{bmatrix} \Delta c_0 & \Delta c_1 & \Delta c_2 & \Delta c_3 & \Delta c_4 & \Delta c_5 \end{bmatrix} \quad (78)$$

To determine what entries of  $\Delta C$  can be nonzero and still have the product  $\Delta C A^{-1} B$  be zero, compute  $A^{-1} B$ :

$$A^{-1} B = \begin{bmatrix} -1 \\ 0 \\ -\frac{(L_r N_{\delta_a} - N_r L_{\delta_a})}{(L_\beta N_r - L_r N_\beta)} \\ 0 \\ \frac{(L_\beta N_{\delta_a} - N_\beta L_{\delta_a})}{(L_\beta N_r - L_r N_\beta)} \\ -\frac{(L_\beta Y_r N_{\delta_a} - L_\beta u_0 N_{\delta_a} - L_r Y_\beta N_{\delta_a} - N_\beta Y_r L_{\delta_a} + N_\beta u_0 L_{\delta_a} + N_r Y_\beta L_{\delta_a})}{(L_\beta N_r - L_r N_\beta) g \cos(\theta_0)} \end{bmatrix} \quad (79)$$

If the entries  $\Delta c_1$  and  $\Delta c_4$  are used to make the output minimum phase and nonzero

high frequency gain, the blended output will track the original output at low frequencies. These entries correspond to the aileron rate,  $\dot{\delta}_a$ , and the roll rate,  $p$ , respectively. This means that the blended output will be a combination of bank angle, roll rate, and aileron rate.

### 4.3. Simulation Environment

The aircraft model used for designing and testing the autopilot was a high fidelity non-linear simulator of a Cirrus SR22. The aircraft is a high performance single-engine, fixed-gear aircraft with a gross takeoff weight of 3,600 lb. Figure 4.4 shows an image of the aircraft in flight.



Figure 4.4. Cirrus SR22 in flight.

The aerodynamic database was obtained through a flight test program and model identification performed by the Eagle Flight Research Center at Embry-Riddle Aeronautical University. The model is implemented in The Mathwork Inc.'s MATLAB<sup>®</sup>/Simulink<sup>®</sup> and includes non-linear regions such as stall, different flap

configurations, and transitions between configurations. In addition, the model has been validated against FAA Part 60 tests. Figure 4.5 shows a plot of the principal stability derivatives of the model. The aircraft model runs in Simulink at 1000 Hz.

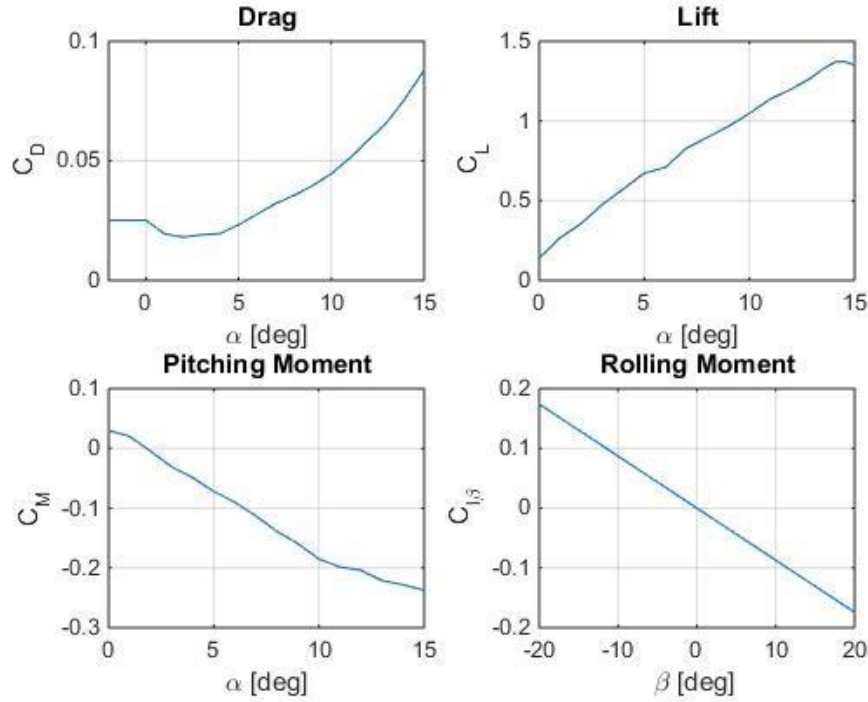


Figure 4.5. Stability derivatives of the SR22 model used.

#### 4.3.1. Sensor Models

The sensors were modeled as second order systems based on representative sensors found in (Berger T. , Tischler, Hagerott, Gangsaas, & Saeed, 2012). Air data sensors had a natural frequency of 4.8 rad/s and a damping ratio of one. Angular rates and attitude angles sensors had a natural frequency of 25 rad/s. All sensors had a damping ratio of 1. Random noise was introduced into all of the sensors. Table 4.2 shows the natural frequency and the amount of random noise used for each of the sensors. The amount of random noise was selected in order to create a realistic sensor package comparable with commercial-grade hardware currently available for GA aircraft.

Table 4.2. Natural frequency and random noise of each sensor.

Sensor	Natural Frequency ( <i>rad/s</i> )	Random Noise	Units
$V_{TAS}$	4.8	1	kts
$h$	50	5	ft
$\phi$	25	1	deg
$\theta$	25	1	deg
$\psi$	25	2	deg
$p$	25	0.1	deg/s
$q$	25	0.1	deg/s

#### 4.3.2. Actuator Models

The actuators were modeled as second order systems based on representative actuators found in (Berger T. , Tischler, Hagerott, Gangsaas, & Saeed, 2012). They have a natural frequency of 22.6 rad/s and a damping ratio of 0.7. The limits for the actuators were obtained from the aircraft's type certificate data sheet. The elevator limits are 25 degrees up and 15 degrees down. The ailerons limits are 12 degrees up and 13 degrees down. Random noise was introduced into the actuator commands. Random noise of 0.5 degrees was introduced into the actuators.

#### 4.3.3. Atmospheric Disturbances

The Dryden Wind Turbulence Model was used to generate atmospheric disturbances. In this model, turbulence is created by passing band-limited white noise through forming filters. The model is based on the mathematical representation in the Military Specification (MIL-SPEC) MIL-F-8785C, and it produces linear wind turbulence as well as rotational components. A detailed explanation of this process can be found in (Beal, 1993). The turbulence level was chosen as moderate based on the autopilot assumptions presented in Section 2. Wind gusts based on the same MIL-SPEC were also

included in the model as persistent disturbances. The gusts are comprised of both linear wind velocities  $(u, v, w)$  and rotational rates  $(p, q, r)$ . This atmospheric turbulence model was chosen because it is one of the two most accepted atmospheric turbulence models in the aviation industry. The von Karman model is usually used for structural analysis, and the Dryden model is most often used for simulating atmospheric turbulence in real-time (Ercole, Cardullo, Kelly, & Houck, 2012).

#### **4.4. Autopilot Architecture**

The autopilot was designed to be equivalent in hardware, capabilities, and performance to current GA autopilots. The autopilot is a two-axis system (roll and pitch). The pilot is responsible for manually operating the rudder, to maintain coordinated flight, and the throttle to apply appropriate power for climbs and descents. The pilot is also responsible for deploying the flaps and/or landing gear when required. Unlike current GA autopilots, the adaptive autopilot does not need sensors to detect the current aircraft configuration. Any changes in the aircraft dynamics due to deployment of flaps and/or landing gear is handled by the adaptive component of the autopilot.

The autopilot can operate in the same modes available in the popular Genesys Aerosystems 55X autopilot. These modes are heading tracking, GPS navigation, approach, altitude hold, and vertical speed tracking. Because the GPS navigation mode makes use of heading tracking, altitude hold, and vertical speed tracking, only the GPS navigation and approach modes were tested.

The autopilot was designed by separating the longitudinal and lateral controllers. The longitudinal controller provides altitude tracking, and the lateral controller provides bank angle tracking. A separate navigational controller provides the required bank and

altitude commands for three-dimensional navigation. An airspeed controller that simulates the pilot operating the throttle to maintain a desired airspeed is also included in the navigation controller.

#### 4.4.1. Longitudinal Controller

The primary objective of the longitudinal autopilot is to control the aircraft's altitude. To accomplish this, two conventional controllers and an adaptive controller were connected in series. In this architecture, altitude is tracked through vertical speed with the use of a Proportional-Integral-Controller (PID) controller. Vertical speed is tracked through pitch angle by means of a PID controller. The pitch angle is tracked using a direct model reference adaptive controller. Figure 4.6 shows the control architecture used.

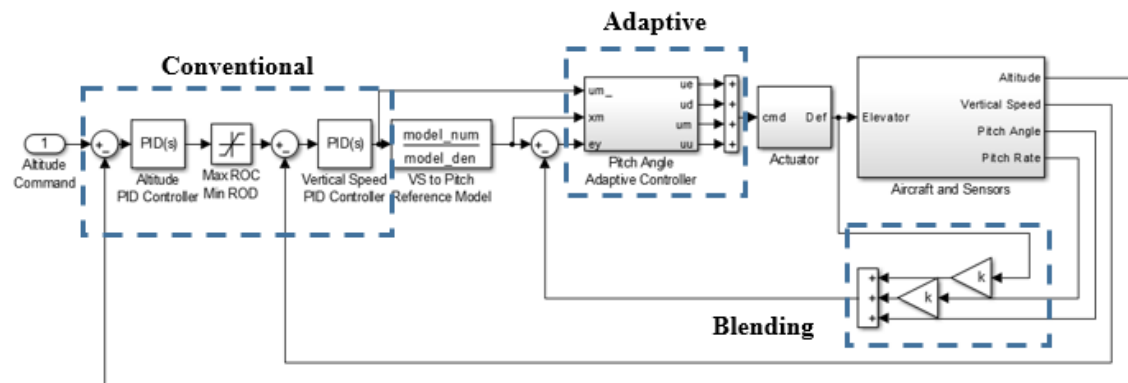


Figure 4.6. Longitudinal controller architecture.

The conventional outer-loop controllers were tuned to control the pitch reference model. This way, the outer loop does not need to be tuned for every make and model of aircraft. The adaptive controller then drives the unknown plant to track the reference model. This allows for a variety of aircraft to be controlled by the same controller as long as the assumptions derived within Section 3 are met.

#### 4.4.2. Lateral Controller

The primary objective of the lateral controller is to track a bank angle command. To achieve this, a conventional controller and a direct model reference adaptive controller were used in series. In this architecture, heading is controlled through rate of turn in the conventional controller. The desired rate of turn is converted to required bank angle using the equations of motion. The desired bank angle is then tracked by the direct model reference adaptive controller. Figure 4.7 shows the control architecture used.

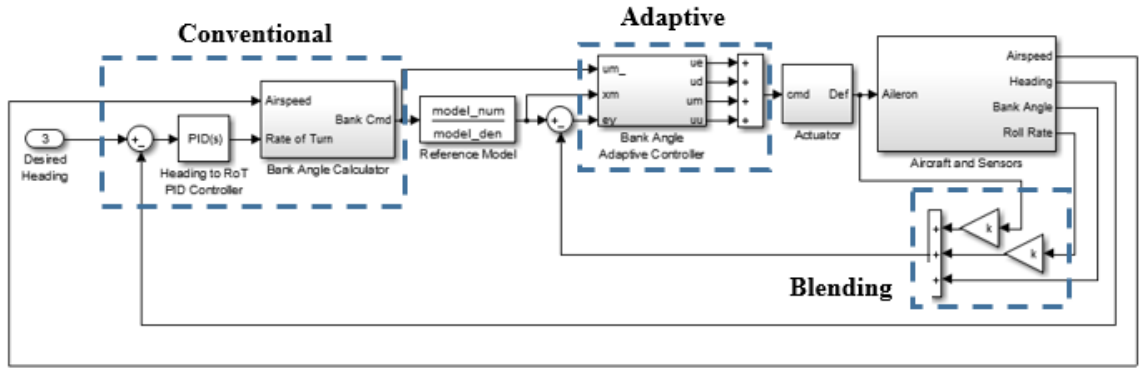


Figure 4.7. Lateral controller architecture.

The conventional outer-loop controller was tuned to the bank angle reference model. The conversion between desired rate of turn and desired bank angle,  $\phi_D$ , in radians, is done using (Monteiro, n.d.):

$$\phi_D = \tan^{-1} \left( \frac{(RoT)(TAS)}{g} \right) \quad (80)$$

where  $RoT$  is the desired rate of turn,  $TAS$  is the true airspeed, and  $g$  is the acceleration due to gravity. This conversion is physics based and does not depend on the dynamics of the specific aircraft being controlled. The adaptive controller then drives the unknown plant to track the reference model. This allows for a variety of aircraft to be controlled by the same controller, as long as the assumptions derived within Section 3 are met.

#### 4.4.3. Navigation Controller

The navigation controller consists of a waypoint navigation mode and an approach mode. The waypoint navigation mode computes the altitude and the heading error between the current aircraft position and the desired waypoint. The heading error,  $\psi_e$ , was computed as the difference between the aircraft's magnetic heading,  $\psi$ , and the waypoint's magnetic heading,  $\psi_w$ , as shown in Figure 4.8.

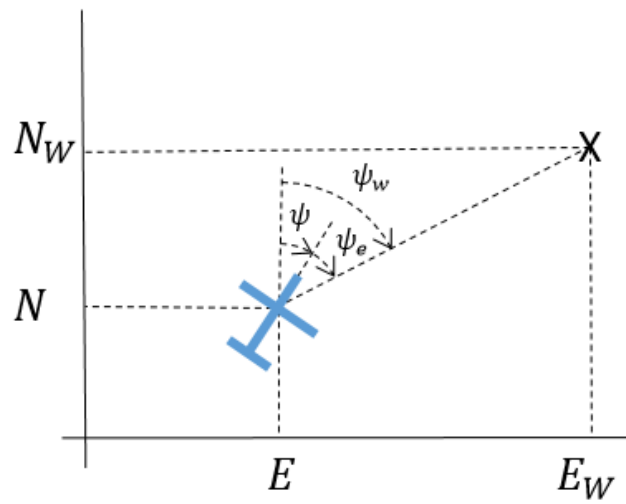


Figure 4.8. Aircraft's heading, waypoint heading, and heading error.

The heading error can be computed from:

$$\psi_e = \psi_w - \psi \quad (81)$$

The waypoint's magnetic heading can be computed using the trigonometric relation:

$$\psi_w = \tan^{-1} \left( \frac{E_w - E}{N_w - N} \right) \quad (82)$$

The approach mode simulates an Instrument Landing System (ILS) approach. It computes the distance from the ILS transmitter and generates a glideslope and a localizer error based on that distance. The aircraft's position relative to the runway was obtained by

computing the aircraft's position in a reference frame with origin at the runway. This is achieved by a coordinate transformation using the runway's heading. The glideslope error is the altitude error between the aircraft's current altitude and the predefined glideslope altitude. The localizer error is the lateral error between the aircraft's current position and the runway extended centerline. Figure 4.9 shows the block diagram used to compute the glideslope and localizer errors. These two errors are then sent to the autopilot to align the aircraft with the runway for landing. The airspeed controller is a low gain proportional controller. It actuates the throttle to maintain the desired airspeed.

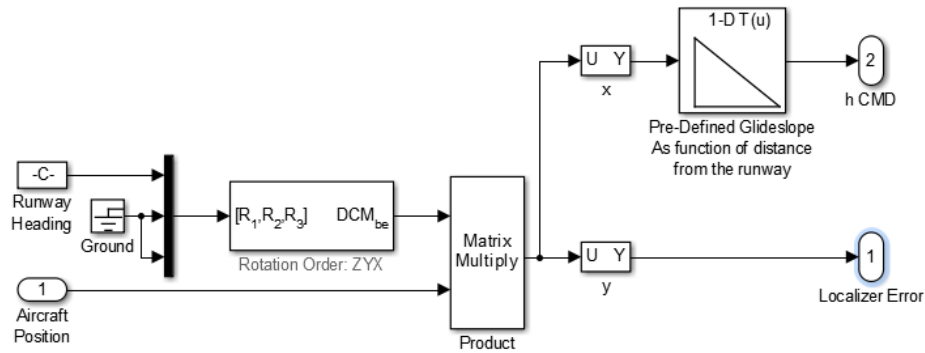


Figure 4.9. Localizer and glideslope errors.

## 4.5. Test Cases

To test the robustness and adaptability of the autopilot, the mathematical requirements of adaptive control theory were verified. Then, the aircraft was flown through a test scenario with increasing amounts of disturbances to verify performance and functionality.

### 4.5.1. Mathematical Requirements

The first test of the autopilot was to ensure that the mathematical requirements of adaptive control theory were met. To do this, Simulink was used to linearize the aircraft

model, and the linearized model was used to verify the following:

1. The plant  $(A, B, C)$  is minimum phase
2.  $CB$  is nonsingular
3. The reference model poles do not coincide with the plant zeros

When these conditions were met, the aircraft was flown through the test scenario described in the next section.

#### **4.5.2. Test Scenario**

The following test scenario was developed: the aircraft starts from a trim condition at cruise altitude and airspeed and descends to 1500 ft AGL where it initiates an ILS approach to 200 ft altitude. At 200 ft altitude, the simulation stops. It is assumed that at this altitude, the pilot would make a decision to land or to go around and take manual control of the aircraft. The aircraft starts the initial descent while slowing down and navigating horizontally. The flaps are deployed gradually as the aircraft slows down into the flaps operating airspeed. The horizontal waypoints were chosen to align the aircraft with the runway. After the last waypoint is reached, an ILS approach is initiated. The ILS approach is flown from 1500 ft to 200 ft AGL. Throughout the flight, moderate turbulence is present. At 400 ft, a gust of 25 ft/s (15 kts) is applied to test the autopilot's ability to maintain positive control of the aircraft. This scenario was chosen because it tests all components of the autopilot, both adaptive and conventional. It also represents worst case operating conditions in terms of turbulence and gusts. It tests the autopilot's ability to adapt to new flap configurations and slower airspeeds. It also tests the robustness to persistent disturbances. Figure 4.10 shows the test horizontal profile, and Figure 4.11 shows the vertical profile.

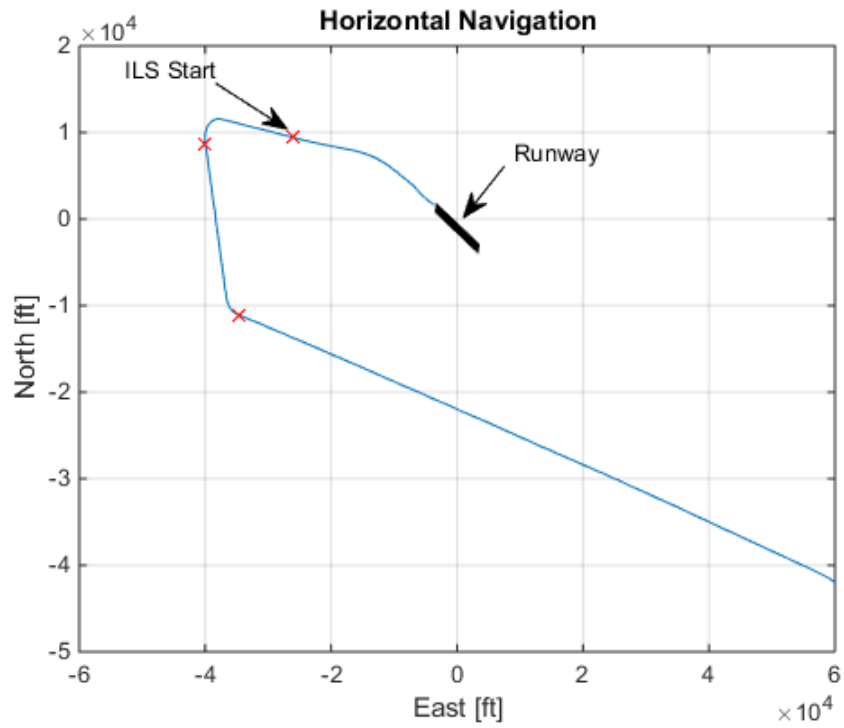


Figure 4.10. Horizontal navigation profile of the test scenario.

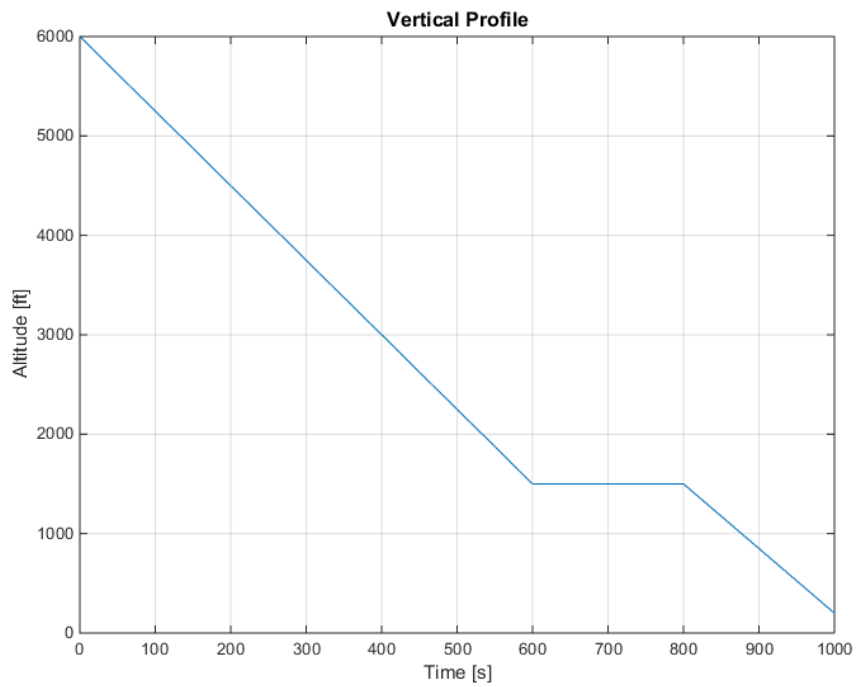


Figure 4.11. Vertical navigation profile of the test scenario.

For comparison purposes, three test cases were designed. The aircraft was first flown through the test scenario in a noise free environment. The noise from the actuators and sensors was removed, and the turbulence and gusts models were not active. This provided a baseline to compare the autopilot's robustness and operation in ideal conditions versus the worst case scenario. To observe the effect of the internal disturbances, the second test case consisted of flying through the test scenario with sensor and actuator noise but with no turbulence. Lastly, the test scenario was performed with sensor noise and turbulence. Table 4.3 shows each of the three test cases and the disturbances present in each.

Table 4.3. Summary of disturbances present on each test case.

	<b>Internal Disturbances</b>	<b>External Disturbances</b>
Test Case 1	OFF	OFF
Test Case 2	ON	OFF
Test Case 3	ON	ON

#### 4.6. Autopilot Transfer

The last step in testing the autopilot was to transfer it to a different aircraft model. The aircraft chosen was a Ryan Navion. The Navion is a single engine GA aircraft with a gross takeoff weight of 3600 lb. The aircraft is shown in Figure 4.12.



Figure 4.12. Navion aircraft in flight.

The nonlinear stability derivatives were obtained through full scale wind tunnel testing. The autopilot was transferred to this aircraft with all sensor models and actuators. The critical test case with sensors and actuator noise and turbulence was performed again as described previously.

## 5. Results

This section explains the results obtained in this investigation in detail. It provides numerical values for all controller gains used, adaptive and conventional, as well as reference models used and blending parameters chosen. It provides all stability analyses and the results to all test cases described in Section 4. Time histories of key autopilot parameters are also presented.

### 5.1. Adaptive Controllers

The adaptive controllers were designed following the theoretical guidelines presented previously. The following subsections describe the longitudinal and the lateral direct model reference adaptive controllers (MRAC).

#### 5.1.1. Longitudinal MRAC

The linearized longitudinal model of the aircraft and elevator actuator combination was found to be:

$$x = \begin{bmatrix} \delta_e & \dot{\delta}_e & \alpha & V_{TAS} & \theta & q \end{bmatrix}^T \quad (83)$$

$$A = \begin{bmatrix} 0 & 1 & 0 & 0 & 0 & 0 \\ -510.76 & -31.64 & 0 & 0 & 0 & 0 \\ 0.0025 & 0 & -2.0263 & -0.0009 & 0 & 0.97 \\ 0 & 0 & 40.36 & -0.022 & -32.12 & 0 \\ 0 & 0 & 0 & 0 & 0 & 1 \\ 0.82 & 0 & -28.76 & 0 & 0 & -4.78 \end{bmatrix} \quad (84)$$

$$B = [0 \ 510.76 \ 0 \ 0 \ 0 \ 0]^T \quad (85)$$

$$C = [0 \ 0 \ 0 \ 0 \ 1 \ 0] \quad (86)$$

The resulting transfer function is minimum phase but has a zero high frequency gain, so sensor blending needed to be performed. In order to determine which entries of the  $\Delta C$  matrix should be used and because  $A$  is invertible,  $A^{-1}B$  was used.

$$A^{-1}B = \begin{bmatrix} -1 \\ 0 \\ -0.028 \\ 58.12 \\ -0.075 \\ 0 \end{bmatrix} \quad (87)$$

By inspection, the entries  $\Delta c_1$  and  $\Delta c_5$ , corresponding to the  $\dot{\delta}_e$  and  $q$  states respectively, would result in the blended output tracking the original output at steady state. The  $\Delta C$  matrix then had the form:

$$\Delta C = [0 \quad \Delta c_1 \quad 0 \quad 0 \quad 0 \quad \Delta c_5] \quad (88)$$

The entry  $\Delta c_1$  is used to make  $CB$  non-singular. A temporary new output matrix,  $C_{temp}$ , that makes  $C_{temp}B$  non-singular was used to transform the system into normal form.

$$C_{temp} = [0 \quad 0.05 \quad 0 \quad 0 \quad 1 \quad 0] \quad (89)$$

The normal form matrices are shown below:

$$\bar{A}_{11} = -31.64 \quad (90)$$

$$\bar{A}_{12} = [-0.3027 \quad 0 \quad 0 \quad 25.59 \quad 1] \quad (91)$$

$$\bar{A}_{21} = \begin{bmatrix} -0.999 \\ 0 \\ 0 \\ -19.975 \\ 0 \end{bmatrix} \quad (92)$$

$$\bar{A}_{22} = \begin{bmatrix} -0.0498 & 0 & 0 & 0.003 & -20 \\ 0 & -2.026 & 0 & -0.003 & 0.966 \\ 1.602 & 40.355 & -0.022 & -0.08 & 0 \\ -0.996 & 0 & 0 & 0.05 & 1 \\ -0.04 & -28.755 & 0 & -0.816 & -4.779 \end{bmatrix} \quad (93)$$

The invertible coordinate transformation,  $W$ , that transforms the system into normal form is given by:

$$W = \begin{bmatrix} 0 & 0.05 & 0 & 0 & 1 & 0 \\ -0.0499 & 0 & 0 & 0 & -20 & 0 \\ 0 & 0 & 1 & 0 & 0 & 0 \\ 0 & 0 & 0 & 1 & 0 & 0 \\ -0.9988 & 0 & 0 & 0 & 1 & 1 \\ 0 & 0 & 0 & 0 & 0 & 1 \end{bmatrix} \quad (94)$$

When transformed to normal form, the  $\Delta C$  matrix has the form:

$$\Delta \bar{C} = \Delta C W^{-1} = [0 \quad \Delta c_1 \quad 0 \quad 0 \quad 0 \quad \Delta c_5] W^{-1} \quad (95)$$

$$\Delta \bar{C} = [20\Delta c_1 \quad 0.998\Delta c_1 \quad 0 \quad 0 \quad -0.0499\Delta c_1 \quad \Delta c_5] \quad (96)$$

Because the state corresponding to  $\Delta c_1$  (elevator rate) was used to provide a non-singular  $CB$ , it was not desired to add any more of it to the blended output, so  $\Delta c_1$  was chosen to be 0. The entry  $\Delta c_5$  was selected to be 1. The blending matrix in normal form was chosen to be:

$$\Delta \bar{C} = [0 \quad 0 \quad 0 \quad 0 \quad 0 \quad 1] \quad (97)$$

with:

$$\begin{aligned} \Delta \bar{C} &= [\Delta \bar{C}_1 \quad \Delta \bar{C}_2] \\ \Delta \bar{C}_1 &= 0 \\ \Delta \bar{C}_2 &= [0 \quad 0 \quad 0 \quad 0 \quad 1] \end{aligned} \quad (98)$$

The transmission zeros of the system were found through the eigenvalues of  $\bar{A}_{22} - \bar{A}_{21}\Delta\bar{C}_2$ :

$$\bar{A}_{22} - \bar{A}_{21}\Delta\bar{C}_2 = \begin{bmatrix} -0.0498 & 0 & 0 & 0.0025 & -19 \\ 0 & -2.026 & 0 & -0.0025 & 0.966 \\ 1.602 & 40.355 & -0.022 & -0.08 & 0 \\ -0.9963 & 0 & 0 & 0.0498 & 20.975 \\ -0.0408 & -28.755 & 0 & -0.816 & -4.779 \end{bmatrix} \quad (99)$$

The eigenvalues are:

$$\begin{aligned} & -2.940 \pm 6.25i \\ \text{eig}(\bar{A}_{22} - \bar{A}_{21}\Delta\bar{C}_2) &= -0.453 \pm 0.687i \\ & -0.0406 \end{aligned} \quad (100)$$

It can be seen that the blended system was minimum phase and  $CB$  non-singular.

The  $\Delta\bar{C}$  matrix was then transformed back to the original coordinates.

$$\Delta C = \Delta\bar{C}W^{-1} \quad (101)$$

$$\Delta C = [0 \quad 0 \quad 0 \quad 0 \quad 0 \quad 1] \quad (102)$$

and the blended output matrix  $C_b$  can be assembled:

$$C_b = C_{temp} + \Delta C \quad (103)$$

$$C_b = [0 \quad 0.05 \quad 0 \quad 0 \quad 1 \quad 1] \quad (104)$$

Because only the entries  $\Delta c_1$  and  $\Delta c_5$  were used in the blending process, the blended output is not only minimum phase and nonzero high frequency gain, but it will track the original output at low frequencies. Table 5.1 compares the original and blended output properties.

Table 5.1. Comparison between longitudinal original and blended outputs.

Output	Zeros	<i>CB</i>
Original	$-1.9195$ $-0.0419$	0
Blended	$-2.940 \pm 6.251i$ $-0.4528 \pm 0.687i$ $-0.0406$	25.54

Figure 5.1 shows a time history of the response of the original and blended outputs to the input shown in Figure 5.2.

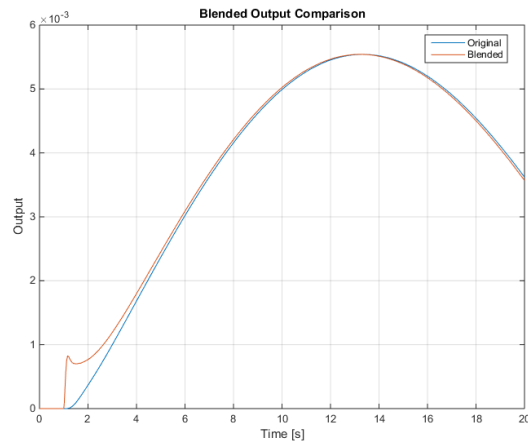


Figure 5.1. Time history comparison of original and blended outputs.

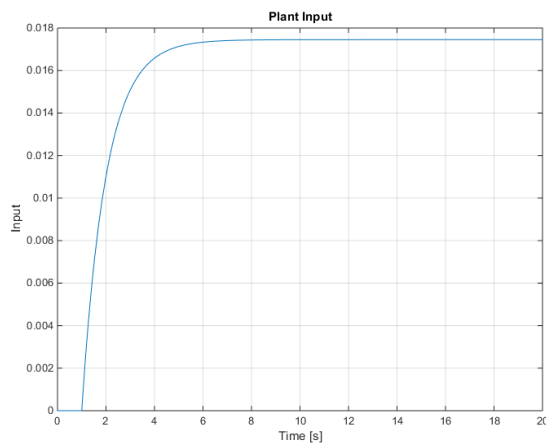


Figure 5.2. Plant input for output comparison.

It can be seen that, as predicted, after an initial high frequency response, the blended output converges to the original output at low frequencies. The blended output then met all the requirements from adaptive control theory. The reference model was then chosen to be:

$$\frac{\theta_{ref}(s)}{\theta_{cmd}(s)} = \frac{100}{s^2 + 14s + 100} \quad (105)$$

This model was chosen to provide tracking of the outer-loop controller. It can be seen that the model poles do not coincide with the plant zeros. The adaptive gains were then chosen to be:

$$\begin{aligned} \dot{G}_e &= -0.01G_e - 400e_y e_y^* \\ \dot{G}_D &= -0.01G_D - 10e_y \\ \dot{G}_m &= -0.01G_m - 50e_y x_m^* \\ \dot{G}_u &= -0.01G_u - 10e_y u_m^* \end{aligned} \quad (106)$$

Note that the disturbance basis function,  $\phi_D$ , has been chosen to be 1. This means that the disturbances are treated as a series of steps of unknown amplitudes.

### 5.1.2. Lateral MRAC

The lateral-directional linear model of the aircraft at 3000 ft and 150 kts is given by:

$$x = \begin{bmatrix} \delta_a & \dot{\delta}_a & \beta & \phi & p & r \end{bmatrix}^T \quad (107)$$

$$A = \begin{bmatrix} 0 & 1 & 0 & 0 & 0 & 0 \\ -510.76 & -31.64 & 0 & 0 & 0 & 0 \\ 0 & 0 & -0.232 & 0.123 & 0.026 & -1.02 \\ 0 & 0 & 0 & 0 & 1 & 0.026 \\ 0.92 & 0 & -33.61 & 0 & -15.83 & 3.66 \\ 0.006 & 0 & 6.50 & 0 & 0.112 & -0.436 \end{bmatrix} \quad (108)$$

$$B = [0 \ 510.76 \ 0 \ 0 \ 0 \ 0]^T \quad (109)$$

$$C = [0 \ 0 \ 0 \ 1 \ 0 \ 0] \quad (110)$$

The resulting transfer function is minimum phase but has a zero high frequency gain, so sensor blending needed to be performed. In order to determine which entries of the  $\Delta C$  matrix should be used and because  $A$  is invertible,  $A^{-1}B$  was used:

$$A^{-1}B = \begin{bmatrix} -1 \\ 0 \\ 0.037 \\ 4.44 \\ -0.014 \\ 0.53 \end{bmatrix} \quad (111)$$

By inspection, the entries  $\Delta c_1$  and  $\Delta c_4$ , corresponding to the  $\delta_a$  and  $p$  states respectively, would result in the blended output tracking the original output at steady state.

The  $\Delta C$  matrix then has the form:

$$\Delta C = [0 \ \Delta c_1 \ 0 \ 0 \ \Delta c_4 \ 0] \quad (112)$$

The entry  $\Delta c_1$  is used to make  $CB$  non-singular. A temporary new output matrix,  $C_{temp}$ , that makes  $C_{temp}B$  non-singular is used to transform the system into normal form.

$$C_{temp} = [0 \ 0.05 \ 0 \ 1 \ 0 \ 0] \quad (113)$$

The normal form matrices are shown below:

$$\bar{A}_{11} = -31.64 \quad (114)$$

$$\bar{A}_{12} = [-0.303 \quad 0 \quad 25.585 \quad 1 \quad 0.0256] \quad (115)$$

$$\bar{A}_{21} = \begin{bmatrix} -0.999 \\ 0 \\ -19.975 \\ 0 \\ 0 \end{bmatrix} \quad (116)$$

$$\bar{A}_{22} = \begin{bmatrix} -0.0498 & 0 & 0.0025 & -20 & -0.512 \\ -0.006 & -0.232 & 0 & 0.026 & -1.019 \\ -0.996 & 0 & 0.05 & 1 & 0.026 \\ -0.046 & -33.613 & -0.920 & -15.833 & 3.660 \\ -0 & 6.498 & -0.006 & 0.112 & -0.436 \end{bmatrix} \quad (117)$$

The invertible coordinate transformation,  $W$ , that transforms the system into normal form is given by:

$$W = \begin{bmatrix} 0 & 0.05 & 0 & 1 & 0 & 0 \\ -0.05 & 0 & 0 & -20 & 0 & 0 \\ 0 & 0 & 1 & 0 & 0 & 0 \\ -0.999 & 0 & 0 & 1 & 0 & 0 \\ 0 & 0 & 0 & 0 & 1 & 0 \\ 0 & 0 & 0 & 0 & 0 & 1 \end{bmatrix} \quad (118)$$

When transformed to normal form, the  $\Delta C$  matrix will have the form:

$$\Delta \bar{C} = \Delta C W^{-1} = [0 \quad \Delta c_1 \quad 0 \quad 0 \quad \Delta c_4 \quad 0] W^{-1} \quad (119)$$

$$\Delta \bar{C} = [20\Delta c_1 \quad 0.998\Delta c_1 \quad 0 \quad -0.0499\Delta c_1 \quad \Delta c_4 \quad 0] \quad (120)$$

Because the state corresponding to  $\Delta c_1$  (aileron rate) was used to provide a non-singular  $CB$ , it was not desired to add any more of it to the blended output, so  $\Delta c_1$  was chosen to be 0. The entry  $\Delta c_4$  was chosen as 2. The blending matrix in normal form resulted

in:

$$\Delta\bar{C} = [0 \ 0 \ 0 \ 0 \ 2 \ 0] \quad (121)$$

with:

$$\begin{aligned} \Delta\bar{C} &= [\Delta\bar{C}_1 \ \Delta\bar{C}_2] \\ \Delta\bar{C}_1 &= 0 \\ \Delta\bar{C}_2 &= [0 \ 0 \ 0 \ 2 \ 0] \end{aligned} \quad (122)$$

The transmission zeros of the system were found through the eigenvalues of

$\bar{A}_{22} - \bar{A}_{21}\Delta\bar{C}_2$ :

$$\bar{A}_{22} - \bar{A}_{21}\Delta\bar{C}_2 = \begin{bmatrix} -0.05 & 0 & 0.0025 & -18.003 & -0.512 \\ -0.006 & -0.232 & 0 & 0.026 & -1.019 \\ -0.996 & 0 & 0.05 & 40.950 & 0.026 \\ -0.046 & -33.612 & -0.919 & -15.833 & 3.660 \\ 0 & 6.498 & -0.006 & 0.112 & -0.434 \end{bmatrix} \quad (123)$$

The eigenvalues are:

$$\begin{aligned} &-0.318 \pm 2.584i \\ \text{eig}(\bar{A}_{22} - \bar{A}_{21}\Delta\bar{C}_2) &= \begin{matrix} -13.095 \\ -2.079 \\ -0.690 \end{matrix} \end{aligned} \quad (124)$$

It can be seen that the system is now minimum phase and  $CB$  non-singular. The  $\Delta\bar{C}$  matrix was then transformed back to the original coordinates:

$$\Delta C = \Delta\bar{C}W^{-1} \quad (125)$$

$$\Delta C = [0 \ 0 \ 0 \ 0 \ 2 \ 0] \quad (126)$$

and the blended output matrix,  $C_b$ , can be assembled:

$$C_b = C_{temp} + \Delta C \quad (127)$$

$$C_b = [0 \ 0.05 \ 0 \ 1 \ 2 \ 0] \quad (128)$$

Because only the entries  $\Delta c_1$  and  $\Delta c_4$  were used in the blending process, the blended output is not only minimum phase and nonzero high frequency gain, but it will track the original output at low frequencies. Table 5.2 compares the original and blended output properties.

Table 5.2. Comparison between lateral original and blended outputs.

Output	Zeros	$CB$
Original	$-0.348 \mp 2.615i$	0
Blended	$-0.318 \mp 2.567i$ -13.095 -2.079 -0.690	25.54

Figure 5.3 shows a time history of the response of the original and blended outputs to the input shown in Figure 5.2.

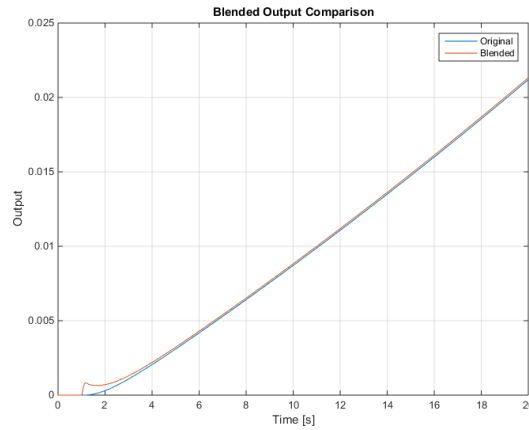


Figure 5.3. Time history of original and blended outputs response.

Once again, it can be seen that the blended output tracks the original output after an initial high frequency response. The reference model for bank angle was chosen to be:

$$\frac{\phi_{ref}(s)}{\phi_{cmd}(s)} = \frac{2500}{s^2 + 90s + 2500} \quad (129)$$

The bank angle reference model was chosen to be significantly faster than the pitch angle model. This is due to the fact that the bank angle needs a much faster response in order to track a heading. It can be seen that the model poles do not coincide with any of the plant zeros. The adaptive gains were chosen to be:

$$\begin{aligned} \dot{G}_e &= -0.05G_e - 400e_y e_y^* \\ \dot{G}_D &= -0.05G_D - 10e_y \\ \dot{G}_m &= -0.05G_m - 50e_y x_m^* \\ \dot{G}_u &= -0.05G_u - 10e_y u_m^* \end{aligned} \quad (130)$$

Once again, the disturbance basis function,  $\phi_D$ , was chosen to be 1 to represent a series of steps of unknown amplitudes.

## 5.2. Conventional Controllers

The conventional controllers were tuned to control the reference models. The adaptive controller drives different plants to the reference models, allowing a conventional controller (tuned to the reference models) to control plants with different dynamics. The following subsections describe these controllers.

### 5.2.1. Altitude Controller

The altitude hold controller is comprised of two linear controllers in series. The first one is a PI controller that converts an altitude error into a vertical speed command with a saturation of 500 fpm and -500 fpm in the navigation mode and 500 fpm to -1500 fpm in the approach mode. The second one is a PID controller that converts the vertical

speed error into a pitch angle command. The pitch angle command is then used as the input to the reference model. The gains for the longitudinal controllers are given in Table 5.3.

Table 5.3. Longitudinal conventional controller gains.

<b>Gain</b>	<b>Altitude Error</b>	<b>Vertical Speed Error</b>
P	0.250	0.120
I	0.005	0.040
D	---	0.035

### 5.2.2. Heading Angle Controller

The heading angle controller allows the aircraft to navigate to waypoints horizontally. It works by converting the heading error into a rate of turn command. The rate of turn command is then used to compute the required bank angle as a function of airspeed to achieve the desired rate of turn. The bank angle command is then sent to the reference model. Heading error is converted to rate of turn command by a proportional controller with a gain of 0.2. Rate of turn command is saturated at 3.9 degrees per second (130% standard rate turn), which is typical of GA autopilots.

### 5.2.3. Airspeed Controller

An airspeed controller was used to simulate the pilot operating the throttle lever to hold a constant airspeed. The airspeed being held was the aircraft's approach velocity. The airspeed controller is a proportional controller with a gain of -0.08.

### 5.3. Test Scenario Results

The aircraft was flown by the autopilot through the test scenario. To establish a baseline, the scenario was first run with no disturbances. The random noise was removed from the sensor and actuator models, and the turbulence and gust were turned off. The test was then repeated with sensor and actuator random noise. Lastly, the test was run with sensor and actuator noise and turbulence. The following subsections contain the results for each of those three runs.

#### 5.3.1. Test Case 1: No disturbances

This section presents the results obtained in the disturbance free case. Figure 5.4 shows the vertical navigation results.

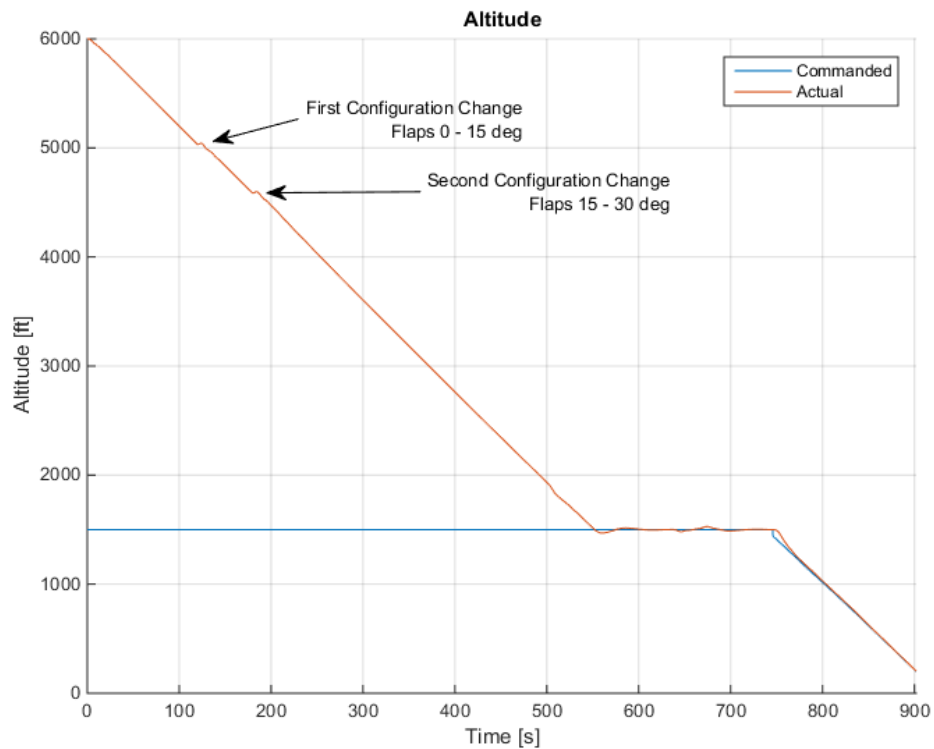


Figure 5.4. Noise-free vertical navigation results for the SR22 aircraft.

It can be seen that the aircraft follows the vertical navigation profile closely. The two configuration changes shown cause the vertical speed of the aircraft to oscillate, but the autopilot adapts adequately and continues through the descent. Figure 5.5 shows the pitch angle tracking results.

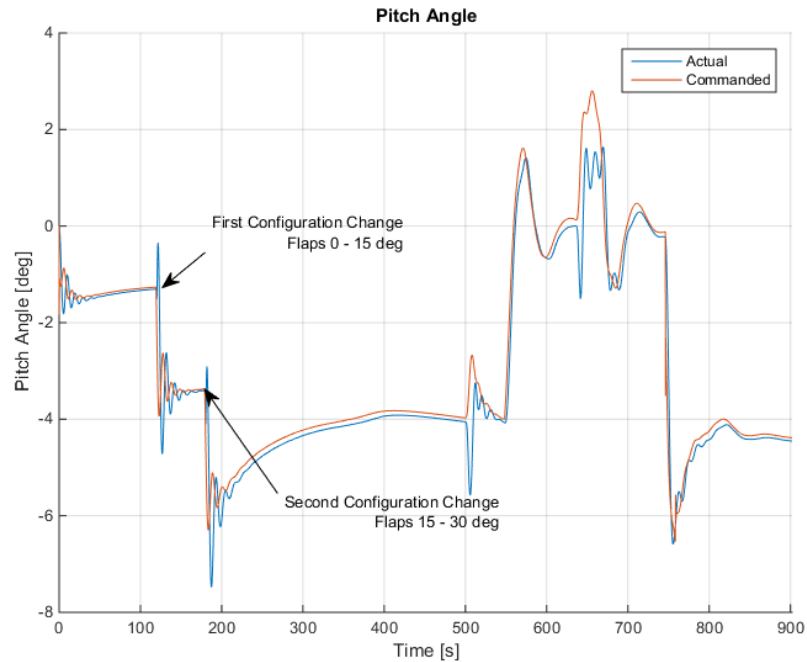


Figure 5.5. Noise-free pitch angle tracking results for the SR22 aircraft.

The pitch angle time history shows that, as expected, the pitch angle tracks the reference model closely despite the fact that the blended output is driving the adaptive controller. Lightly damped, low frequency, commanded oscillations are present in the pitch angle. These oscillations have a peak-to-peak amplitude of one degree and a period of 10 seconds. These oscillations do not present a problem for the aircraft occupants due to their small amplitude and low frequency, and because they subside after three cycles. Flap deployment results in a very noticeable decrease in pitch angle. Figure 5.6 shows the time history of the longitudinal adaptive gains.

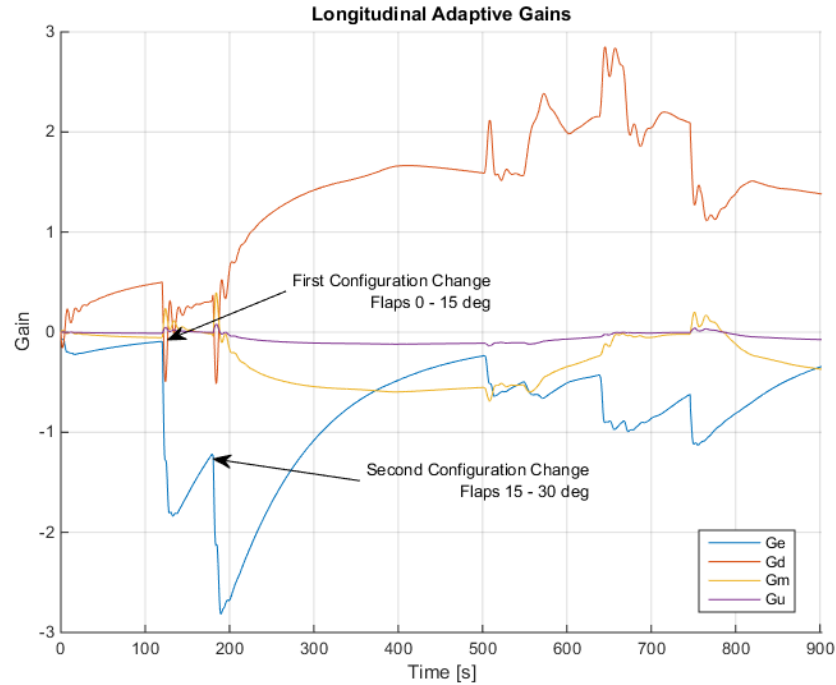


Figure 5.6. Time history of longitudinal adaptive gains for the SR22 aircraft.

The adaptive gains remain bounded throughout the simulation. The adaptive gain  $G_e$  that corresponds to the error between the reference model and the blended output experiences abrupt changes during each of the configuration changes. The gain is able to adapt adequately. Other abrupt changes to  $G_e$  occur when the aircraft banks and loses some altitude. However, these changes are significantly smaller in magnitude than those that occur as a result of a configuration change. When there are no configuration changes or turns, the leakage term slowly returns the gain to zero. Figure 5.7 shows the horizontal navigation results.

The horizontal navigation results show that the autopilot is able to navigate the course and align the aircraft with the runway. Figure 5.8 shows the bank angle tracking results.

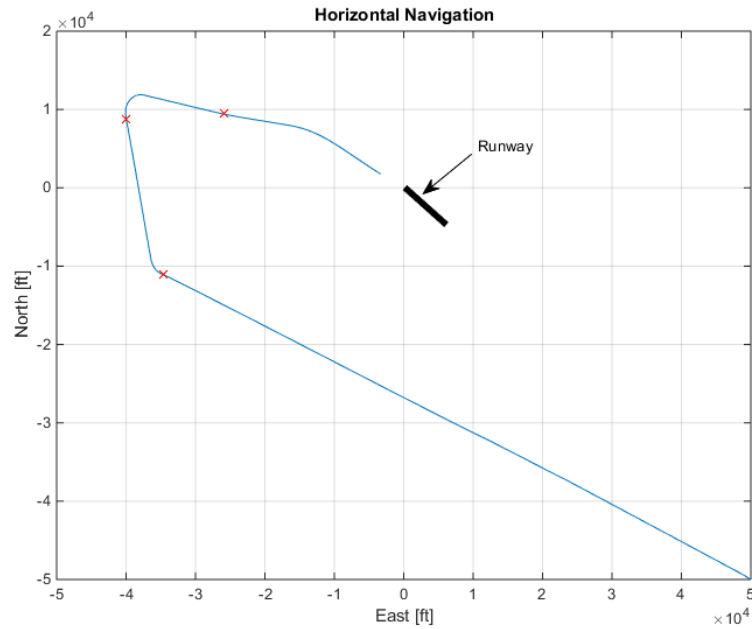


Figure 5.7. Noise-free horizontal navigation results for the SR22 aircraft.

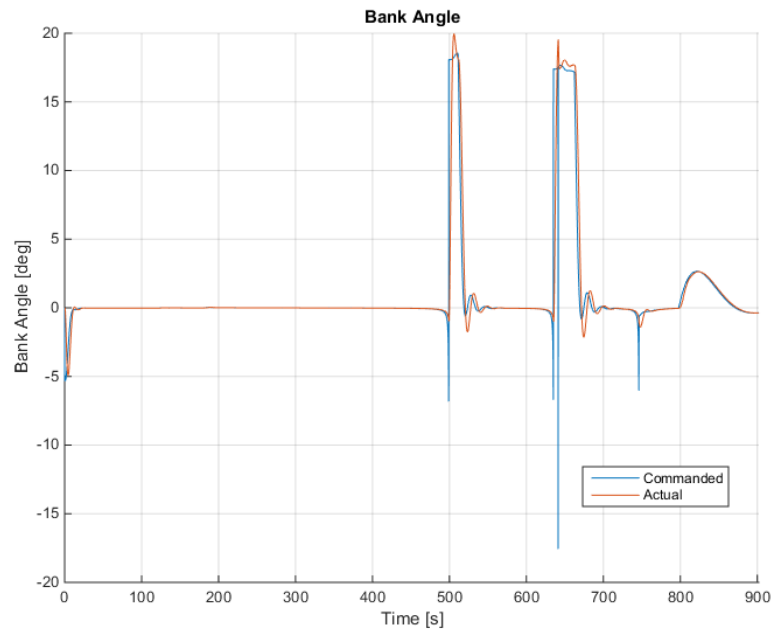


Figure 5.8. Noise-free bank angle tracking results for the SR22 aircraft.

The bank angle time history shows adequate tracking of the reference bank angle.

Longitudinal configuration changes do not affect the aircraft's bank angle. The localizer

error time history is shown in Figure 5.9.

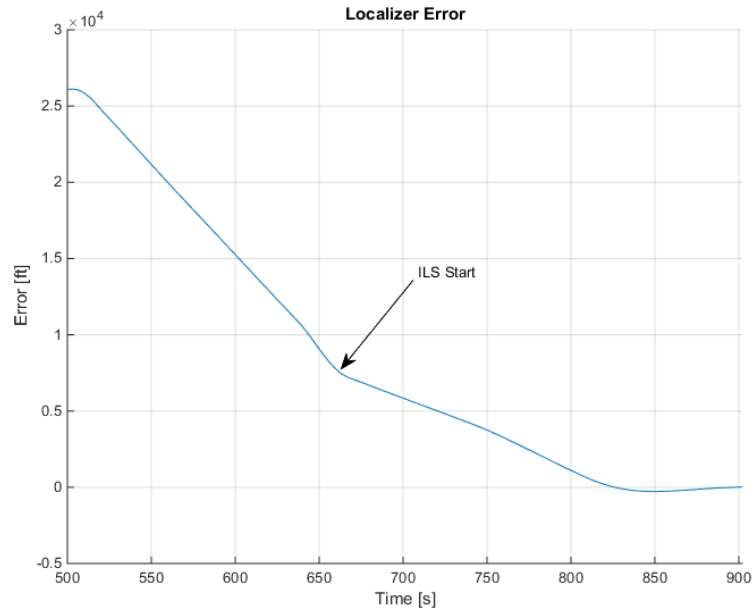


Figure 5.9. Noise-free localizer time history results for the SR22 aircraft.

The autopilot is able to intercept and follow the localizer signal. The time history for the lateral adaptive gains can be seen in Figure 5.10.

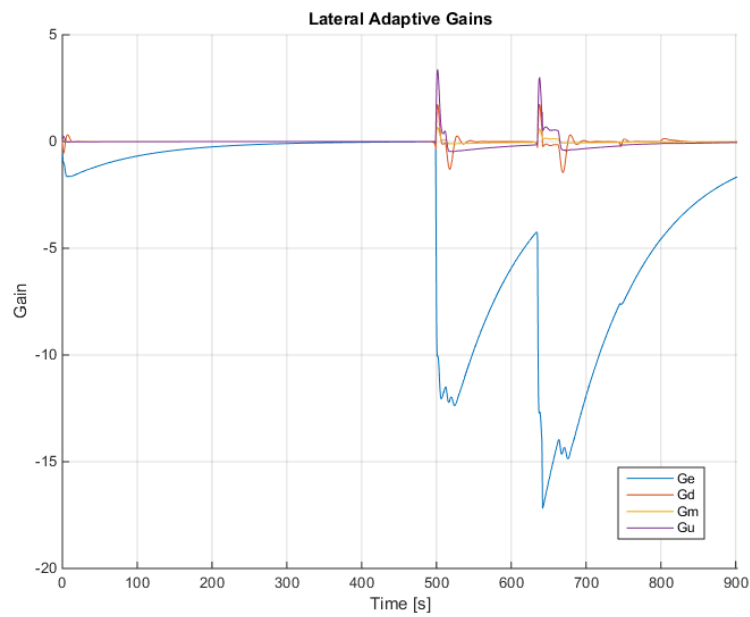


Figure 5.10. Time histories for the lateral adaptive gains for the SR22 aircraft.

The lateral adaptive gains remain bounded throughout the flight. Once again, it can be seen that the changes in configuration do not have an effect on the lateral adaptive gains. Abrupt changes to the lateral gains occur when the aircraft turns, but after it returns to level flight, the leakage term returns the gains to zero. After the test was complete sensor and actuator noise was introduced into the model to observe the effects of internal disturbances.

### 5.3.2. Test Case 2: Internal Disturbances

The vertical navigation results for Test Case 2 are shown in Figure 5.11. The vertical navigation results are not significantly different from the results from Test Case 1. The adaptive autopilot has accommodated the disturbances, and therefore, they do not reduce the ability of the conventional autopilot to track altitude. The internal disturbances are visible in the pitch angle results.

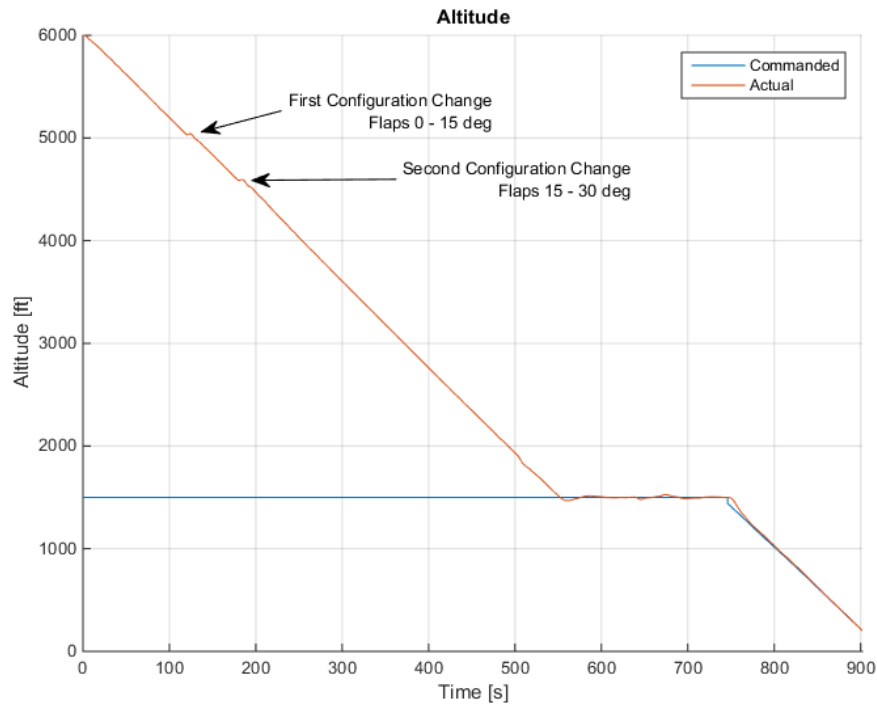


Figure 5.11. Vertical navigation results for the SR22 aircraft with sensor noise.

The pitch angle tracking results are shown in Figure 5.12.

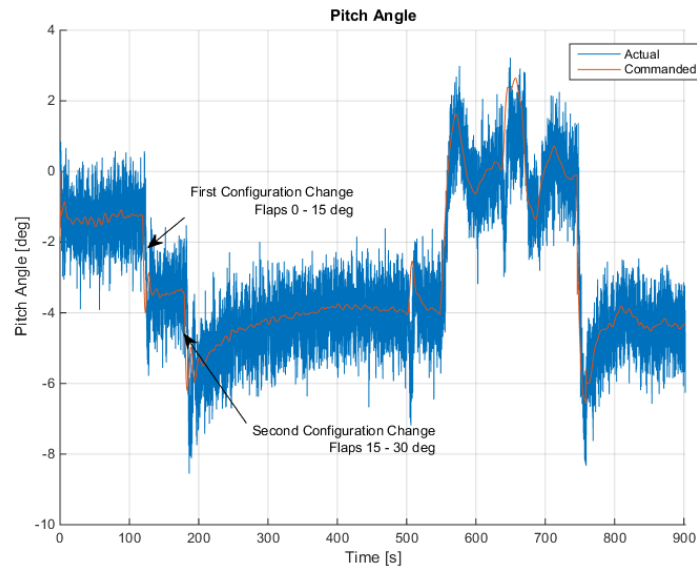


Figure 5.12. Pitch angle tracking results for the SR22 aircraft with sensor noise.

The pitch angle results are similar to the noise free results. The commanded oscillations are still present, and the change in pitch angle due to configuration changes are obvious. The time history of the longitudinal adaptive gains is shown in Figure 5.13.

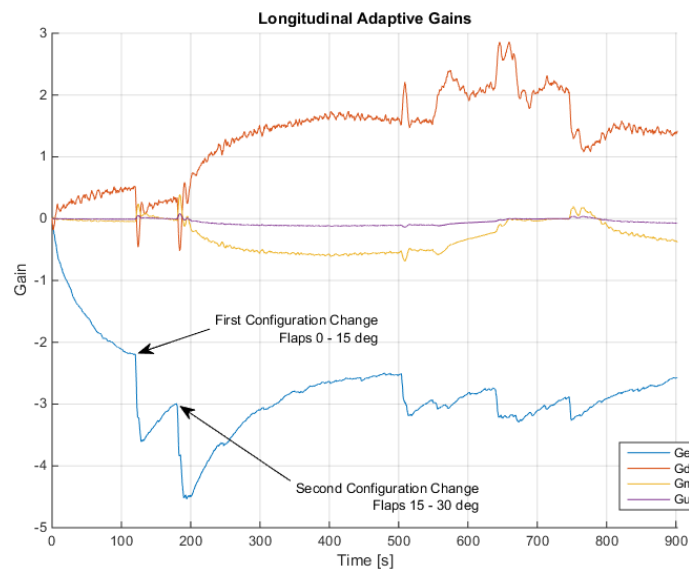


Figure 5.13. Longitudinal adaptive gains time history for the SR22 aircraft with sensor noise.

The longitudinal adaptive gains have the same behavior as in the noise free case. The most important difference can be seen on  $G_D$ , corresponding to disturbances. In the noise free case,  $G_D$  is smooth. After the disturbances are introduced,  $G_D$  is no longer smooth because it adapts to accommodate these disturbances at each time step. All adaptive gains exhibit a similar behavior, but it is significantly more apparent in  $G_D$ . The horizontal navigation results are shown in Figure 5.14.

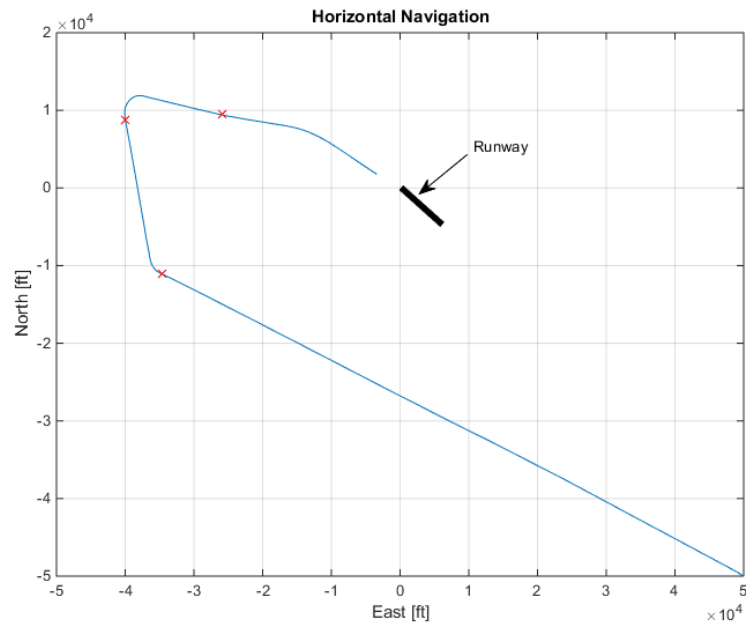


Figure 5.14. Horizontal navigation results for the SR22 aircraft with sensor noise.

The horizontal navigation results are nearly identical to the noise free case. The lateral adaptive controller has accommodated the disturbances, and therefore they do not reduce the capacity of the conventional autopilot to navigate horizontally. The bank angle tracking results are shown in Figure 5.15. Once again, the changes in configuration do not affect the aircraft's bank angle. The localizer error for the ILS approach is shown in Figure 5.16.

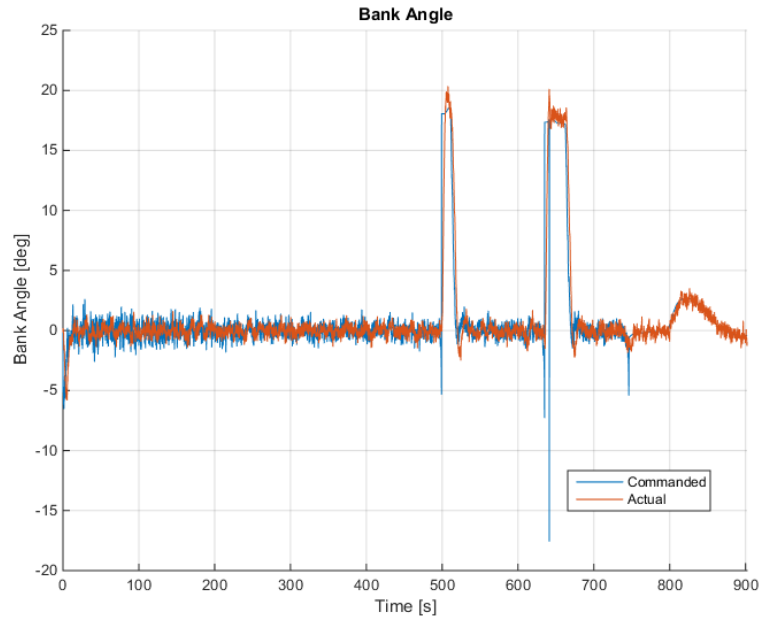


Figure 5.15. Bank angle tracking results for the SR22 aircraft with sensor noise.

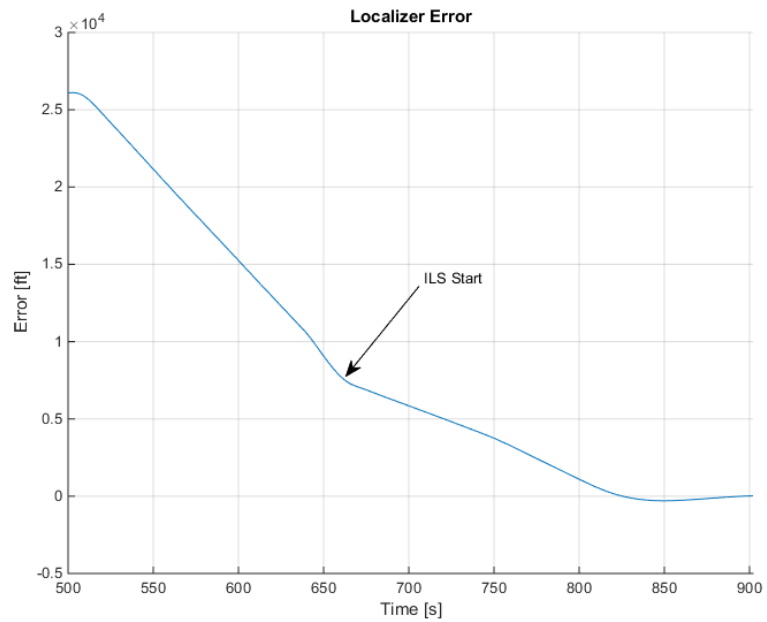


Figure 5.16. Localizer error time history for the SR22 aircraft with sensor noise.

Even in the presence of internal disturbances, the autopilot is capable of aligning the aircraft with the runway. The time history of the lateral adaptive gains is shown in Figure 5.17.

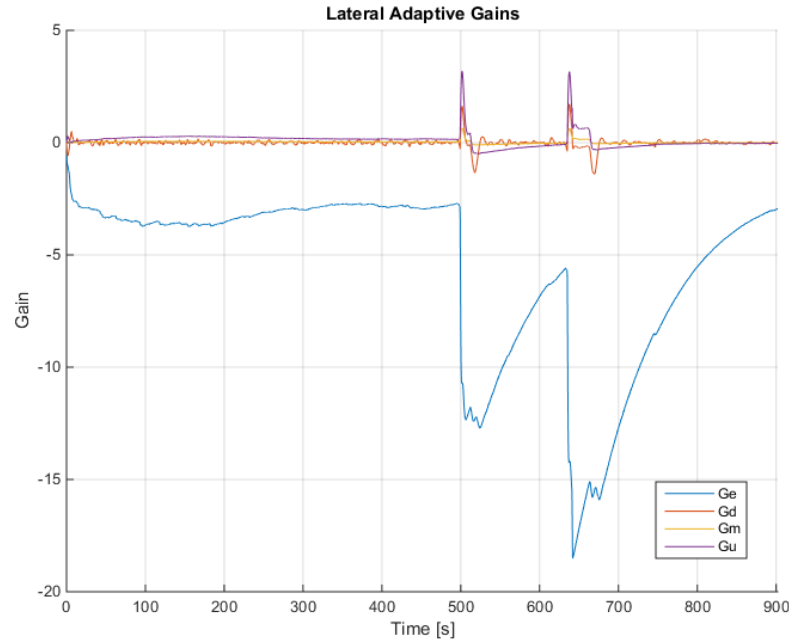


Figure 5.17. Lateral adaptive gains time history for the SR22 aircraft with sensor noise.

As with the longitudinal adaptive gains, the lateral adaptive gains are similar to the noise free case, with  $G_D$  accommodating the disturbances. After Test Case 2 was completed, the final and most critical test was performed. The results are shown in the next section.

### 5.3.3. Test Case 3: Internal and External Disturbances

Test Case 3 includes sensor and actuator random noise as well as turbulence. It also includes a 15 kts gust on final approach when the aircraft reaches an altitude of 400 ft. This test is the most critical because it represents a worst case scenario. Figure 5.18 shows the vertical navigation results. The aircraft starts at the trim condition at cruise altitude and begins a 300 fpm descent to prevent over-speeding. After the airspeed is below the flap operating airspeed, the flaps are deployed manually by the pilot. When the flaps are deployed, the aircraft initiates a 500 fpm descent to the target altitude of 1500 ft. The

airplane then performs an ILS approach down to 200 ft. It can be seen that the autopilot maintained altitude tracking through different airspeeds, altitudes, and flap configurations in the presence of internal and external disturbances.

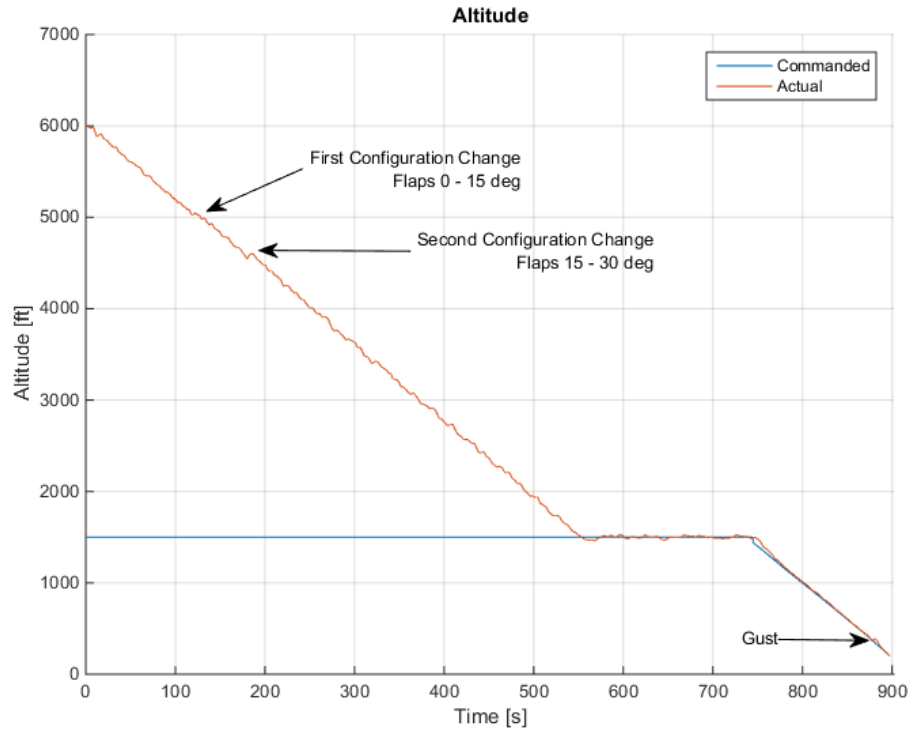


Figure 5.18. Vertical navigation results for the SR22 aircraft.

Figure 5.19 shows the pitch angle tracking by the adaptive autopilot. It can be seen that the pitch angle follows the reference model closely. This shows that the blended output does, in fact, track the original output of interest (the pitch angle). It can be seen that the autopilot adapts appropriately to changes in configuration. Figure 5.20 shows the time history of the longitudinal adaptive gains. As predicted by the theory, all adaptive gains remained bounded. Unlike the disturbance free case, the configuration changes are not as noticeable in the adaptive gains. The horizontal navigation results are shown in Figure 5.21.

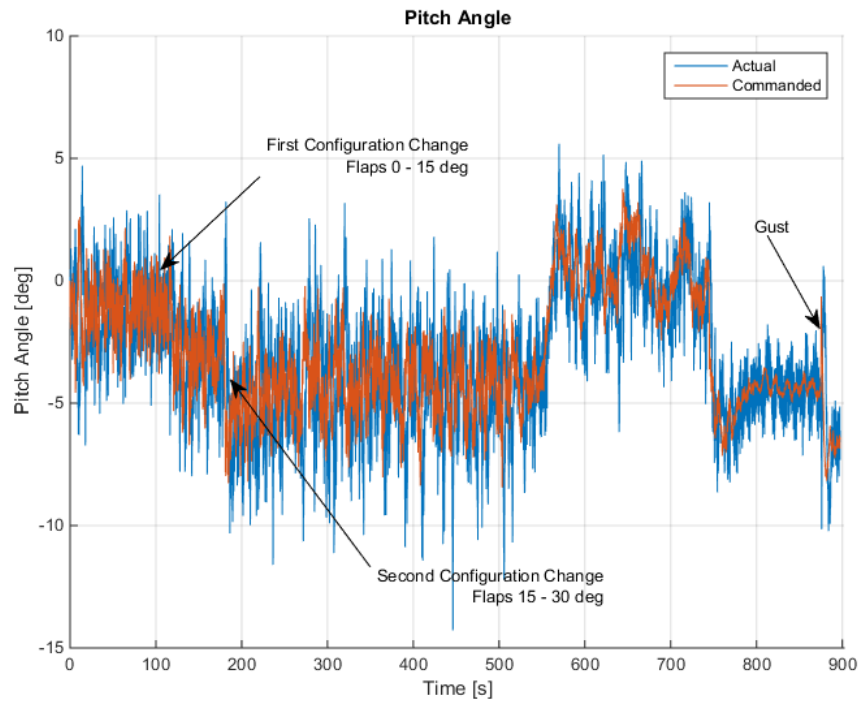


Figure 5.19. Pitch angle tracking results for the SR22 aircraft.

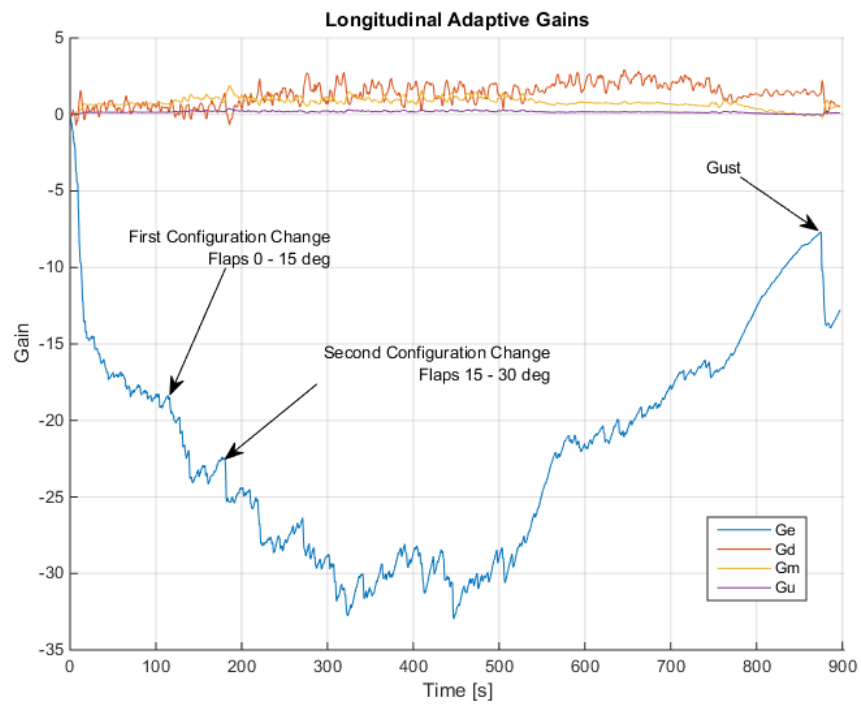


Figure 5.20. Longitudinal adaptive gains time history for the SR22 aircraft.

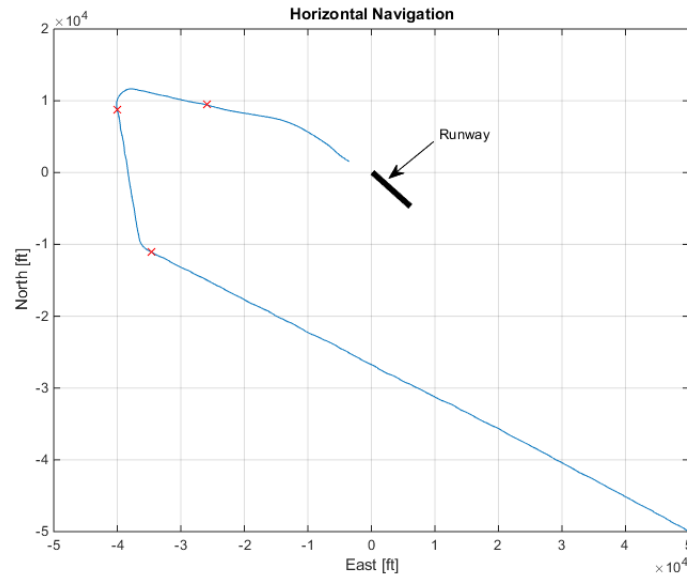


Figure 5.21. Horizontal navigation results for the SR22 aircraft.

The aircraft navigates appropriately through all the waypoints to position itself to start the ILS approach. After the ILS starts, the aircraft aligns itself with the runway while following the glideslope. The localizer error for the last 400 seconds of the flight is shown in Figure 5.22.

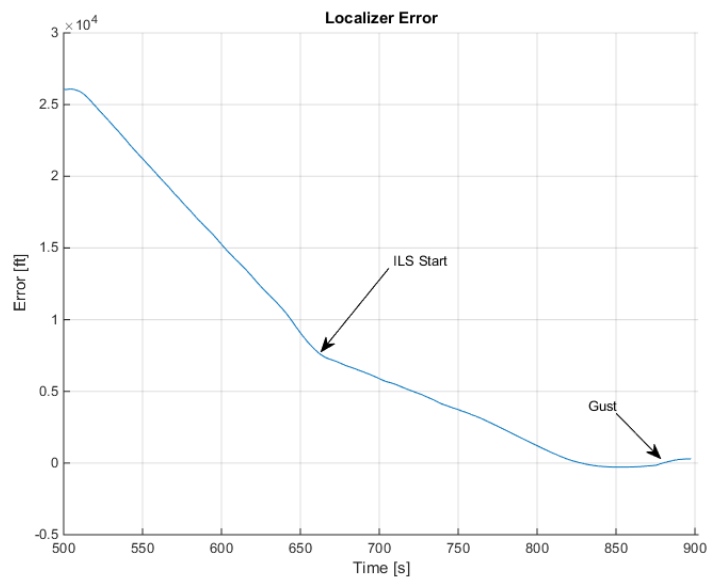


Figure 5.22. Localizer error time history for the SR22 aircraft.

The autopilot is able to align the aircraft with the runway. When the gust hits at 400 ft (890 seconds into the flight), the aircraft is displaced from the localizer. The autopilot is able to bank the aircraft to remain within the operating distance of the ILS transmitter and realigns the aircraft with the runway. The bank angle tracking is shown in Figure 5.23.

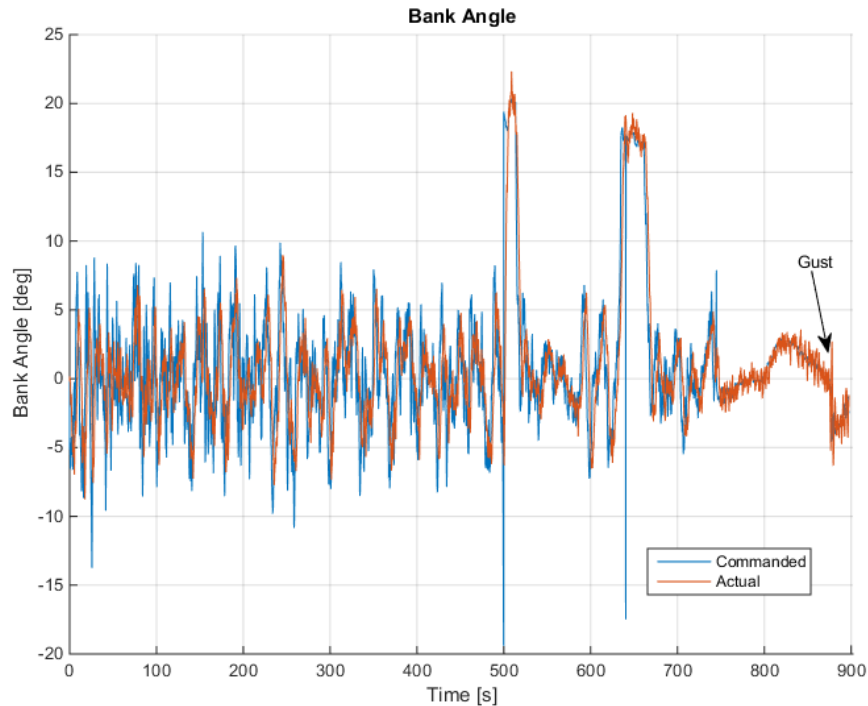


Figure 5.23. Bank angle tracking results for the SR22 aircraft.

The bank angle tracks the reference model closely. The bank angle response has a higher frequency once the ILS approach starts, but the bank angle remains close to the reference model. The lateral adaptive gains are shown in Figure 5.24.

Once again, as predicted by the theory, all adaptive control gains remained bounded. After the test scenario was completed successfully by the autopilot on the aircraft used for design, the autopilot was transferred, without modification, to a different GA aircraft. The following section describes the autopilot transfer process and results.

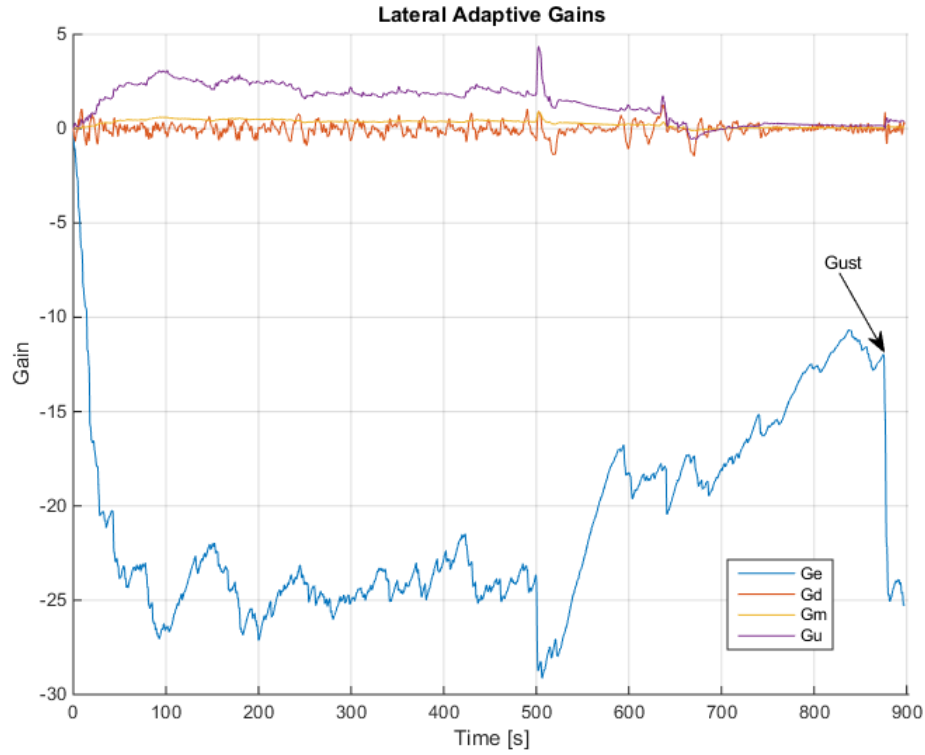


Figure 5.24. Lateral adaptive gains time history for the SR22 aircraft.

#### 5.4. Autopilot Transfer Results

The autopilot was transferred to a Ryan Navion nonlinear simulator. The model was then linearized to verify that the blended outputs are minimum phase and have a nonzero high frequency gain. The longitudinal transfer function from elevator to blended pitch angle was found to be:

$$\frac{\theta_b(s)}{\delta_e(s)} = \frac{25.54s^5 + 94.03s^4 + 2978s^3 + 6729s^2 + 4303s + 336.4}{s^6 + 35.32s^5 + 635.8s^4 + 2152s^3 + 4393s^2 + 307.1s + 245.3} \quad (131)$$

Similarly, the lateral transfer function from aileron deflection to blended bank angle was found to be:

$$\frac{\phi_b(s)}{\delta_a(s)} = \frac{25.54s^5 + 164.2s^4 + 1.365 \times 10^4 s^3 + 1.53 \times 10^4 s^2 + 3.215 \times 10^4 s + 1.35 \times 10^4}{s^6 + 38.07s^5 + 720.4s^4 + 3494s^3 + 3590s^2 + 6882s + 75.23} \quad (132)$$

Table 5.4 shows the zeros and the high frequency gain for each of these transfer functions.

Table 5.4. Zeros and high frequency gain of blended outputs in the Navion aircraft.

<b>Transfer Function</b>	<b>Zeros</b>	<b>High Frequency Gain</b>
$\frac{\theta_b(s)}{\delta_e(s)}$	$-0.6739 \pm 10.5598i$ $-1.1218 \pm 0.2054i$ $-0.0905$	25.54
$\frac{\phi_b(s)}{\delta_a(s)}$	$-0.3145 \pm 1.4068i$ $-2.6592 \pm 22.78i$ $-0.4834$	25.54

It can be seen that following the methodology described earlier resulted in minimum phase, nonzero high frequency gain blended outputs in the new aircraft. In addition, the zeros of the blended outputs do not coincide with the reference model poles. It is expected that, by blending the outputs in this manner, the blended outputs will track the original outputs at low frequencies, allowing the generic conventional controller to navigate the aircraft through the test case scenario while being subjected to internal and external disturbances.

After it was verified that the mathematical requirements of the adaptive controller were satisfied in the new aircraft, Test Case 3 was run. The simulation was started from a trim condition at 6000 ft and 110 kts and stopped at 200 ft. Figure 5.25 shows the vertical navigation results.

It can be seen that the autopilot successfully navigated the aircraft from cruise altitude to 200 ft. The autopilot was able to adapt to changes in altitude, airspeed, and configuration. The glideslope was also followed. To do this, the adaptive autopilot tracked the reference model pitch angle. The results are shown in Figure 5.26.

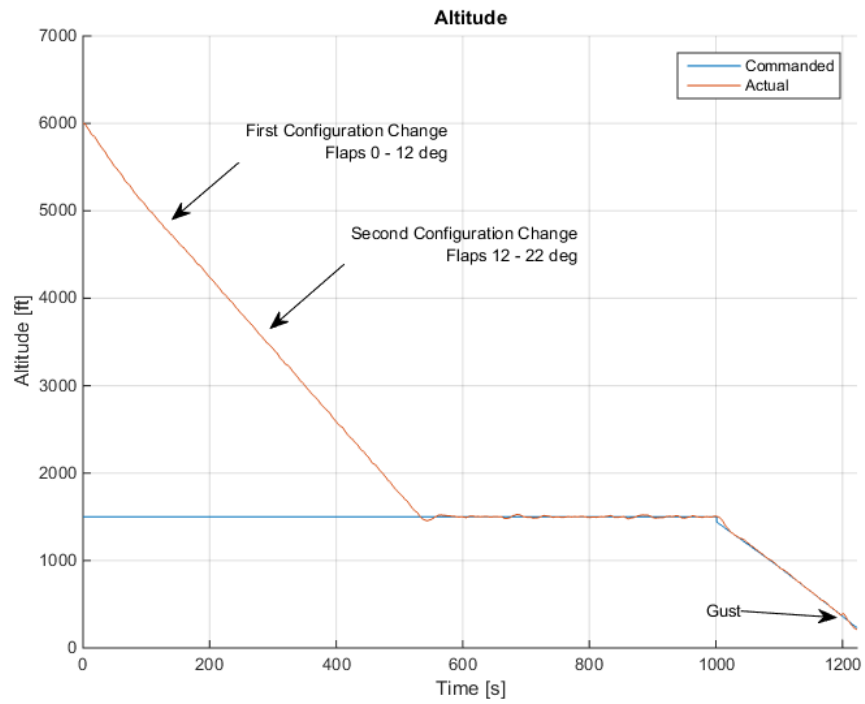


Figure 5.25. Vertical navigation results for the Navion aircraft.

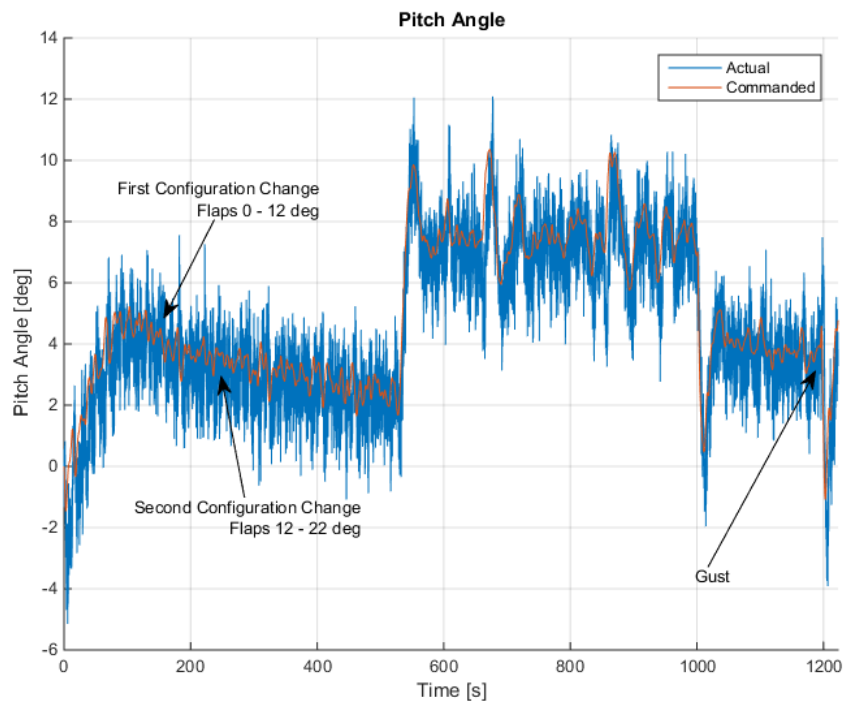


Figure 5.26. Pitch angle tracking results for the Navion aircraft.

The pitch angle was tracked correctly throughout the test scenario. The blended output converged to the pitch angle, allowing the pitch angle to track the reference model.

The longitudinal adaptive gains are shown in Figure 5.27

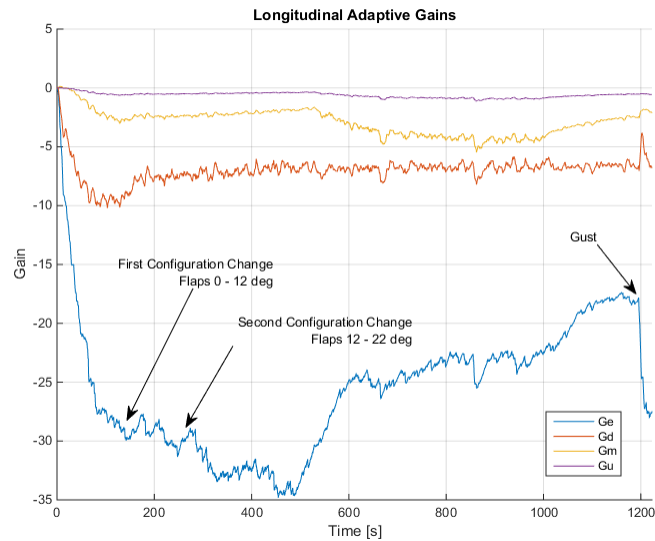


Figure 5.27. Longitudinal adaptive gains time history for the Navion aircraft.

The adaptive gains remained bounded throughout the simulation. The horizontal navigation results are shown in Figure 5.28.

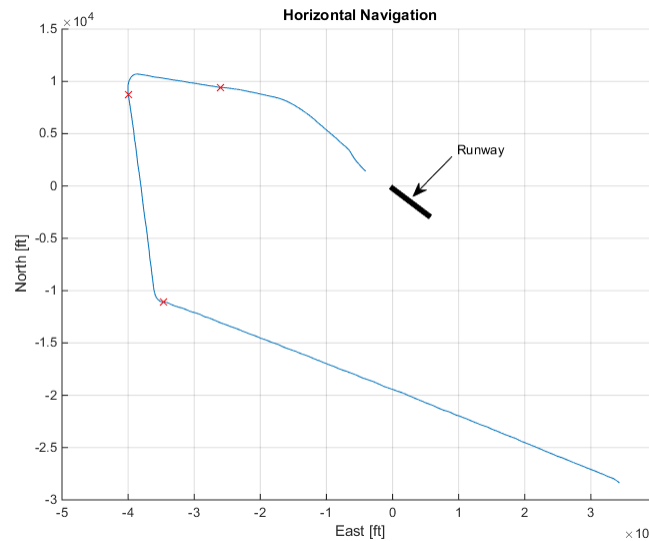


Figure 5.28. Horizontal navigation results for the Navion aircraft.

The aircraft was navigated successfully through all the waypoints. The localizer was then used to align the aircraft with the runway. Figure 5.29 shows the time history of the localizer error from the start of the ILS at 1500 ft until the end of the simulation. It can be seen that the autopilot successfully aligned the aircraft with the runway.

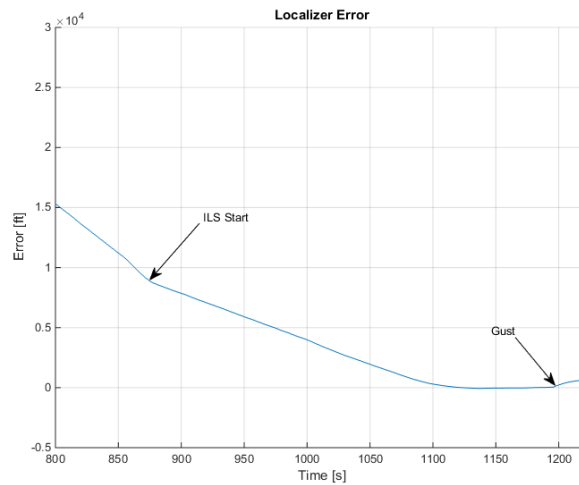


Figure 5.29. Localizer error time history for the Navion aircraft.

The bank angle tracking is shown in Figure 5.30. It can be seen that the bank angle follows the reference model closely. Once again, the ILS demands higher frequency bank angle commands, but the autopilot is able to track adequately.

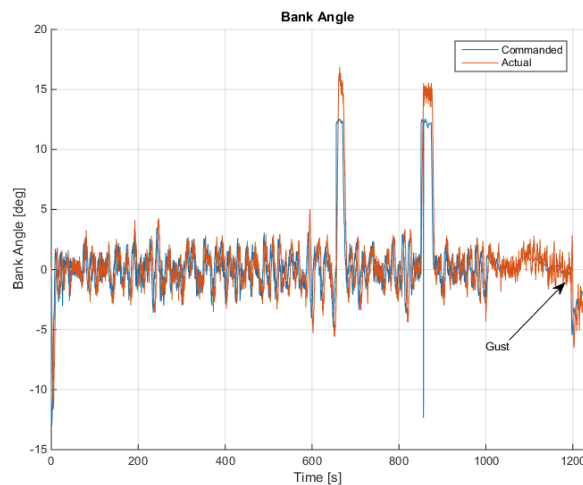


Figure 5.30. Bank angle tracking results for the Navion aircraft.

Figure 5.31 shows a time history of the lateral adaptive gains. Once again, as predicted by the theory, the adaptive gains remain bounded.

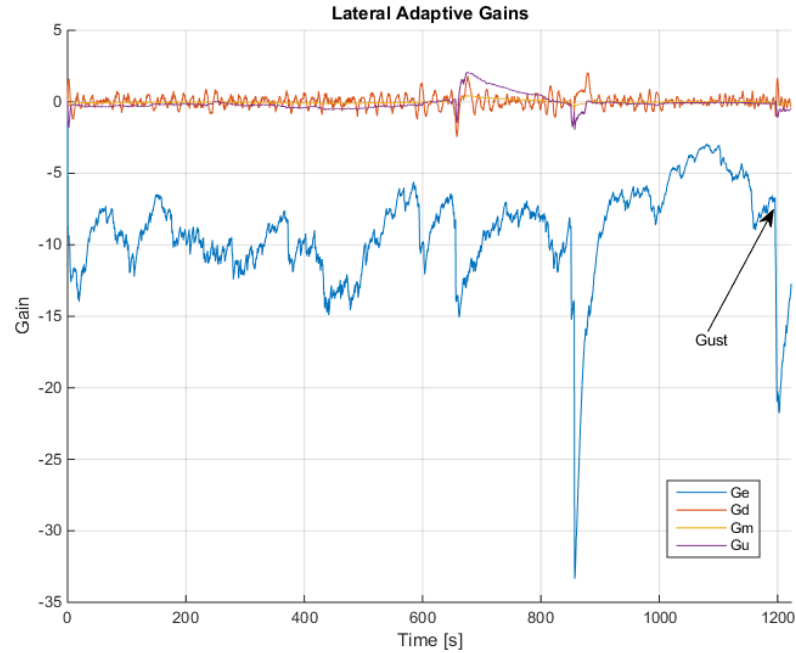


Figure 5.31. Lateral adaptive gains time history for the Navion aircraft.

The results show that the autopilot was able to adapt to both aircraft. Without *a priori* knowledge of each aircraft's dynamics, the autopilot adapted quickly enough to perform its intended functions successfully. Changes of aircraft configuration were also handled appropriately. The autopilot was robust enough to operate in the presence of both internal and external disturbances. It was also capable of performing an ILS approach, and to maintain positive control of the aircraft after being disturbed by a 15 kts gust.

## 6. Conclusion

In conclusion, LOC is a serious problem in aviation that primarily impacts GA aircraft. Technological advancements can help mitigate the problem, but the FAA certification process makes certain solutions economically unfeasible. Autopilots are one of such solutions. It is estimated that autopilots could reduce 50% of GA LOC IFR accidents if they were installed on every IFR-capable aircraft.

Autopilots must be certified for every make and model of aircraft, making the purchasing price extremely high, especially when compared to their uncertified counterparts. Autopilots for experimental aircraft do not need to be certified and therefore cost a fraction of the price of GA autopilots, while they are comprised of essentially the same hardware and possess the same capabilities. The difference in price, thus, can be primarily attributed to certification costs. If a generic autopilot could be designed and certified for several makes and models of aircraft, the certification cost could be divided among all units sold. Even if the initial certification cost is higher than usual, dividing the cost among several makes and models would result in a reduction in price per unit. This investigation presented a methodology for designing such a generic autopilot and demonstrated its feasibility.

In order to design a generic autopilot, adaptive augmentation of a conventional autopilot was used. Using this controller structure, a conventional autopilot was designed for a reference aircraft. A direct model reference adaptive controller was then used to make an unknown aircraft behave like the reference aircraft. When connected in series, the conventional controller provides the outer-loop guidance and navigation, while the adaptive controller ensures that the unknown aircraft behaves in a predictable manner and

provides robustness to internal and external disturbances.

The use of an adaptive controller in a GA aircraft presented several challenges. The nonlinear nature of adaptive controllers makes them non-deterministic. Currently, the FAA does not allow non-deterministic autopilots to be certified. Because not every possible situation can be tested beforehand, safety assurance of non-deterministic controllers cannot be done in the same way it is done for deterministic controllers. In this investigation, the safety of the controller was demonstrated through mathematical analysis.

Robust asymptotic stability of direct adaptive controllers has been previously demonstrated through a thorough mathematical analysis. This stability proof makes assumptions on the plant they are controlling. If these assumptions are met, then the proof is valid. This presented a challenge when applying direct adaptive control to GA aircraft, because most of these aircraft do not readily meet these assumptions. In some cases, a process known as sensor blending can be used to make the plant meet these assumptions. Although the sensor blending process works extremely well for regulating the plant's states to zero, it can sometimes lead to large steady state errors when tracking a nonzero reference. The sensor blending process was expanded for tracking a nonzero reference with zero steady state error. This was used to ensure that the GA aircraft met the controller assumptions while being able to track a non-zero reference.

Additionally, GA aircraft are usually equipped with lower-grade hardware than commercial and military aircraft. The generic autopilot was designed as a replacement of current autopilots. It was desired to minimize the additional hardware required for the generic autopilot. Therefore, the adaptive controller had to be designed with sufficient robustness to compensate for less accurate sensors and slower actuators.

The generic autopilot was designed along with an implementation methodology. The autopilot was then implemented on a high fidelity simulator of an SR22 aircraft. After it was verified that methodology ensured that the controller assumptions were met, the aircraft was flown through a test scenario. The test consisted of three-dimensional navigation at different altitudes, airspeeds, and configurations. The autopilot then guided the aircraft in an ILS approach from 1500 to 200 ft. The test was conducted three times. The first time was a noise-free, ideal case. The second time, sensor and actuator noise were introduced. The third time, moderate atmospheric turbulence and wind gusts were introduced. The autopilot was able to fly the aircraft through the test scenario in all three cases.

The autopilot was able to adapt appropriately to the aircraft. It was able to perform its task safely. The autopilot also adapted to changes in configuration, airspeed, and altitude. In the presence of turbulence, the autopilot was able to maintain control of the aircraft. The autopilot was also able to perform the ILS approach in ideal conditions and under moderate turbulence. A gust of 15 kts was applied at 400 ft, and the autopilot was able to maintain the aircraft under control and realign it with the runway.

After the autopilot was tested successfully on one high fidelity simulator, it was transferred, without modification, to a high fidelity simulator of a different aircraft using the developed methodology. All controller assumptions were verified and the aircraft was flown through the last case of the test scenario. The autopilot was able to adapt to the unknown aircraft and navigate it successfully through different airspeeds, altitudes, and changes in configuration. The adaptive gains remained bounded and were able to accommodate all disturbances. Once again, the ILS approach was completed successfully,

and the autopilot maintained positive control of the aircraft even in the presence of a 15 kts gust.

This investigation demonstrated the feasibility of a generic autopilot through the use of adaptive augmentation. A methodology was developed for the implementation of the autopilot that provides the autopilot with a strong theoretical stability proof. An adaptive autopilot is a sensible approach to the introduction of adaptive controls to the GA fleet. In case of a malfunction, the autopilot can be safely and immediately disengaged, returning control to the pilot. The work presented here can serve as a starting point to increasing levels of automation in GA aircraft in an economically feasible way. This work can be expanded, as the certification process begins to change and confidence in theoretical proofs increases, to more flight critical aspects of aviation. The following section provides recommendations for future work in this area.

## 7. Recommendations

This section includes recommendations for future work in the area of adaptive controls applied to GA aircraft. The generic autopilot was designed using current consumer-grade hardware available in GA aircraft. It is of interest to determine the minimum quality of the actuators and sensors that can be used while still maintaining acceptable performance of the autopilot. The mathematical proof of controller stability does not use any hard coded values for actuator speed or sensor noise, so it is theoretically possible to use extremely slow actuators and noisy sensors. In practice, however, there will be a limit in which the autopilot will no longer be able to perform its intended functions satisfactorily. It would be highly desirable to know this practical limitation of the autopilot. This could be done by conducting a sensitivity analysis by gradually degrading the sensors' and actuators' speed and accuracy. This knowledge would be of interest to regulators and manufacturers.

Similarly, the adaptive controller places the requirement that the plant have no unstable transmission zeros. However, there is no guideline as to how stable the zeros must be. While transferring the generic autopilot to a different plant without modification of the sensor blending, the transmission zeros will change location. For this reason, the sensor blending was performed to place the plant's transmission zeros at a conservative location, so that when the autopilot is transferred to a different plant, the zeros remain stable. It is of interest to determine, if possible, a systematic procedure to determine how much the zeros will move, and in what direction, as a function of parameters that can be determined without detailed knowledge of the plant. For example, as a function of the aircraft's natural modes' frequencies. This could then be used to develop, if not absolute bounds, general

recommendations for autopilot transfer.

This investigation provides a proof of concept generic autopilot that was tested on two different aircraft simulators. It is of interest to test this autopilot and implementation methodology on a higher number of aircraft simulators. Testing on a wider variety of high fidelity simulators would increase confidence in the autopilots adaptability. After the autopilot has been tested more exhaustively, it would be of interest to implement this generic autopilot on an actual aircraft. Implementing the autopilot on an aircraft without *a priori* knowledge of the aircraft's dynamics would be the ultimate test on the autopilots adaptability to unknown plants.

Autopilots are often designed as SISO systems, and this process was followed in the design of the generic autopilot. Adaptive controllers, however, often benefit from a MIMO design approach. Unstable transmission zeros have been known to become stable, or disappear entirely, when a MIMO approach is used. It would be of interest to design a generic autopilot using this approach, to observe the changes in the aircraft's zeros and any improvements in autopilot performance.

This investigation consisted of the design and implementation of a generic autopilot with no knowledge of the specific aircraft that is being controlled. Additionally, the autopilot was limited by existing hardware in current GA autopilots. Significant performance and functionality improvements can be achieved by removing these constraints. The work presented here could be expanded to more flight critical tasks if approximate knowledge of the aircraft was available. Additionally, if more information about the aircraft was available, such as angle of attack and normal acceleration, this work could be expanded to design fly-by-wire adaptive controllers.

## REFERENCES

- 14 CFR Part 23 Reorganization Aviation Rulemaking Committee. (2013). *Recommendations for Increasing the Safety of Small General Aviation Airplanes Certificated to 14 CFR Part 23*. Federal Aviation Administration.
- Aditya, R., Balas, M. J., & Doman, D. B. (2016). Direct Adaptive Stability and Command Augmentation of an Air-Breathing Hypersonic Vehicle. *IEEE Aerospace Conference*. Big Sky.
- Anderson, C. (2013). *The Effects of Aircraft Certification Rules on General Aviation Accidents*. Unpublished doctoral dissertation, Embry-Riddle Aeronautical University, Daytona Beach.
- Astrom, K. J. (1980). Self-tuning regulators - Design principles and applications. In K. S. Narendra, & R. V. Monopoli (Eds.), *Applications of Adaptive Control* (pp. 1-68). New York: Academic Press.
- Baker, C. (1993). Fuzzy Logic Control in Flight Control Systems. In *Fuzzy Logic Control - Software and Hardware Applications* (pp. 363-373). Prentice Hall Series on Environmental and Intelligent Systems.
- Balas, M. J. (1995). Finite-Dimensional Direct Adaptive Control for Discrete-Time Infinite-Dimensional Linear Systems. *Journal of Mathematical Analysis and Applications*, 196, 153-171.
- Balas, M. J., & Frost, S. A. (2014). Robust Adaptive Model Tracking for Distributed Parameter Control of Linear Infinite-dimensional Systems in Hilbert Space. *IEEE/CAA Journal of Automatica Sinica*, 1, 3.
- Balas, M. J., & Frost, S. A. (2016). A Zero Filter Augmentation for Robust Adaptive Control of Weakly Minimum Phase Finite-Dimensional Systems. *AIAA Infotech at Aerospace*. San Diego.
- Balas, M. J., & Frost, S. A. (2016). Adaptive Model Tracking Control for Weakly Minimum Phase Linear Infinite-Dimensional Systems in Hilbert Space Using a Zero Filter. *AIAA Scitech*. San Diego: AIAA.
- Balas, M. J., & Frost, S. A. (2017). Sensor Blending for Direct Adaptive Control of Non-minimum Phase Linear Infinite-Dimensional Systems in Hilbert Space. *American Control Conference*. Seattle: American Automatic Control Council.
- Balas, M. J., & Fuentes, R. (2004). A Non-orthogonal Projection Approach to Characterization of Almost Positive Real Systems with an Application to Adaptive Control. *IEEE American Control Conference*. Boston.
- Beal, T. R. (1993). Digital Simulation of Atmospheric Turbulence for Dryden and von Karman Models. *Journal of Guidance, Control, and Dynamics*, 16(1), 132-138.
- Belcastro, C. M., & Foster, J. V. (2010). Aircraft Loss of Control Accident Analysis. *AIAA Guidance, Navigation, and Control Conference*.
- Bellman, R., & Kalaba, R. (1959, November). On Adaptive Control Processes. *IRE Transactions on Automatic Control*, 4, 1-9.
- Berger, T., Tischler, M. B., Hagerott, S. G., Gangsaas, D., & Saeed, N. (2012). Longitudinal Control Law Design and Handling Qualities Optimization for a Business Jet FLIGHT Control System. *AIAA Guidance, Navigation, and Control Conference*. Minneapolis.
- Berger, T., Tischler, M. B., Hagerott, S. G., Gangsaas, D., & Saeed, N. (2013). Lateral/Directional Control Law Design and Handling Qualities Optimization for a

- Business Jet Flight Control System. *AIAA Atmospheric Flight Mechanics Conference*. Boston: AIAA.
- Bhattacharyya, S., Cofer, D., Musliner, D. J., Mueller, J., & Engstrom, E. (2015). *Certification Considerations for Adaptive Systems*. NASA.
- Boskovic, J. D. (2012). A New Decentralized Retrofit Adaptive Fault-Tolerant Flight Control Design. *International Journal of Adaptive Control and Signal Processing*.
- Bruner, H. S. (2007, May). A Model Following Inverse Controller with Adaptive Compensation for General Aviation Aircraft. *Doctoral Dissertation*. Wichita, Kansas, USA: Wichita State University Dissertations Publishing.
- Campbell, S. F., & Kaneshige, J. T. (2010). A Nonlinear Dynamic Inversion L1 Adaptive Controller for a Generic Transport Model. *American Control Conference*. Baltimore: IEEE.
- Cao, C., & Hovakimyan, N. (2007). Novel L1 Neural Network Adaptive Control Architecture with Guaranteed Transient Performance. *IEEE Transactions on Neural Networks*, 18(4), 1160-1171.
- CH Robotics. (n.d.). *Understanding Euler Angles*. Retrieved September 17, 2016, from CH Robotics: <http://www.chrobotics.com/library/understanding-euler-angles>
- Chandramohan, R., Steck, J. E., Rokhsaz, K., & Ferrari, S. (2007). Adaptive Critic Flight Control for a General Aviation Aircraft: Simulations for the Beech Bonanza Fly-By-Wire Test Bed. *AIAA Infotech@Aerospace Conference and Exhibit*. Rohnert Park: AIAA.
- Clough, B. T. (2002). Metrics, schmetrics! How the Heck do you Determine a UAV's Autonomy Anyway? *Performance Metrics for Intelligent SYstems Conference*. Gaithersburg.
- Duerksen, N. (1996). *Fuzzy Logic Decoupled Longitudinal Control for General Aviation Airplanes*. Hampton: NASA Contractor Report 201639.
- Ercole, A. V., Cardullo, F. M., Kelly, L. C., & Houck, J. A. (2012). *Algorithm for Simulating Atmospheric Turbulence and Aeroelastic Effects on Simulator Motion Systems*. NASA/TM-2012-217601.
- Federal Aviation Administration. (n.d.). *14 CFR Part 23 Reorganization Aviation Rule Making Committee*. Retrieved October 1, 2015, from Federal Aviation Administration Website: [http://www.faa.gov/regulations\\_policies/rulemaking/committees/documents/media/Part23RARC-81511.pdf](http://www.faa.gov/regulations_policies/rulemaking/committees/documents/media/Part23RARC-81511.pdf)
- Federal Aviation Administration. (2009). *Part 23 - Small Airplane Certification Process Study*. Federal Aviation Administration.
- Federal Aviation Administration. (2015, September). *14 Code of Federal Regulations*. Retrieved from E-CFR Website: [http://www.ecfr.gov/cgi-bin/text-idx?node=pt14.1.23#se14.1.23\\_11](http://www.ecfr.gov/cgi-bin/text-idx?node=pt14.1.23#se14.1.23_11)
- Federal Aviation Administration. (2015). *Fact Sheet: General Aviation Safety*. Retrieved from FAA Website: [https://www.faa.gov/news/fact\\_sheets/news\\_story.cfm?newsId=19134](https://www.faa.gov/news/fact_sheets/news_story.cfm?newsId=19134)
- Federal Aviation Administration. (2015). *Fly Safe: Prevent Loss of Control Accidents*. Retrieved from FAA Website: [http://www.faa.gov/news/updates/?newsId=83285&omniRss=news\\_updatesAoc&cid=101\\_N\\_U](http://www.faa.gov/news/updates/?newsId=83285&omniRss=news_updatesAoc&cid=101_N_U)

- Federal Aviation Administration. (2016). *Verification of Adaptive Systems*. New Jersey: Department of Transportation.
- Field, E. J. (1995). *Flying Qualities of Transport Aircraft: Precognitive or Compensatory?* PhD Thesis. Cranfield University.
- Fuentes, R. J., & Balas, M. J. (2000). Direct Adaptive Rejection of Persistent Disturbances. *Journal of Mathematical Analysis and Applications*, 251, 28-39.
- Galloway, A., Paige, R. F., Tudor, N. J., Weaver, R. A., Toyn, I., & McDermid, J. (2005). Proof vs Testing in the Context of Safety Standards. *Digital Avionics Systems Conference*. IEEE.
- Gat, E. (2004). Autonomy Software Verification and Validation Might not be as Hard as it Seems. *Aerospace Conference*. IEEE.
- General Aviation Joint Steering Committee. (2014). *Loss of Control Working Groups*. General Aviation Joint Steering Committee (GAJSC).
- Gregory, I. M., Cao, C., Xargay, E., Hovakimyan, N., & Zou, X. (2009). L1 Adaptive Control Design for NASA AirSTAR Flight Test Vehicle. *AIAA Guidance, Navigation, and Control Conference*. Chicago: AIAA.
- Gregory, I. M., Xargay, E., Cao, C., & Hovakimyan, N. (2010). Flight Test of an L1 Adaptive Controller on the NASA AirSTAR Flight Test Vehicle. *AIAA Guidance, Navigation, and Control Conference*. Toronto, Ontario: AIAA.
- Hartman, A. (2011). *Adaptive Control of Nonminimum Phase Systems Using Sensor Blending with Application to Launch Vehicle Control*. Wyoming: Master's Thesis University of Wyoming.
- Jacklin, S. A. (2008). Closing the Certification Gaps in Adaptive Flight Control Software. *AIAA Guidance, Navigation and Control Conference and Exhibit*. Honolulu.
- Jacklin, S. A. (2012). Certification of Safety-Critical Software Under DO-178C and DO-278A. *Infotech@Aerospace*. Garden Grove: AIAA.
- Jacklin, S. A., Schumann, J. M., Gupta, P. P., Richard, M., Guenther, K., & Soares, F. (2005). Development of Advanced Verification and Validation Procedures and Tools for the Certification of Learning Systems in Aerospace Application. *Infotech@Aerospace*. Arlington: AIAA.
- Jacobson, S. R. (2010). Aircraft Loss of Control Causal Factors and Mitigation Challenges. *AIAA Guidance, navigation and control conference*. Toronto.
- Kailath, T. (1980). *Linear Systems*. Prentice-Hall.
- Kaneshige, J., Bull, J., & Totah, J. J. (2000). Generic Neural Flight Control and Autopilot System. *AIAA Guidance, Navigation and Control Conference and Exhibit*. Denver: AIAA.
- Kim, B. S., & Calise, A. J. (1997). Nonlinear Flight Control Using Neural Networks. *Journal of Guidance, Control, and Dynamics*, 20(1), 26-33.
- Klein, V., & Morelli, E. A. (2006). *Aircraft System Identification Theory and Practice*. Reston: AIAA Education Series.
- Lavretsky, E., & Wise, K. A. (2005). Adaptive Flight Control for Manned/Unmanned Military Aircraft. *American Control Conference*. IEEE.
- Lemon, K. A., Steck, J. E., Hinson, B. T., Nguyen, N., & Dimball, D. (2010). Model Reference Adaptive Flight Control Adapted for General Aviation: Controller Gain Simulation and Preliminary Flight Testing on a Bonanza Fly-By-Wire Testbed. *AIAA Guidance, Navigation, and Control Conference*. Toronto, Ontario: AIAA.

- Liu, Y., Tao, G., & Joshi, S. M. (2010). Modeling and Model Reference Adaptive Control of Aircraft with Asymmetric Damage. *Journal of Guidance, Control, and Dynamics*, 33(5), 1500-1517.
- Mamdani, E. H. (1993). Twenty Years of Fuzzy Control. Experiences Gained and Lessons Learnt. *IEEE International Conference on Fuzzy Systems* (pp. 339-344). IEEE.
- McFarland, M. B., & Calise, A. J. (1997). Multilayer Neural Networks and Adaptive Nonlinear Control of Agile Anti-Air Missiles. *Guidance, Navigation, and Control Conference*. New Orleans: AIAA.
- Meikel, P. J., Steele, B. S., Lemon, K. A., Steck, J. E., & Rokhsaz, K. R. (2013). Flight and HIL Testing of a Longitudinal Model Reference Adaptive Controller on a High-Lag General Aviation Aircraft. *AIAA Guidance, Navigation, and Control Conference*. Boston: AIAA.
- Monteiro, L. R. (n.d.). *Bank Angle and the Physics of Standard Rate Turns*. Retrieved September 18, 2016, from Aviation Education: [http://www.luizmonteiro.com/Article\\_Bank\\_Angle\\_for\\_Std\\_Rate\\_09.aspx](http://www.luizmonteiro.com/Article_Bank_Angle_for_Std_Rate_09.aspx)
- Narendra, K. S., & Annaswamy, A. M. (1989). *Stable Adaptive Systems*. Prentice Hall.
- Nelson, R. C. (1998). *Flight Stability and Automatic Control*. USA: McGraw-Hill Higher Education.
- Noriega, A., Balas, M. J., & Anderson, R. P. (2016). Robust Adaptive Control of a Weakly Minimum Phase General Aviation Aircraft. *Complex Adaptive Systems*. Los Angeles.
- Noriega, A., Balas, M. J., & Anderson, R. P. (2017). Sensor Blending with an Application to Robust Direct Adaptive Control of a Non-Minimum Phase Aircraft. *AIAA SciTech*. Grapevine: AIAA.
- Noriega, A., Balas, M. J., & Martos, B. (2017). Adaptive Augmentation of a Linear Controller for a Plant with Unmatched Uncertainties with an Application to Aircraft Fly-by-Wire Control. *AIAA Aviation*. Denver: AIAA.
- Patel, V. V., Cao, C., Hovakimyan, N., Wise, K. A., & Lavretsky, E. (2007). L1 Adaptive Controller for Tailless Aircraft. *American Control Conference*. New York City: IEEE.
- Rajagopal, K., Balakrishnan, S. N., Steck, J. E., & Kimball, D. (2010). Robust Adaptive Control of a General Aviation Aircraft. *AIAA Atmospheric Flight Mechanics Conference*. Toronto, Ontario Canada: AIAA.
- Rajagopal, K., Mannava, A., Balakrishnan, S. N., Nguyen, N., & Krishnakumar, K. (2009). Neuroadaptive Model Following Controller Design for Non-affine Non-square Aircraft System. *AIAA Guidance, Navigation, and Control Conference*. Chicago: AIAA.
- Romanski, G. (2001). The Challenges of Software Certification. *CrossTalk J Def Software Engineering*, 14(9).
- Rushby, J. (2007). Just-in-Time Certification. *IEEE International Conference on Engineering Complex Computer Systems* (pp. 15-24). IEEE.
- Rysdyk, R., Nardi, F., & Calise, A. J. (1999). Robust Adaptive Nonlinear Flight Control Applications using Neural Networks. *American Control Conference*. San Diego: IEEE.
- Sharma, M., Lavretsky, E., & Wise, K. A. (2006). Application and Flight Testing of an Adaptive Autopilot on Precision Guided Munitions. *AIAA Guidance, Navigation,*

- and Control Conference and Exhibit*. Keystone: AIAA.
- Shuguang, Z. (1994). Fuzzy Control for Roll Agility. *ICAS Congress* (pp. 2296-2301). Anaheim: AIAA.
- Snell, A. (2002). Decoupling of Nonminimum Phase Plants and Applications to Flight Control. *AIAA Guidance, Navigation, and Control Conference and Exhibit*. Monterey: AIAA.
- Steck, J. E., Rokhsaz, K., Pesonen, U., & Duerksen, N. (2004). An Advanced Flight Control System for General Aviation APplication. *SAE International*. 2004-01-1807.
- Steinberg, M. (1992). Potential Role of Neural Networks and Fuzzy Logic in Flight Controller Design and Development. *Aerospace Design Conference*. Irvine: AIAA.
- Stepanyan, V., Krishnakumar, K., Nguyen, N., & Van Eykeren, L. (2009). Stability and Performance Metrics for Adaptive Flight Control. *AIAA Guidance, Navigation, and Control Conference*. Chicago: AIAA.
- Stroosma, O., Damveld, H. J., Mulder, J. A., Choe, R., Xargay, E., & Hovakimyan, N. (2011). A Handling Qualities Assessment of a Business Jet Augmented with an L1 Adaptive Controller. *AIAA Guidance, Navigation, and Control Conference*. Oregon: AIAA.
- Urnes, J. E. (1999). *NASA F-15 Intelligent Flight Control*. Final Report Boeing Report No. STL 99P0040.
- Wang, C., Santone, M., & Chengyu, C. (2012). Pilot-Induced Oscillation Suppression by Using L1 Adaptive Control. *Journal of Control Science and Engineering*.
- Ward, D. E. (1998). *Self Designing Controller*. Final Report AFRL WL-TR-97-3095.
- Wen, J. T., & Balas, M. J. (1989). Robust Adaptive Control in Hilbert Space. *Journal of Mathematical Analysis and Applications*, 143, 1-26.
- Wise, K., Brinker, J., Calise, A., Enns, D., Elgersma, M., & Voulgaris, P. (1999). Direct Adaptive Reconfigurable Flight Control for a Tailless Advanced Fighter Aircraft. *International Journal of Robust Nonlinear Control*, 9, 999-1012.

### A. Robust Stabilization Theorem Proof

Consider the positive definite function:

$$V \equiv (Pe, e) + \frac{1}{2} \text{tr}[\Delta G \gamma^{-1} \Delta G^T] \quad (133)$$

Taking the time derivative of this and substituting (35) yields:

$$\dot{V} = \text{Re}(PA_c e, e) + (e, PA_c e) + (PBw, e) + \text{tr}[\Delta \dot{G} \gamma^{-1} \Delta G^T] + (Pe, v) \quad (134)$$

where  $w \equiv \Delta G \eta$ . Knowing that  $(A, B, C)$  is SD, and using  $x^T y = \text{tr}[yx^T]$  yields:

$$\begin{aligned} \dot{V} &= \text{Re}(PA_c e, e) + \langle e_y, w \rangle - a \text{tr}[G \gamma^{-1} \Delta G^T] - \text{tr}(e_y \eta^T \Delta G^T) + (Pe, v) \\ &\leq -q_{\min} \|e\|^2 - a \text{tr}[(\Delta G + G^*) \gamma^{-1} \Delta G^T] + (Pe, v) \\ &\leq -\left(q_{\min} \|e\|^2 + a \text{tr}[\Delta G \gamma^{-1} \Delta G^T]\right) + a \left|\text{tr}[G^* \gamma^{-1} \Delta G^T]\right| + |(Pe, v)| \\ &\leq -\left(\frac{2q_{\min}}{p_{\max}} \frac{1}{2} (Pe, e) + 2a \frac{1}{2} \text{tr}[\Delta G \gamma^{-1} \Delta G^T]\right) + a \left|\text{tr}[G^* \gamma^{-1} \Delta G^T]\right| + |(Pe, v)| \\ &\leq -2aV + a \left|\text{tr}[G^* \gamma^{-1} \Delta G^T]\right| + |(Pe, v)| \end{aligned} \quad (135)$$

with  $\langle e_y, w \rangle \equiv e_y^* w$ . Using the Cauchy-Schwartz inequality:

$$\left|\text{tr}[G^* \gamma^{-1} \Delta G^T]\right| \leq \|G^*\|_2 \|\Delta G\|_2 \quad (136)$$

and

$$|(Pe, v)| \leq \left\|P^{\frac{1}{2}} v\right\| \left\|P^{\frac{1}{2}} e\right\| = \sqrt{(Pv, v)} \sqrt{(Pe, e)} \quad (137)$$

then (135) becomes:

$$\begin{aligned} \dot{V} + 2aV &\leq a \|G^*\|_2 \|\Delta G\|_2 + \sqrt{p_{\max}} \|v\| \sqrt{(Pe, e)} \\ &\leq a \|G^*\|_2 \|\Delta G\|_2 + \left(\sqrt{p_{\max}} M_v\right) \sqrt{(Pe, e)} \\ &\leq \left(a \|G^*\|_2 + \sqrt{p_{\max}} M_v\right) \sqrt{2} \left[\frac{1}{2} (Pe, e) + \frac{1}{2} \|\Delta G\|_2^2\right]^{\frac{1}{2}} \end{aligned} \quad (138)$$

Therefore,

$$\frac{\dot{V} + 2aV}{V^{\frac{1}{2}}} \leq \sqrt{2} \left( a \|G^*\|_2 + \sqrt{p_{max}} M_v \right) \quad (139)$$

Then, using the identity  $tr[ABC] = tr[CAB]$ :

$$\begin{aligned} \|G^*\|_2 &\equiv \left[ \text{tr} \left( G^* \gamma^{-1} (G^*)^T \right) \right]^{\frac{1}{2}} = \left[ \text{tr} \left( (G^*)^T G^* \gamma^{-1} \right) \right]^{\frac{1}{2}} \\ &\leq \left[ \left( \text{tr} \left( (G^*)^T G^* (G^*)^T G^* \right) \right)^{\frac{1}{2}} \left( \text{tr} \left( \gamma^{-1} \gamma^{-1} \right) \right)^{\frac{1}{2}} \right] = \left[ \text{tr} (G^* (G^*)^T) \right]^{\frac{1}{2}} \left[ \text{tr} (\gamma^{-1}) \right]^{\frac{1}{2}} \\ &\leq \frac{M_v}{a M_G} M_G = \frac{M_v}{a} \end{aligned} \quad (140)$$

which implies that

$$\frac{\dot{V} + 2aV}{V^{\frac{1}{2}}} \leq \sqrt{2} \left( 1 + \sqrt{p_{max}} \right) M_v \quad (141)$$

From:

$$\frac{d}{dt} \left( 2e^{at} V^{\frac{1}{2}} \right) = e^{at} \frac{\dot{V} + 2aV}{V^{\frac{1}{2}}} \leq \sqrt{2} e^{at} \left( 1 + \sqrt{p_{max}} \right) M_v \quad (142)$$

Integrating this expression yields:

$$e^{at} V(t)^{\frac{1}{2}} - V(0)^{\frac{1}{2}} \leq \frac{\left( 1 + \sqrt{p_{max}} \right) M_v}{a} (e^{at} - 1) \quad (143)$$

$$V(t)^{\frac{1}{2}} \leq +V(0)^{\frac{1}{2}} e^{-at} + \frac{\left( 1 + \sqrt{p_{max}} \right) M_v}{a} (1 - e^{-at}) \quad (144)$$

The function  $V(t)$  is a norm function of state  $e(t)$  and matrix  $G(t)$ . Since  $V(t)^{\frac{1}{2}}$  is bounded for all time, then  $e(t)$  and  $G(t)$  are bounded. Using  $\sqrt{p_{min}} \|e(t)\| \leq V(t)^{\frac{1}{2}}$  in (144) yields an exponential bound on state  $e(t)$ :

$$\|e(t)\| \leq \frac{e^{-at}}{\sqrt{p_{\min}}} V(0)^{\frac{1}{2}} + \frac{(1 + \sqrt{p_{\max}}) M_v}{a\sqrt{p_{\min}}} (1 - e^{-at}) \quad (145)$$

Taking the limit superior yields:

$$\lim_{t \rightarrow \infty} \|e(t)\| \leq \frac{(1 + \sqrt{p_{\max}})}{a\sqrt{p_{\min}}} M_v \equiv R_* \quad (146)$$

This concludes the proof of the Robust Stabilization Theorem.